Drp1 ablation in the adult mouse forebrain

Inauguraldissertation
zur
Erlangung der Würde eines Doktors der Philosophie
vorgelegt der
Philosophisch-Naturwissenschaftlichen Fakultät
der Universität Basel

von

Björn Oettinghaus

aus Frankfurt am Main, Deutschland

Berlin, 2014

Genehmigt von der Philosophisch-Naturwissenschaftlichen Fakultät

auf Antrag von

Fakultätsverantwortlicher:	Prof. Dr. Markus Rüegg
Dissertationsleiter:	Prof. Dr. Stephan Frank
Korreferent:	Prof. Dr. Christoph Handschin

Basel, den 20.5.2014
(Datum der Genehmigung durch die Fakultät)

_____

Unterschrift des Fakultätsverantwortlichen

Prof. Dr. Jörg Schibler
(Dekan)

Preface

The following dissertation was written by the author. The INTRODUCTION is based on an updated version of a previous review (Oettinghaus et al., 2012).

The RESULTS section of this dissertation consists of a manuscript written by the author that will shortly be submitted for publication. Please refer to the author contributions section of the manuscript where the contribution of each co-author to this work is listed.

Acknowledgements

I would like to express my warmest gratitude towards my supervisor Stephan Frank for giving me the opportunity to prepare my PhD thesis at the University Hospital of Basel on the exciting topic of mitochondrial dynamics.

I would further like to thank Luca Scorrano for the teaching years in his lab in Geneva and for providing the opportunity to characterize this knockout mouse model.

Special thanks go out to Maria Licci and Lisa Restelli who spent a considerable amount of time helping me with this project and contributed essential ideas.

Last but not least I would like to thank the technicians of the Neuropathology division for being a big help in preparing tissue sections and histological stainings.

This work was supported by Swiss National Science Foundation grant 31003A_127308 and the Novartis Foundation for Medical-Biological Research.

Abstract

Due to their high energy demand, their highly polarized nature and the sheer length of their processes, neurons - more than any other cell type - depend on a well-balanced dynamic mitochondrial network. Drp1, the only known mammalian mediator of mitochondrial fission, is essential for neuronal development. Apart from studies in Purkinje cells, not much is known about the role of Drp1 in the postnatal brain. Tamoxifen-inducible Drp1 ablation in the forebrain leads to a swollen, perinuclearly aggregated mitochondrial phenotype and mitochondrial depletion from synapses resulting in impaired synaptic transmission. In contrast to Drp1-ablated neuronal cultures however, dendritic morphology and synapse numbers are not affected; however, Drp1-ablated neurons show an increased sensitivity to ischemia. Forebrain-specific Drp1-ablated mice also develop a complex metabolic phenotype characterized by weight loss, increased lipolysis and elevated corticosterone levels. Investigating this catabolic shift we found evidence for the activation of the unfolded protein response pathway (UPR) and altered ER morphology in Drp1-ablated brain regions, culminating in the induction of the multifaceted metabolic cytokine Fgf21. Fgf21 is normally produced in liver, fat and skeletal muscle in response to metabolic stress as fasting or exercise. It increases insulin sensitivity, regulates lipolysis in adipocytes and stimulates corticosterone production via receptors in the hypothalamus, thus explaining essential aspects of the observed catabolic phenotype. In summary, our results show that brain tissue can signal metabolic stress via Fgf21 induction, which induces a systemic metabolic shift.

Table of content

Introduction

Mitochondria play important roles in life and death of eukaryotic cells, providing most of the ATP required for metabolic cell processes via oxidative phosphorylation. Moreover, in addition to regulating several other metabolic pathways, such as Krebs cycle, fatty acid metabolism, gluconeogenesis, and haem-synthesis, mitochondria also control intracellular calcium signaling and apoptosis.

Although early, high-resolution electron microscopy images of the organelles - which were obtained by Palade in the early fifties and which have since coined the standard depictions for ensuing text book generations - displayed static, bean-shaped mitochondrial units (Palade, 1953), observations of living cells dating back to 1914 had already revealed that mitochondria are extremely dynamic organelles, modulating their morphology through fusion and fission processes that create highly interconnected tubular networks as well as punctiform solitary organelles (Lewis and Lewis, 1914). Research efforts during the last decade have deciphered the basic molecular mechanisms governing mitochondrial fusion and fission.

Mitochondrial fusion

For lipid bilayer fusion, membranes must first aggregate by coming into nanometer proximity. In order to approximate further to Ångstrom distance they need to overcome the negative charges of the outward facing sulfate groups of the hydrophilic phospholipid heads of the lipid bilayer. For this to happen, membranes need to be dehydrated and negative charges of hydrophilic phospholipid heads need to be neutralized. The two membranes to connect via a hemifusion state in which the components of the two lipid bilayers can mix while their lumen is not yet connected. At one point this hemifusion state may destabilize resulting in the formation of a fusion pore, and the lumen of both bilayers may join. In biological membranes the fusion process is mediated by proteins. The SNARE protein family is the best-studied membrane fusion-mediating protein family. SNARE proteins consist of a transmembrane domain and a cytosolic domain which participates in the formation of SNARE complexes which form between two SNARE proteins of opposing membranes and cytosolic proteins sharing similar protein domains. Several models exist that postulate a role for SNARE complexes in the formation of the hemifusion state and the formation of subsequent fusion pores (Söllner, 2003).

The continuous changes in mitochondrial morphology are controlled by a group of evolutionary conserved large GTPases that share structural homology with prototypical dynamins (Smirnova et al., 1998). Dynamins, ranging in size between 70-100 kDa, are mechanochemical enzymes that - through GTP hydrolysis-driven assembly into multimeric spirals around the collars of invaginating vesicles - are mainly involved in the scission of nascent endo- and exocytic vesicles (van der Bliek, 1999; Morlot and Roux, 2013). In mammals, Mitofusin 1 and 2 (Mfn1/Mfn2) are dynamin-like GTPases that regulate fusion of the outer mitochondrial membrane (OMM). Both proteins are anchored in the OMM and share structural homology, given by a cytoplasmatic N-terminal GTPase domain, two hydrophobic heptad repeats and two C-terminal transmembrane domains connected by a very short loop domain located in the intermembrane space (IMS). Mfn1 is primarily expressed on the OMM while Mfn2 is also expressed on the endoplasmic reticulum (ER) installing trans-organelle connections (de Brito and

Scorrano, 2008). The biophysics of membrane fusion mediated by mitofusins are not clear and it is unknown whether they only participate in the approximation of two membranes or if they also facilitate the formation of a hemifusion state and membrane pore formation. Opa1, another dynamin-related protein with eight known alternative splicing-derived isoforms in humans, is embedded in the inner mitochondrial membrane (IMM) through a transmembrane domain that resides nearby the N-terminus and protrudes the major portion into the IMS. The two non-interrelated functions of Opa1 consist in promoting Mfn1-mediated mitochondrial fusion as well as in regulating the intrinsic apoptotic pathway by impairing cristae maintenance and cytochrome *c* release. Therefore, it is comprehensible that Opa1 downregulation not only leads to enhanced mitochondrial fragmentation, but also to an altered structure of the cristae. Interestingly, the above-mentioned splicing variants of Opa1 give rise to either membrane bound long isoforms or solube short isoforms that are released into the IMS. It has been demonstrated that tightness of cristae junctions correlates with the oligomerization of these two forms of Opa1 (Cipolat et al., 2006; Frezza et al., 2006). Fusion events can be divided into two categories: (1) those in which the OMM of two mitochondria only enter a hemifusion state and separate again shortly thereafter and (2) complete fusion events, where OMM and IMM fuse entirely and mitochondria form a syncytium. The number of complete fusion events greatly depends on Opa1 expression levels. This suggests that Opa1 is of particular importance for IMM fusion (Liu et al., 2009).

Mitochondrial fission

Membrane fission in the eukaryotic cell occurs mainly during membrane vesicle trafficking, mitochondrial dynamics and cytokinesis. This involves firstly the deformation of the membrane into spherical or tubular buds as exemplified by the formation of clathrin-coated pits in endocytosis (Cocucci et al., 2012) and ER tubule outgrowth (English and Voeltz, 2013). This step needs to be followed by the mechanical membrane constriction until a luminal contact point between two opposing membrane sites is established. From here on the reverse mechanistic principles apply as in membrane fusion, and final fission is achieved via the formation of a hemifission state. Membrane constriction of clathrin-coated pits is performed by dynamins and several models of the biophysics responsible for final membrane fission are currently being evaluated (Morlot and Roux, 2013). During cytokinesis membrane fission is mediated via the constriction of an intracellular, constrictive ring composed of actin and myosin filaments and final fission is mediated by SNARE proteins (Glotzer, 2005).

Dynamin-related protein 1 (Drp1) is the only known protein actively mediating mitochondrial fission. In humans, Drp1 is highly expressed in tissues with particular energy demands, such as brain and muscle, whereas moderate to low expression levels are found in liver, lung, placenta, kidney, and pancreas (Smirnova et al., 1998). The molecular structure of Drp1 largely corresponds to that of other proteins of the dynamin superfamily, except for the lack of the C-terminal proline-rich domain termed pleckstrin homology domain (PH) present in most members of the superfamily which is important for dynamin-membrane interactions (Figure 1) (Chang and Blackstone, 2007). On the cellular level, almost the entire Drp1 pool is cytosolic with only about 3% of the total protein content residing at the mitochondrial surface. In order to induce organelle fission, cytosolic Drp1 requires activation and subsequent translocation to the OMM. Here, Drp1 oligomers form ring-like multimeric structures on

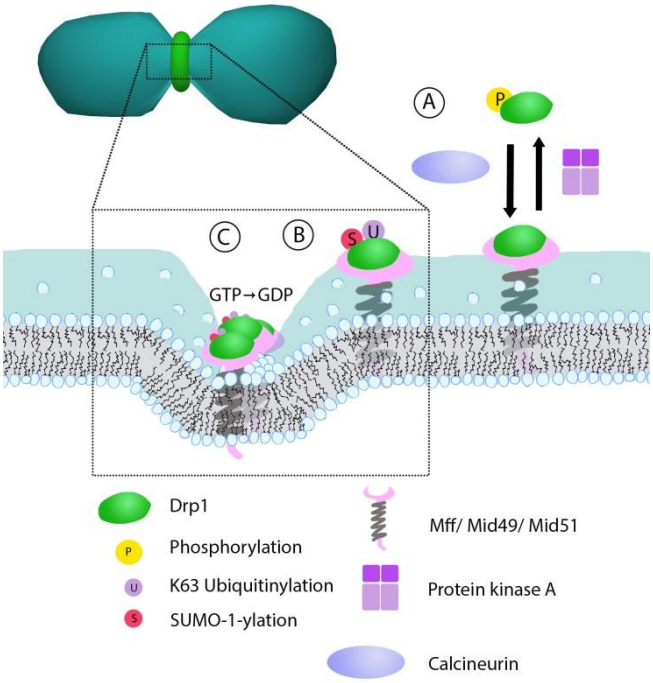

Figure 1 Molecular regulation of Drp1-mediated mitochondrial fission
(A) Activation of Drp1 by e.g. calcineurin-mediated dephosphorylation targets the protein to mitochondria where it is thought to bind one of the adaptor proteins Mff, Mid49 or Mid51. **(B)** Additional posttranslational Drp1 modifications such as ubiquitination and SUMOylation stabilize Drp1 on the OMM. **(C)** Following oligomerization, Drp1 assembles into constrictive ring-like multimers that, upon GTP hydrolysis, mediate membrane constriction.

prospective OMM fission sites through a self-assembling process (Ingerman et al., 2005), followed by GTP hydrolysis-driven conformational changes that – via ring constriction - lead to membrane severing and subsequent organelle division (Lackner et al., 2009; Mears et al., 2011) (Figure 1C). Accordingly, integration of mutated Drp1 molecules (e.g. of the K38A mutation with incapacitated GTP hydrolysis) into the ring-like Drp1 multimers inhibits their constriction through dominant-negative effects, resulting in blocked organelle fission (Smirnova et al., 1998) (Figure 2). Membrane constriction driven by Drp1 structurally closely resembles constriction driven by dynamin. There are a few structural differences that are of major importance. Prototypic dynamin possesses a PH domain which allows it to directly bind to membranes whereas Drp1 does not have a similar domain. In the cryo-EM reconstruction of polymerized Drp1 a gap of 3-4 nm between the assembled Drp1 molecules and the underlying membrane can be appreciated (Mears et al., 2011). It therefore appears likely that Drp1 recruitment to mitochondria requires an adaptor protein to attach to the OMM. Dynamin mediates the constriction of 25 nm membrane tubules to 10 nm *in vitro*. These measurements match the size of the membrane neck of clathrin-coated pits, and the final membrane scission could be driven by shear force. Drp1 however drives the fission of 110 nm tubules and constricts them to 35 nm. The diameter of a mitochondrial tube on the other hand is as large as 500 nm and a 35 nm gap between two membranes makes a spontaneous membrane separation unlikely (Bui and Shaw, 2013). Structural evidence therefore suggests that other mechanisms initiate and complete mitochondrial membrane fission upstream and downstream of Drp1. Preceding Drp1 recruitment, ER tubules have been observed to wrap around potential mitochondrial fission sites (Friedman et al., 2011), a phenomenon termed ER-associated mitochondrial division (ERMD). Drp1 recruitment is also known to be F-actin dependent (DuBoff et al., 2012; De Vos et al., 2005); recently, it was shown that the ER membranes wrapping around mitochondrial fission sites are enriched in inverted formin 2 (INF2) which recruits actin to polymerize between the ER and the mitochondrial membrane (Korobova et al., 2013). Lately also

myosin was shown to participate in ERMD (DuBoff et al., 2012; Korobova et al., 2014). This growing body of evidence suggests that mitochondrial fission is initiated by the ER and driven by the constriction of actin and myosin filaments until the mitochondrial tubule is narrow enough for Drp1 polymerization. The final fission from a 35 nm to a 10 nm tubule could be driven by a member of the dynamin family that mediates fission of other cellular membranes in this range. Another theory involves the modulation of the fission range of Drp1 by an adaptor molecule. Drp1 recruitment to the mitochondria requires an adaptor protein integrated into the OMM. Three mammalian adaptor proteins have been identified so far - Mid49, Mid51 and Mff – all of which can mediate Drp1 recruitment and mitochondrial fission on their own (Losón et al., 2013; Otera et al., 2010; Palmer et al., 2013; Richter et al., 2014; Zhao et al., 2009). Interestingly, in concert with Mid49, Drp1 increases the minimal membrane fission diameter from 35 nm to 14 nm *in vitro* (Koirala et al., 2013), which indicates that adaptor proteins are needed to drive final membrane division. In yeast, Fis1 is the only adaptor for Drp1. The mammalian paralogue Fis1 does only exert little fission activity which might be cell type-specific (Losón et al., 2013; Otera et al., 2010; Shen et al., 2014). Recently, Fis1 has been proposed to form a complex with Drp1 and Mff and to be indispensable for mitophagy (Gomes and Scorrano, 2008; Shen et al., 2014).

At the moment, it is completely unclear how fission of the IMM is achieved. Maybe, in the future, an inner mitochondrial fission machinery will be discovered that is similar to the ftsZ rings driving bacterial and chloroplastic division. Interestingly, mitochondrial DNA molecules localize to Drp1- and Mff-marked fission sites, and their distribution is Drp1-dependent (Ban-Ishihara et al., 2013) suggesting that the OMM fission complex is connected to the mitochondrial matrix. This leads to the speculation that the entire mitochondrial fission machinery is in fact a large complex spanning the ER and both mitochondrial membranes thus connecting cytosol and mitochondrial matrix.

Posttranslational Drp1 modifications

Changes in mitochondrial shape are tightly coupled to essential organellar and cellular functions, as exemplified during mitosis, when the balance between fusion and fission temporarily shifts towards fission to enable equal mitochondrial distribution to daughter cells (Taguchi et al., 2007). In order to allow for rapid adaptation to continuously changing cellular needs, extensive posttranslational modifications such as phosphorylation, SUMOylation and ubiquitination are in place which, by regulating the activity of mitochondrial morphogenic proteins, directly impinge on organelle morphology (Figure 2). When activated by increased cAMP levels, protein kinase A (PKA) phosphorylates Drp1 at residue S637, thereby inhibiting its GTPase activity as well as intermolecular Drp1 interactions resulting in elongated mitochondria (Cereghetti et al., 2008; Chang and Blackstone, 2007; Cribbs and Strack, 2007). This mechanism is being exploited during starvation where mitochondrial elongation resulting from PKA-mediated Drp1 phosphorylation can protect starving cells from autophagy (Gomes et al., 2011). PKA-mediated Drp1 phosphorylation at S637 is counteracted by calcineurin, whose activation leads to organelle fragmentation by boosting Drp1 translocation to mitochondria (Cereghetti et al., 2008; Wang et al., 2011b). As calcineurin activation occurs in response to increased cytosolic Ca^{2+} levels, this mechanism could be activated in Ca^{2+}-mediated neuronal injury, e.g. during ischemia or excitotoxicity. Of note, increased calcineurin activity and

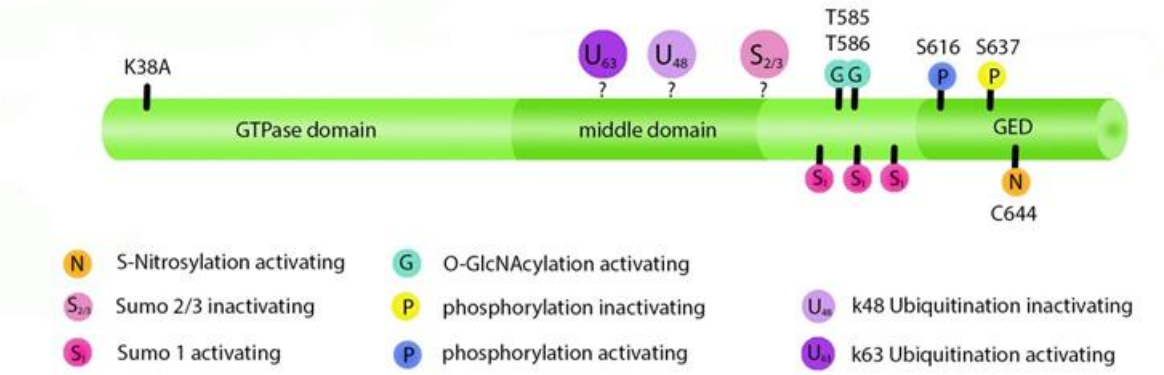

Figure 2 Drp1 structure and posttranslational modifications
Drp1 is composed of a N-terminal GTPase domain, a middle domain and a C-terminal GTPase effector domain (GED), the latter - through impacting GTP hydrolysis - influencing Drp1 oligomerisation. The K38A mutation alters catalytic core residues within the GTPase domain; however, K38A mutant Drp1 can still oligomerize with wildtype Drp1, thus acting as a dominant-negative mutation. The E3-ligases March5 and parkin can ubiquitinate Drp1 at currently unknown sites. March5 mediated k63-linked ubiquitination stabilizes the mitochondrial Drp1 pool while parkin-mediated k48-linked ubiquitination targets Drp1 for proteasomal degradation. Phosphorylation of Drp1 can exert either activating or inactivating effects. Drp1 phosphorylation at S616 by the CDK1/CyclinB complex triggers Drp1-mediated mitochondrial fission during mitosis. In contrast, PKA mediated phosphorylation at S637 inhibits mitochondrial Drp1 translocation; this effect can be antagonized by the phosphatase calcineurin. SUMO-1-ylation of Drp1 can occur at multiple sites between the middle and GED domains, and is mediated by various SUMO-1 ligases such as Sumo1, Ubc9, and MAPL. Removal of SUMO1 is performed by the SUMOprotease SenP5. SUMO-1-ylation of Drp1 stabilizes its association with mitochondria while SUMO-2/3-ylation stbilizes the cytosolic location of Drp1. SUMO-2/3-ylation occurs at an unknown site of Drp1 by unknown SUMO-2/3 ligases during ischemia. Removal of SUMO-2/3 is mediated by SenP3. Mitochondrial fission in the context of Alzheimer`s disease involves Aβ-mediated S-nitrosylation of Drp1 at position C644 which activates Drp1. Lastly O-linked-N-acetyl-glucosamine glycoslysation of Drp1 at T585 and T586 occurs in cardiomyocytes and mediates mitochondrial fission.

subsequent mitochondrial fission have been shown to participate in neuronal toxicity in a Huntington disease mouse model (Costa et al., 2010).

During mitosis, Drp1 phosphorylation at S616 also activates Drp1, triggering mitochondrial fission to enable even mitochondrial distribution to cellular progeny. This phosphorylation event is mediated by the Cdk1/CyclinB complex under the control of the small Ras-like GTPase RALA and its effector RALBP1 (Kashatus et al., 2011; Taguchi et al., 2007). Although cell-cycle coupled events are obviously less significant in postmitotic cells, increased levels of Drp1 S616 phosphorylation were recently found in Alzheimer's disease-affected brains (Wang et al., 2009). In postmitotic neurons, the S616 site can alternatively be phosphorylated by protein kinase C δ (PKCδ) *in vitro* as well as *in vivo*, as demonstrated in a rat model where hypertensive encephalopathy was shown to be associated with mitochondrial fission, accompanied by increased Drp1/PKCδ interactions on mitochondria (Qi et al., 2011).

In addition to the various phosphorylating posttranslational modifications discussed above, Drp1 is subject to ubiquitination. k48-linked ubiquitination marks proteins for proteasomal degradation and ubiquitin-polylinkage at residue k63 is proteasome-independent. To date, MARCH5 as well as parkin have been shown to act as E3 ligases with substrate specificity to Drp1. However, MARCH5-mediated, k63-linked ubiquitination stabilizes Drp1 on mitochondria (Karbowski et al., 2007; Park et al., 2010), while parkin-mediated, k48-linked ubiquitination promotes the proteasomal degradation of Drp1 (Wang et al., 2011a).

SUMOylation of Drp1 is mediated by the small ubiquitin modifier (SUMO). Three different variants of SUMO exist. SUMO-1 and SUMO-2/3 share only 50% sequence homology while SUMO-2 and SUMO-3 differ by just three N-terminal amino acids. SUMO-1 linkage stabilizes Drp1 on mitochondria, thereby supporting mitochondrial fragmentation. SUMOylation of Drp1 is performed by the SUMO ligases Sumo1, Ubc9 and MAPL (Braschi et al., 2009; Figueroa-Romero et al., 2009; Harder et al., 2004; Wasiak et al., 2007; Zunino et al., 2009), while deSUMOylation is mediated by the SUMO protease SenP5 (Zunino et al., 2007, 2009). SUMO-2/3 conjugation of Drp1 stabilizes its cytosolic location during ischemia. SUMO protease SenP3 activity is necessary for the removal of SUMO-2/3 conjugates of Drp1 (Guo et al., 2013a).

Another posttranslational modification has been identified in an Alzheimer`s disease (AD) context. S-nitrosylation at residue C644 in AD brains promotes mitochondrial fission (Cho, Nakamura et al. 2009; Wang, Su et al. 2009; Nakamura, Cieplak et al. 2010).

This multitude of different posttranslational Drp1 modifications is complemented by the discovery of two O-linked-N-acetyl-glucosamine glycosylation (O-GlcNAcylation) sites in cardiomyocytes: T585 and T586. O-GlcNAcylation of Drp1 activates its translocation to mitochondria (Gawlowski et al., 2012).

Non-mitochondrial roles of Drp1

Apart from promoting mitochondrial fission Drp1 has been shown to participate in the maintenance of other cellular organelles. Drp1 has been shown to also regulate peroxisomal fission in mammals (Koch et al., 2003; Wakabayashi et al., 2009; Waterham et al., 2007) dependent on the Drp1 adaptor proteins Fis1 and Mff (Delille and Schrader, 2008; Gandre-Babbe and Bliek, 2008; Koch et al., 2005). Even a role for Drp1 in vesicle trafficking of the Golgi complex could be shown for some cell lines (Bonekamp et al., 2010). Drp1 has also been shown to localize to the ER (Pitts et al., 1999). In β cells treatment with free fatty acids induces the fusion of ER tubules to ER cisternae, a process which is dependent on Drp1 (Wikstrom et al., 2013). Drp1 has also been implicated in highly specialized fission processes in the plasma membrane. In hippocampal neurons it has been shown that Drp1 is recruited probably via Mff to clathrin-coated pits that are retrieving transmitters from the synaptic cleft, and loss of Drp1 function leads to misshaped synaptic vesicles (Li et al., 2013). These results suggest that membrane shaping proteins may not be as specialized as previously thought and that they have evolutionarily adapted to modulate a variety of cellular membranes, probably in a cell type-specific manner.

Drp1 has been found to be subjected to alternative splicing and different isoforms are expressed in different tissues, but no specialized functions could previously be assigned to different Drp1 isoforms. Lately, specialized isoforms have been identified that bind to microtubules and apparently aid in their

stabilization. Their association with microtubules is regulated in a cell cycle-dependent manner via phosphorylation of S616 (Strack et al., 2013). Strikingly, it seems that Drp1 not only has the ability to polymerize around membrane stretches but also to polymerize around fibrillar protein structures. Possibly, the microtubular localization of Drp1 serves to attach mitochondria to the cytoskeleton (Ferraro et al., 2011; Varadi et al., 2004; Yoon et al., 1998).

Drp1 in neuronal morphogenesis, homeostasis, and neurodegeneration

It is a well-known fact that most neurodegenerative diseases occur sporadically, with age being the most significant risk factor. Remarkably, more than one third out of 106 genes that have so far been linked to neurodegenerative diseases, are key regulators of mitochondrial function (Schon and Przedborski 2011). Mutations in two of the mitochondria-shaping proteins have been causally linked to familial neurodegenerative diseases. Whereas autosomal-dominant Mfn2 mutations are pathogenically underlying Charcot Marie Tooth Disease type 2A (CMT2A), a peripheral axonal neuropathy, Opa1 mutations lead to autosomal-dominant optic atrophy (ADOA) (Westermann, 2010). In addition, the mitochondrial fission protein Drp1 can sporadically be affected by mutations in humans, as exemplified by the report of a lethal syndromic birth defect attributable to a heterozygous Drp1 mutation (Waterham et al., 2007). In this case, a newborn presented clinically with truncal hypotonia and insufficient-to-absent optic and motor reflexes accompanied by persistent lactic acidemia; the infant died at day 37 after birth. Workup of that case revealed marked microcephaly, abnormal brain development with abnormal gyral patterns as well as optic atrophy. This severe developmental phenotype hinted – for the first time – at a crucial role of Drp1 in brain development. Given the early embryonic lethality of mice genetically ablated for the mitochondrial fusion proteins Mfn1, Mfn2 (Chen et al., 2003) as well as of constitutive Drp1 knockout mice (see below), it seems plausible that Drp1 mutations may cause early embryonic lethality in humans as well, with a high chance of going undetected in clinical practice. The importance of Drp1 for neuronal development has recently been confirmed beyond doubt by two murine models of genetic Drp1 ablation, each resulting in early embryonic lethality (E11.5). Drp1-ablated embryos display pronounced defects in organ development affecting liver, heart and the neural tube, and lack the trophoblast giant cell layer (Ishihara et al., 2009; Wakabayashi et al., 2009). Both groups were able to generate neuronal-specific Drp1 knockout mice using different approaches. In both models, murine embryos seem to develop normally, but die at postnatal day 0. Employing the engrailed1 (EN1) promoter, Wakabayashi and coworkers ablated Drp1 specifically in the midbrain and the cerebellum, which appeared smaller, devoid of lobar structures, and showed decreased numbers of Purkinje neurons containing fewer mitochondria (Wakabayashi et al., 2009). Ishihara et al. ablated Drp1 pan-neurally using the nestin promoter, which normally gets activated at around day E9.5 (Ishihara et al., 2009). At E18.5, a reduction of forebrain size with white matter hypoplasia and periventricular leukomalacia was observed, accompanied by markedly enlarged subdural and ventricular spaces. In addition, hypoplasia of brain stem and cerebellum was noted. Further analyses revealed significantly increased numbers of TUNEL-positive neurons in deep cortical layers. Interestingly, Drp1 is highly expressed in layer V of the adult mouse neocortex (Belgard et al., 2011), roughly correlating with the many TUNEL-positive cells at the cortex-white matter junction of Drp1-ablated mice (Ishihara et al., 2009). On the cellular level, it is interesting to note that neurons

express mitochondria-shaping proteins at particularly high levels, which very likely reflects the peculiar morphological and biochemical characteristics of this highly ATP-dependent cell type. *In vitro*, expression of the dominant-negative Drp1 mutant K38A in rat hippocampal neurons reduces the number of dendritic spines, underscoring again the importance of Drp1 for neuronal morphogenesis (Li et al., 2004) (Figure 3C). In line with these observations, mixed neuronal cultures derived from nestin-Cre Drp1 knockout mice also feature decreased synapse formation and exhibit decreased neurite numbers (Ishihara et al., 2009) (Figure 3C), whereas in postnatal cortical mouse neurons Drp1 downregulation or expression of a dominant-negative Drp1 mutant causes cell death (Uo et al., 2009). Also activity-stimulated formation of excitatory synapses is blocked by expression of dominant-negative Drp1 mutants, whereas synapse formation is potentiated by the expression of wildtype Drp1 (Li et al., 2004). Interestingly, in Alzheimer disease brains, Mfn1, Mfn2, Opa1 and Drp1 are simultaneously down regulated and this state seems to be associated with perinuclear mitochondrial aggregation and decreased numbers of dendrites and synapses (Wang et al., 2009). Lastly, it should be noted here that synapses in *Drosophila* Drp1 mutants are largely devoid of mitochondria, apparently without synapse function impairment. However, significant defects in the ATP-dependent recruitment of reserve pool vesicles exist, indicating that mitochondria present in the synaptic compartment are required to satisfy sustained local energy needs (Verstreken et al., 2005).

Mitochondria are abundant at synapses (Rowland et al., 2000) as well as within the active growth cones of developing neurons (Morris and Hollenbeck, 1993). As will be discussed later, mitochondrial trafficking is an energy-dependent process that requires appropriate morphology and function of the organelles. Mitochondria in neurons lacking functional Drp1 tend to aggregate in the perikarya (Ishihara et al., 2009; Li et al., 2004; Uo et al., 2009) (Figure 3C). In developmental models, the neuronal demise that follows the inactivation of Drp1 seems to be largely dependent on impaired synapse formation and neurite outgrowth, both of which can probably, at least in part, be attributed to mitochondrial trafficking problems. Curiously, the mitochondrial phenotypes that can be observed in neurons with reduced Drp1 activity are not uniform, ranging from an elongated organelle network that branches out into neurites (Figure 3B) to aggregated perinuclear mitochondrial accumulations (Figure 3C).

This phenotypic variability seems to depend on specific experimental conditions, and especially on the time between Drp1 ablation and mitochondria visualization. A number of publications describe an elongated mitochondrial network that branches out into neurites as depicted in Figure 3B. Of note, the time of mitochondria visualization after Drp1 inactivation was indicated with 2-5 days (Barsoum et al., 2006), 2-4 days (Meuer et al., 2007; Yuan et al., 2007) or 18-24h (Han et al., 2008), respectively. The publications describing an aggregated perinuclear mitochondrial morphology specify the time between Drp1 inactivation and visualization as 4 days (Li et al., 2004), 5 days (Uo et al., 2009), 9 days (Ishihara et al., 2009) or 20 days, respectively (Kageyama et al., 2012).

It is thus tempting to speculate that the elongated mitochondrial morphology branching into neurites and dendrites (Figure 3B) represents a transient state that can be observed shortly after functional Drp1 inactivation, whereas the perinuclear mitochondrial clustering associated with degeneration of neuronal processes (Figure 3C) may result from long-term Drp1 deprivation.

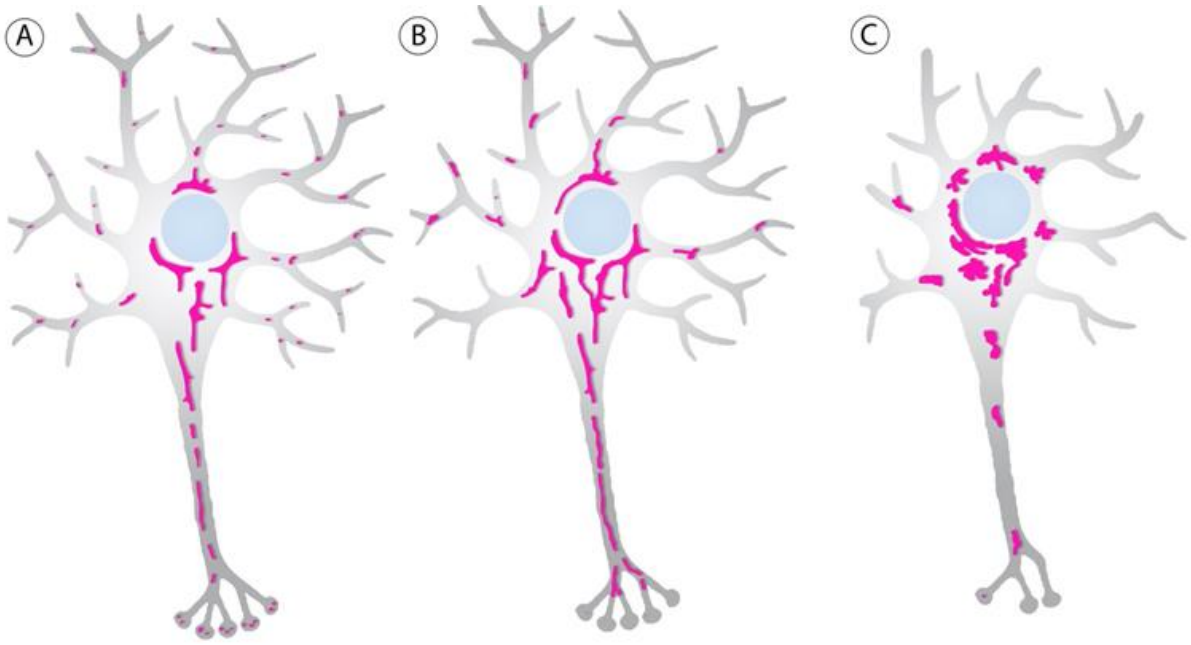

Figure 4 Mitochondrial phenotypes in fission-incompetent neurons
(A) Different mitochondrial phenotypes have been reported for Drp1-deficient neurons. Wildtype mitochondrial morphology is characterized by evenly-distributed organelles in the axonal, neuritic and perikaryon compartments. (B) Following functional Drp1 inactivation in neurons an elongated mitochondrial morphology that branches out into the neurites can be observed; under these conditions, mitochondria do not fragment during apoptosis and are protected from cell death (Barsoum et al., 2006; Cheung et al., 2007; Costa et al., 2010; Dagda et al., 2008; Grohm et al., 2012; Meuer et al., 2007; Park et al., 2011; Tian et al., 2009; Young et al., 2010; Yuan et al., 2007; Zhang et al., 2013). (C) Others found impaired mitochondrial trafficking with elongated organelles aggregating within the perikaryon, accompanied by decreased numbers of neurites and synapses (Ishihara et al., 2009; Li et al., 2004; Uo et al., 2009).

A recent report has studied the effects of neuronal Drp1 ablation in Purkinje cells and confirmed this assumption. Transgenic mice with a floxed Drp1 locus were crossed with mice expressing Cre recombinase under the control of the L7 promoter which is active in Purkinje cells 3 weeks after birth. In Purkinje cells of one-month-old mice the mitochondrial network appeared at first elongated, whereas in two-month-old mice it appeared aggregated, which finally leads to Purkinje cell degeneration within the first three months of age (Kageyama et al., 2012).

Drp1 and aberrant mitochondrial trafficking in neurons

Neurons as the longest human cells exceeding lengths of one meter in certain motor- and sensory neurons are especially dependent on a proper mitochondrial distribution. Distinct long- and short-distance mitochondrial transport mechanisms exist in order to satisfy the particularly high local energy demands at synapses and nodes of Ranvier. Significantly, aberrant mitochondrial trafficking is likely the primary cause underlying the CNS developmental defects including perturbed synapse formation in Drp1 knockout mice. In neurons, microtubule tracks are used as long-distance transport rails to cargo membrane vesicles and cellular organelles including mitochondria. Axonal transport of mitochondria is bidirectional and thought to be coordinated with neuronal outgrowth (Morris and Hollenbeck 1993). Whereas anterograde (i.e. synapse-bound) cargo movement is mediated by

kinesins, dynein/dynactin act promiscuously in retrograde (i.e. perikaryon-bound) organelle transport. The protein couple Miro/Milton, acting in concert with kinesins, is responsible for anterograde mitochondrial trafficking, with Ca^{2+} binding Miro being anchored to the OMM. In a calcium-unbound state, Miro binds to Milton, which in turn can bind to kinesin motorproteins. Upon exposure to high calcium levels, as they occur e.g. within the pre- or postsynaptic compartments, the molecular Miro/Milton interaction gets disrupted, releasing mitochondria (Schwarz, 2013) The only mitochondria-shaping protein so far directly implicated in this process is Mfn2, which interacts with the Miro/Milton complex (Misko et al., 2010). The multimeric dynein complex comprising dynactin and its subunit p50/dynamitin is responsible for retrograde mitochondrial transport. Interestingly, mitochondrial Drp1 foci colocalize with microtubules (Varadi et al., 2004; Yoon et al., 1998). Disruption of the dynein complex or expression of the Drp1 K38A mutant interrupt Drp1/microtubule colocalization, thereby blocking mitochondrial transport (Varadi et al., 2004). Collectively, the available evidence strongly points to a co-dependence of Drp1 and dynein for long-distance mitochondrial trafficking, which is of obvious importance in highly polarized neurons. Short-distance mitochondrial transport in synapses is mediated by actin filaments. In analogy to the disruption of dynein complexes, disruption of actin filaments has been shown to attenuate mitochondrial Drp1 translocation and organelle fission (De Vos et al., 2005).

Drp1 and impairment of neuronal mitochondrial quality control

The turnover of mitochondrial material is fast and efficient . The entire mitochondrial protein content of a liver cell is turned over within a few days as validated in pulse-chase experiments (Lipsky and Pedersen, 1981). Similar experiments have not been performed in neurons; however, as these cells are highly efficient in clearing autophagosomes, similar rates of mitochondrial turnover can be expected (Boland et al., 2008). Basically, there are three different mechanisms that allow for the degradation of mitochondrial material. Firstly, there is the degradation of unfolded proteins by AAA protease complexes in the IMM (Langer et al., 2001) and the degradation of individual proteins by the proteasome system in the cytosol (Karbowski and Youle, 2011). Secondly, there is the formation of mitochondria-derived vesicles that selectively target damaged mitochondrial proteins and lipids for lysosomal degradation. Notably, this process is independent of Drp1 (McLelland et al., 2014; Soubannier et al., 2012). Thirdly, there is the targeted digestion of entire mitochondria through mitophagy, a specialized form of autophagy. Double membrane layered structures that are marked by the microtubule-associated light chain 3 protein (LC3) engulf cytosolic membrane structures including entire cellular organelles and fuse with lysosomes to form autolysosomes. In healthy mitochondria, PTEN-induced kinase 1 (PINK1) is readily imported into the IMM where it is degraded by the rhomboid-like protease PARL. In depolarized mitochondria PINK1 import is blocked at the OMM and PINK1 is able to recruit the ubiquitin ligase parkin to the OMM by phosphorylation (Narendra et al., 2008, 2010). Mitochondrially recruited parkin in turn ubiquitinates mitochondrial proteins, among them Mfn2 and Miro. The ubiquitination on the OMM is detected by p62 which serves as an adaptor for LC3 and targets mitochondria for autophagosomal engulfment (Ashrafi and Schwarz, 2013).

Upstream of mitophagy, Drp1-mediated fission is needed to reduce the size of the mitochondria. Expression of mutant Drp1 is able to block mitochondria removal (Arnoult et al., 2005). Moreover, it

has been shown that Drp1-mediated fission can give rise to depolarized single mitochondrial units that subsequently undergo mitophagy (Twig et al., 2008). In line with this fundamental observation, Drp1 ablation leads to an accumulation of oxidized proteins in mitochondria (Parone et al., 2006; Twig et al., 2008). The Drp1 receptor Fis1 has also been found to be essential for the trafficking of mitochondria to autophagosomes (Gomes and Scorrano, 2008) and just recently it was shown that lack of Fis1 leads to the accumulation of bulk vesicles containing LC3-positive mitochondrial and ER membranes which led to the speculation that components of the ERMD fission complex are needed for the removal of mitochondrial autophagosomes (Shen et al., 2014). Lately, the physiological relevance of parkin-mediated targeting of depolarized mitochondria for mitophagy has been questioned, because this phenomenon has so far only been observed after artificially induced uncoupling of mitochondria *in vitro*. The scarcity of mitophagic events under physiological conditions makes them a difficult phenomenon to observe. It is also difficult to experimentally measure mitophagic events as LC3 and p62 are also involved in targeting cargo other than mitochondria for the engulfment by autophagosomes (Ashrafi and Schwarz, 2013).

Although mammalian neurons are greatly dependent on the expression of autophagic genes, they maintain a very low level of autophagosomes under basal conditions and even under starvation conditions, autophagosome formation is not increased (Yue et al., 2009). It is unclear which role parkin plays in the removal of defective neuronal mitochondria. *In vivo* parkin failed to translocate to mitochondria of dopaminergic neurons in the substantia nigra that were depolarized by a genetically induced respiratory defect (Laar et al., 2011). *In vitro* parkin also failed to translocate to neuronal mitochondria under standard uncoupling conditions (Sterky et al., 2011; Yu et al., 2011). In SH-SY5Y cells a 2-h treatment with the standard chemical uncoupler CCCP (20µM) is sufficient to translocate parkin to 80% of the mitochondria while in neurons a 24-h treatment under the same conditions is needed to translocate parkin to 20% of the mitochondria, even though CCCP treatment induces mitochondrial uncoupling as efficiently in neurons as in SH-SY5Y cells (Cai et al., 2012). Parkin recruitment to mitochondria seems to be locally restricted to the somatodendritic region while parkin-independent removal of axonal mitochondria could also be observed (Cai et al., 2012). While parkin and PINK1 *Drosophila* null mutants show severe neuronal defects (Clark et al., 2006; Greene et al., 2003; Park et al., 2006; Yang et al., 2006), parkin and PINK1 knockout mice are viable and have only subtle phenotypes (Kitada et al., 2007; Palacino et al., 2004; Zhou et al., 2007). It seems that compensatory mechanisms during embryonic development can compensate for a loss in either of these proteins. Deletion of parkin in adult dopaminergic neurons in the substantia nigra, however, induces neurodegeneration in this neuronal population (Shin et al., 2011). However, the authors contribute the neurodegeneration to the failure of parkin to ubiquitinate PARIS, an inhibitor of PGC-1α transcription (Shin et al., 2011). Many more functions than translocation to depolarized mitochondria are attributed to parkin. For example, it exerts an antiapoptotic function by impinging on NF-κB signaling leading to the subsequent upregulation of Opa1 (Müller-Rischart et al., 2013). It also ubiquitinates miro and Mfn2, stopping mitochondrial transport and fusion (Wang et al., 2011c). The same goes for PINK1 which, in addition to parkin, phosphorylates complex I and thereby regulates respiratory efficiency (Morais et al., 2009). In summary, it is unclear how mitophagy is regulated in neurons and the PINK1/parkin pathway might only play a minor role. Due to the scarcity of adult

neurogenesis, postmitotic neurons are indispensable to the organism and autophagic processes in these cells are under tight control by regulatory processes likely to be unique compared to other cell types. For example, neuronal autophagy is likely to occur only in the soma where most lysosomes are located, and might therefore be inhibited in other regions of the cell.

Another aspect of mitochondria quality control is the distribution of mtDNA molecules. Single mitochondrial organelles carry several mtDNA copies, ensuring that intact mtDNA molecules can compensate for damaged (i.e. mutated) ones. It is thus believed that - via fusion of the organelles - mitochondria constantly exchange their mtDNA content within single cells. Proof of functionally important mtDNA exchange was first provided more than a decade ago through a very elegant approach (Ono et al., 2001): through hybridizing two cell lines each carrying one specific mtDNA mutation associated with respiratory deficiency, normal respiration rates could be restored (Ono et al., 2001). In addition, experiments with mice carrying mtDNA mutations proved that, in fact, a population of mitochondria within one cell shares a common pool of mtDNA (Nakada et al., 2001). The process of mitochondrial complementation is highly dependent on organelle fusion as demonstrated in a murine muscle-specific Mfn2-knockout model, where mtDNA mutations accumulate at similar rates as in mice expressing a proof-reading defective mitochondrial DNA polymerase mutant (Chen et al., 2010). In wildtype cells mitochondrial mtDNA molecules locate to mitochondrial fission sites and Drp1 downregulation leads to clustering and apparent loss of mtDNA molecules (Ban-Ishihara et al., 2013; Parone et al., 2008) .This indicates, that Drp1-mediated mitochondrial fission is required for the spatial organisation of mtDNA.

Drp1 in apoptosis

Soon after Drp1`s discovery as a mitochondrial fission protein, it was observed that the mitochondrial fragmentation occurring during apoptosis could be inhibited by overexpression of the dominant-negative Drp1 mutant K38A. Blocking Drp1 function not only inhibited fragmentation of the organelles but, more importantly, also delayed mitochondrial cytochrome *c* release and subsequent apoptotic cell death (Frank et al., 2001). However, the general necessity of mitochondrial fission for apoptosis remains a matter of debate largely attributable to specific experimental setups (including cell lines, specific stimuli, differential sensitivity of various cell death detection assays, as well as different means of Drp1 functional inactivation) (Sheridan and Martin, 2010; Wasilewski and Scorrano, 2009).

We would like to restrict our discussion here to comment on the differential results reported for the available Drp1 knockout mouse models (Ishihara et al., 2009; Wakabayashi et al., 2009). Whereas Wakabayashi et al., using non-immortalized mouse embryonic fibroblasts in their cell death assays, did not observe a delay in apoptosis, the Mihara group using immortalized fibroblasts were able to show just that (Ishihara et al., 2009; Wakabayashi et al., 2009). Interestingly, complete Drp1 ablation did not block, yet delayed mitochondrial fragmentation during apoptosis (Ishihara et al., 2009). Perhaps, this effect is attributable to compensatory changes in expression levels of other mitochondria shaping proteins, which are already altered at steady state in Drp1 null fibroblasts (Ishihara et al., 2009). In summary, genetic Drp1 ablation delays programmed cell death, but is not sufficient to block it.

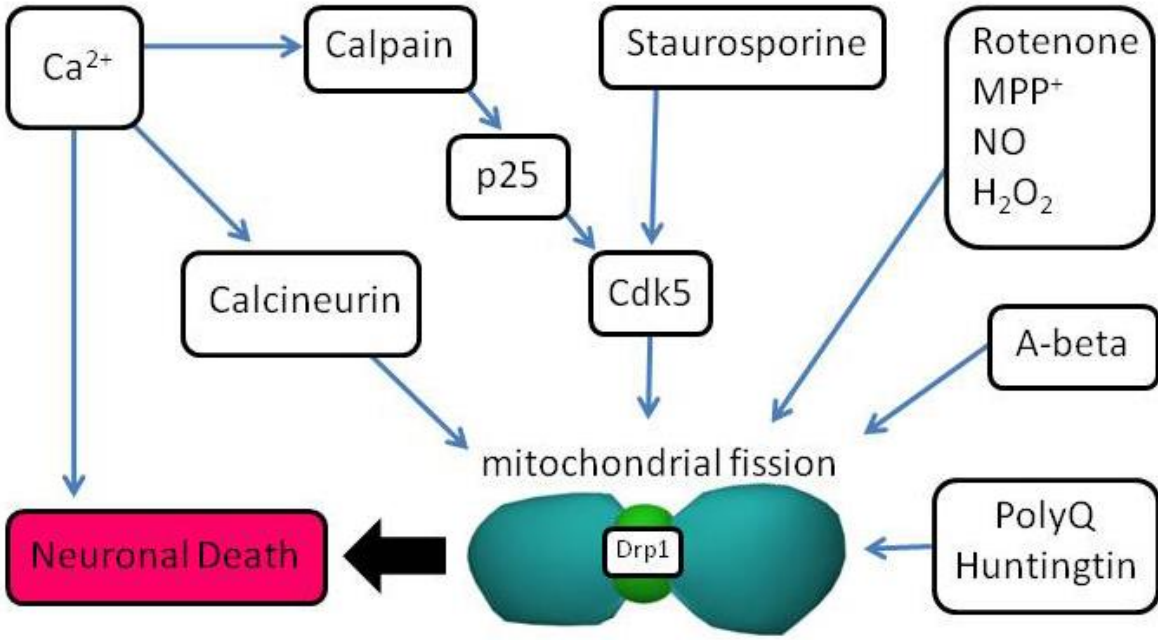

Figure 5 Mitochondrial fission in neuronal death
Mitochondrial fission has been implicated in the pathogenesis of several neurodegenerative diseases. Compounds mimicking neurotoxicity as it occurs in neurodegeneration have *in vitro* been shown to mediate neuronal death dependent on mitochondrial fission. Interestingly, Cdk5, implicated in the pathogenesis of several neurodegenerative conditions, functions as an upstream regulator of mitochondrial fission during neuronal apoptosis. The protein also plays a prominent role in Ca^{2+}-mediated cell death pathways. Here, Ca^{2+}-activated calpains process the p35 Cdk5 activator protein to yield p25, resulting in enhanced Cdk5 activity. In addition, Ca^{2+} can also trigger mitochondrial fragmentation directly by calcineurin-mediated Drp1 S637. On the organelle level, intramitochondrial Ca^{2+} accumulation may lead to organelle swelling and OMM rupture, opening of the permeability transition pore, culminating in the release of proapoptotic factors such as cytochrome *c* from the mitochondria into the cytosol.

On the organelle level, Drp1 has been proposed to facilitate apoptotic cell death by impinging either on outer mitochondrial membrane permeabilization or, alternatively, on mitochondrial cristae remodeling. Key mediators of OMM permeabilization are the “multidomain proapoptotics” Bax and Bak. Both proteins belong to the Bcl-2 family of proteins and get activated in the OMM by so-called “BH3-only” proteins, a Bcl-2 family subset. Once activated, mitochondria release proapoptotic factors such as cytochrome *c* into the cytosol, where subsequent activation of downstream effector caspases occurs via formation of the apoptosome, a specialized protein complex containing APAF1 and pro-caspase-9 (Wasilewski and Scorrano, 2009). Of note, in healthy cells, about 85% of the soluble cytochrome *c* pool reside within the cristae compartment, made up by specialized IMM structures. During apoptosis, dramatic morphological changes termed cristae remodeling take place, facilitating the release of cytochrome *c* during programmed cell death (Bernardi and Azzone, 1981; Scorrano et al., 2002). Expression of the dominant-negative Drp1 mutant K38A can rescue cristae remodeling induced by overexpression of the proapoptotic Bcl-2 protein Bik (Germain et al., 2005) as well as by expression of

mutant huntingtin (Costa et al., 2010). As to now, a plausible answer on how a cytosolic protein such as Drp1 that is targeted to the OMM, can influence cristae remodeling, is lacking. Indirect effects on the proteolytic processing of Opa1, a key regulator of cristae morphology, may represent a plausible scenario as, in fact, levels of proteolytically derived Opa1 isoforms are altered in several Drp1-ablated cell models (Ishihara et al., 2009; Mopert et al., 2009). During apoptosis, Bax translocation from the cytosol to the OMM is dependent on Drp1 and facilitated by cardiolipin, a mitochondrial lipid residing in the IMM. It has been postulated that, in addition to modulating cristae remodeling, Drp1 is involved in the formation of hemifusion sites that bring inner and outer mitochondrial membranes into close contact with each other, thereby enabling the exchange of lipids between the two membranes and facilitating Bax membrane integration (Montessuit et al., 2010). Previously Bax has been shown to localize to mitochondrial fission sites during apoptosis, colocalizing with Drp1 and Mfn2 (Karbowski et al., 2002). This mechanism could be particularly important in neurons, where nitric oxide donor–induced translocation of Bax to mitochondria is Drp1-dependent (Yuan et al., 2007). Of note, the neuronal death in this model requires Drp1 and Bax but no caspase activation, exemplifying a mode of neuronal damage engaging certain modules of the molecular apoptosis cascade without following the complete pathway of classical intrinsic programmed cell death.

Neuronal apoptosis related to changes in mitochondrial morphology has poorly been investigated so far. It is generally difficult to detect *in vivo* as cells dying by apoptosis are swiftly removed by the immune system. Drp1-knockout neurons, which display an aggregated mitochondrial morphology, are more sensitive to the pan-kinase inhibitor staurosporine (STS) as well as to ceramide, a Ca^{2+} stress inducing drug (Ishihara et al., 2009). In contrast, neurons transiently deprived of functional Drp1 display an elongated mitochondrial phenotype (Figure 3B) and show resistance to various apoptotic stimuli such as STS (Costa et al., 2010; Meuer et al., 2007; Young et al., 2010), rotenone (Barsoum et al., 2006; Dagda et al., 2008), MPP^+ (Barsoum et al., 2006), A-β peptide 25-35 (Barsoum et al., 2006), nitric oxide (Barsoum et al., 2006; Yuan et al., 2007), hydrogen peroxide (Cheung et al., 2007), and methamphetamine (Tian et al., 2009) (Figure 4). The discrepancy between these conditions of functional Drp1 inactivation with respect to cell death susceptibility may, as already discussed, be related to the timing of Drp1 ablation: whereas long-term Drp1 ablation favors neuronal death, short-term ablation seems to exert neuroprotective effects. The lack of mitochondrial fission under conditions of genetic Drp1 ablation is likely compensated for by the degradation of the Opa1 protein along with downregulated expression of Mfn1 and Mfn2, all of which result in decreased fusion of the organelles (Ishihara et al., 2009; Mopert et al., 2009).

Ca^{2+} influx is an important inducer of neuronal death. In the context of apoptosis, increased mitochondrial Ca^{2+} uptake can trigger mitochondrial permeability transition, organelle swelling with rupture of the OMM, culminating in the release of proapoptotic factors into the cytosol. In addition, Ca^{2+} activates calpains which trigger apoptosis by cleavage of the BH3-only protein Bid and by processing of the Cdk5 activator p35 to yield the more active p25 form (Lopes and Agostinho, 2011). When activated, Cdk5 mediates STS-induced caspase-dependent neuronal death that is preceded by mitochondrial fragmentation (Meuer et al., 2007). In summary, for neurons, currently available evidence suggests a tight interplay between pathways of Ca^{2+}-mediated neuronal death and classical apoptosis that in both cases involves dysregulated mitochondrial dynamics (Figure 4).

Drp1 in ischemic brain damage and excitotoxicity

Blocking of brain blood vessels by thrombosis can immediately cut off nutrient and blood supply of affected brain regions. Surrounding the necrotic ischemic core where neurons perish by necrosis as an immediate consequence of lacking nutrients, the penumbra receives reduced nutrient supply and remains metabolically active. Cells within the penumbra are susceptible to apoptotic cell death, which occurs primarily as a consequence of excitatory amino acids and proteolytic enzymes released from the necrotic core region. As the penumbra can make up more than half of the total infarction size and apoptotic pathways can be targeted with increasing success, understanding the pathophysiology of ischemic brain damage is imperative for the successful development of neuroprotective strategies targeting such socio-economically important conditions as ischemic stroke (Broughton et al., 2009). In murine models of cerebral ischemia mitochondria within the penumbra have been shown to fragment (Barsoum et al., 2006). As Drp1-mediated mitochondrial fragmentation is commonly observed early during apoptosis - with its inhibition delaying programmed cell death in most experimental scenarios - chemical inhibition of Drp1 using small molecule inhibitors has recently emerged as a promising therapeutic strategy. This is exemplified by mdivi-1, a Drp1-inhibiting compound (Cassidy-Stone et al., 2008) which significantly increases neuronal survival in rodent brain ischemia models (Grohm et al., 2012; Zhang et al., 2013) as well as in rodent retinal ganglion ischemia (Park et al., 2011). Remarkably, mdivi-1 is also effective in reducing infarct sizes in renal (Brooks et al., 2009) and cardiac ischemia (Ong et al., 2010). In this context it is interesting to note that transgenic mice overexpressing miR-499 show reduced myocardial infarction sizes when subjected to cardiac ischemia (Wang et al., 2011b). miR-499 is a micro RNA targeting calcineurin (a cytosolic phosphatase which under normal conditions favors mitochondrial fragmentation via Drp1 dephosphorylation (Cereghetti et al., 2008)). During brain ischemia, SUMO-2/3-ylation is reported to globally increase in the affected brain regions and also to affect Drp1. SUMO-2/3-ylation prevents the translocation of Drp1 to mitochondria and subsequently inhibits mitochondrial fragmentation and cytochrome *c* release. During ischemia, the unfolded protein response pathway (UPR) is activated that leads to the inactivation of the SUMO protease SenP3, that under steady-state conditions readily removes SUMO2/3 from Drp1 which prevents neuronal apoptosis. Upon reoxygenation during reperfusion of the infarct area, UPR stress is lifted and SenP3 activity is restored, making neurons again susceptible to apoptosis (Guo et al., 2013a). This suggests that Drp1 inhibition prior to restoring perfusion may be of utmost importance for the clinical treatment of stroke or myocardial infarct patients.

In addition to limited nutrient supply, neurons within in the cerebral penumbra are exposed to extreme Ca^{2+}-mediated excitotoxic stress. Energy depletion inhibits membrane potential maintenance with subsequent depolarization triggering the release of synaptic vesicles that contain excitatory amino acids. Moreover, excitotoxic stress induced by activation of ionotropic NMDA receptors on presynaptic membranes allows for Ca^{2+} influx, thereby dramatically elevating intracellular Ca^{2+} levels which - when exceeding the uptake capacities of the ER – may result in neuronal cell death. Sharp rises in mitochondrial Ca^{2+} can activate Drp1 through calcineurin-mediated dephosphorylation, and trigger mitochondrial permeability transition with subsequent activation of the mitochondrial gateway to apoptosis. In addition, Ca^{2+} influx into neurons is known to activate calpains (a class of calcium-dependent cysteine proteases). Calpains have been shown to stimulate neuron-specific cyclin-

dependent kinase 5 (Cdk5) forcing cell cycle reentry of postmitotic neurons and promoting neuronal death (Broughton et al., 2009; Lopes and Agostinho, 2011). Moreover, glutamate stimulation of neuronal NMDA receptors leads to reduced mitochondrial motility and fragmentation of the organelles, finally culminating in cell death (Jahani-Asl et al., 2011; Rintoul et al., 2003; Young et al., 2010). Of note, death induced by NMDA receptor-stimulated Ca^{2+} influx can be blocked by overexpression of Opa1 (Jahani-Asl et al., 2011) and, *in vivo,* by overexpression of the endogenous calpain inhibitor, calpastatin (Higuchi et al., 2005). Overstimulation of NMDA receptors also occurs during epileptic seizures. The Drp1 inhibitor mdivi-1 has been shown to limit neuronal loss during status epilepticus elicited by pilocarpine in a rat model (Qiu et al., 2013).

Taken together, the currently available evidence suggests that Drp1-mediated mitochondrial fission contributes to neuronal cell loss under ischemic and excitotoxic conditions. Pharmacological inhibition of the fission machinery, e.g. by the small molecule Drp1 inhibitor mdivi-1, appears to represent a plausible approach that should extensively be tested for its potential as a neuroprotective therapeutic strategy.

Drp1 in Alzheimer's disease

Clinically characterized by progressive decline of cognitive functions and memory, Alzheimer's disease (AD) is a late-onset neurodegenerative disease that leads to the most common form of dementia. Traditional, pathological hallmark features of AD comprise the formation of neurofibrillar tangles composed of hyperphosphorylated tau protein, as well as senile plaques formed by aggregated amyloidogenic A-β-peptides derived from proteolytic cleavage of amyloid precursor protein (APP). During the last few years evidence has been emerging indicating that dysregulated mitochondrial morphology may represent an important component in the complex pathogenesis of AD. Neurons that either overexpress APP or are exposed to toxic A-β peptides display abnormal levels of mitochondria-shaping proteins in association with a perinuclearly aggregated mitochondrial phenotype (Barsoum et al., 2006; Manczak et al., 2011; Wang et al., 2008, 2009). These findings are paralleled by studies of AD patient brains reporting abnormal expression levels of mitochondrial morphogenic proteins (Manczak and Reddy, 2012; Manczak et al., 2011; Wang et al., 2009) and mitochondria aggregated in the perikarya (Wang et al., 2009). Of note, specific, abnormal interactions between Drp1 and A-β have recently been identified in AD brains (Manczak et al., 2011). In addition, a direct interaction between hyperphosphorylated tau and Drp1 could be shown in AD patients as well as in two different AD mouse models (Manczak and Reddy, 2012). Different mouse models expressing mutant forms of tau feature impaired mitochondrial morphology. One model expressing inducible P301L mutant tau displays abnormal mitochondrial distribution in neurons but no increase in mitochondrial size (Kopeikina et al., 2011). In another model, mice and flies also carrying the tau P301L mutation display an elongated mitochondrial phenotype in their neurons; this elongation is due to actin filament disruption by tau which inhibits Drp1 translocation to mitochondria (DuBoff et al., 2012). It seems that both Drp1 overstimulation and Drp1 inhibition can lead to an AD-like phenotype. The complex interplay of A-β, tau and mitochondrial morphology has recently been reviewed (DuBoff et al., 2013). Lastly, specific posttranslational Drp1 modifications have recently been associated with AD. For example, increased levels of Drp1 phosphorylation at position S616 are found in AD brains (Wang, Su et al.

2009). Moreover, Drp1 can undergo S-nitrosylation at residue C644 in an AD context, promoting mitochondrial fission (Cho, Nakamura et al. 2009; Wang, Su et al. 2009; Nakamura, Cieplak et al. 2010).

Drp1 in Huntington's Chorea

A progressive monogenic neurodegenerative disorder, Huntington's disease (HD) is inherited in an autosomal-dominant pattern. It is clinically characterized by involuntary movements such as chorea and dystonia, accompanied by psychiatric disturbances and cognitive decline leading to dementia. Albeit most of the patients experience initial symptoms in their midlife, HD also includes juvenile onset forms. On the molecular level, an intragenic CAG-triplet expansion within the huntingtin (Htt) gene on chromosome 4 results in an abnormal stretch of polyglutamine residues, determining age of onset and disease severity. Histopathological correlates include: progressive neuronal loss affecting in particular striatal GABAergic spiny neurons, and atrophy and gliosis in basal ganglia, cortex, and hippocampus. With several theories existing on the neurotoxicity of mutant Htt aggregates, the exact pathobiology of HD remains to be determined. Transcriptional dysregulation, defective intracellular trafficking, and abnormal mitochondrial bioenergetics and dynamics are all currently being discussed as pathogenic factors (Walker, 2007). HD-like phenotypes can easily be recapitulated in transgenic mice expressing full-length mutant Htt or a N-terminal Htt fragment. Pharmacological inhibition of electron transport chain (ETC) complex II also induced HD-like symptoms in mice indicating a strong mitochondrial component of the disease (Brouillet et al., 1998). Recent studies in HD patient lymphoblasts as well as in primary striatal neurons isolated from HD mouse models revealed a fragmented mitochondrial morphology in concert with an increased susceptibility to apoptotic stimuli. Additionally, increased calcineurin activity paralleled by dephosphorylation and association of Drp1 with mitochondria has been reported (Costa et al., 2010). Intriguingly, this phenotype is accompanied by changes in mitochondrial ultrastructure. Of note, the effects of mutant Htt on mitochondrial fragmentation can be rescued either by the expression of Opa1, the dominant-negative Drp1 mutation K38A, or a dominant-negative calcineurin mutant. The fact that, unlike Opa1, expression of the mitochondrial fusion protein Mfn1 is unable to counteract the increased apoptosis susceptibility of mutant Htt cells emphasizes the importance of Opa1-dependent cristae maintenance, which provides protection from inappropriate cytochrome *c* release and ensuing apoptotic cell death (Costa et al., 2010). In addition to increased mitochondrial fragmentation and neuronal cell death susceptibility, impaired mitochondrial trafficking has also been demonstrated in mutant Htt cell lines. Mutant huntingtin binds to mitochondria, where it assembles into large oligomers at prospective fission sites, similar to Drp1 complexes. Apparently, the co-localization of Drp1 and mutant Htt at mitochondrial fission sites is based on specific Drp1/Htt interactions, that are much weaker in the case of wildtype in comparison to mutated Htt (Shirendeb et al., 2012; Song et al., 2011). In human HD brain, the occurrence of mutant Htt aggregates correlates well with the expression of mitochondrial fission-mediating proteins. In particular in striatal and cortical specimens from HD patients, mitochondrial fission genes Drp1 and Fis1 are expressed at higher mRNA and protein levels, whereas Opa1, Mfn1 and Mfn2 fusion proteins are decreased. Finally, an increased expression of mitochondrially encoded ETC genes as well as significant oxidative DNA damage have been demonstrated in human HD brains, once again reflecting the pathogenically

important relationship between mutant HTT and mitochondrial dysfunction in HD (Shirendeb et al., 2011). Recently, a novel Drp1 inhibitor, P110-TAT, was able to relieve HD symptoms in a mouse model (Guo et al., 2013b), implying that HD patients may benefit from pharmacological reduction of Drp1 activity.

Drp1 in Parkinson's disease

Parkinson`s disease (PD) is the second most common neurodegenerative disease affecting roughly 1% of the population aged 65 years or above (von Campenhausen et al., 2005). Roughly 10% of all cases are associated with mutations in different PARK gene loci, the remaining cases being sporadic with age being the major risk factor. PD pathology is characterized by the loss of dopaminergic neurons in the substantia nigra pars compacta and the formation of intraneuronal inclusions known as Lewy bodies (LB) (Ehringer and Hornykiewicz, 1960; Fearnley and Lees, 1991). On the molecular level, PD pathogenesis has long been regarded as being primarily caused by mitochondrial dysfunction, and, more recently, also by impaired protein turnover causing accumulation of toxic protein aggregates. Apart from LB formation, levels of core components of the ubiquitin-proteasome system are decreased (St. P. McNaught et al., 2003), paralleled by an increase in autophagic vacuoles in PD brains (Anglade et al., 1997). Further, it has long been known that exposure to ETC complex I-inhibiting toxins such as 1-methyl-4-phenylpiridinium (MPP^+), rotenone or paraquat can rapidly induce PD-like symptoms in humans and laboratory animals (Langston et al., 1983; Meredith et al., 2008). In addition, complex I deficiency (Schapira et al., 1990) and elevated reactive oxygen species (ROS) levels (Yan et al., 2013) are frequently observed in PD patients. Moreover, two of the PARK genes, *parkin* and *pink1*, play pivotal roles in the removal of damaged mitochondrial organelles via mitophagy (Narendra et al., 2008, 2010), and other work has identified Drp1 as one of the targets of the E3 ubiquitin ligase, parkin (Wang et al., 2011a). Interestingly, expression of PKA or of the Drp1 S637D phosphomimetic mutation (this S637 phosphorylation is mediated by PKA) can revert the mitochondrial pro-fission phenotype of PINK1-deficient cells (Dagda et al., 2011). In addition, PINK1-deficient cells display increased calcineurin activity; accordingly, their pro-fission phenotype can be reverted by treatment with the calcineurin inhibitor FK506 (Sandebring et al., 2009). *α-synuclein*, another PARK gene and major LB component (Spillantini et al., 1997), associates with mitochondria and induces Drp1-independent mitochondrial fragmentation (Nakamura et al., 2011) which it achieves by disrupting ER-mitochondria contacts (Guardia-Laguarta et al., 2014). In summary, mitochondrial dysfunction significantly contributes to PD pathology. To what extent dysregulated mitochondria morphogenesis and turnover contribute to the pathogenesis of sporadic PD remains to be elucidated.

Aim of the thesis

Ablation of Drp1 in developing neuronal tissue has been shown to have disastrous effects in mice and in humans (Ishihara et al., 2009; Wakabayashi et al., 2009; Waterham et al., 2007). This contrasts the beneficial effects of Drp1 ablation during neuronal apoptosis and ischemia (Barsoum et al., 2006; Cheung et al., 2007; Costa et al., 2010; Dagda et al., 2008; Grohm et al., 2012; Meuer et al., 2007; Park et al., 2011; Tian et al., 2009; Young et al., 2010; Yuan et al., 2007; Zhang et al., 2013).

The first aim of this thesis was to separate the role which Drp1 plays during neurodevelopment from its role during neuronal death *in vivo*. We therefore sought to ablate Drp1 in postmitotic neurons in the adult mouse brain when brain development is completed. We crossed transgenic mice with a floxed Drp1 locus (*Drp1*$^{flx/flx}$) with mice expressing an inducible Cre recombinase transgene under the control of the CamKIIα promoter (Cre^{+}) which is active in the hippocampus and the cortex of adult mice. Forebrain-specific Drp1 ablation would be induced when the offspring of these crosses would be 8 weeks old and puberty and brain development completed, thereby eliminating the neurodevelopmental defects that occur due to constitutive Drp1 ablation. The mice would then be surgically subjected to ischemia and status epilepticus to test for neuroprotective effects of genetic Drp1 ablation. This genetic model has the advantage of restricting Drp1 ablation to neurons and not to systemically inhibit Drp1 in all tissues as a synthetic Drp1 inhibitor would. Furthermore, this model has the benefit of eliminating possible off-target effects of Drp1 inhibitors.

The second aim of this work was to study the long-term effects of adult Drp1 ablation on neurons *in vivo*. Protocols for the genetic manipulation of primary neuronal cultures involve electroporation, transfection or lentiviral infection while the neurons are still not fully differentiated. Long-term Drp1 ablation in these cultures led to a decrease in dendritic structures and synapses (Ishihara et al., 2009; Li et al., 2004; Uo et al., 2009). In this work we aimed to study the effect of Drp1 ablation on synapses and dendrites in an *in vivo* setting when synapse and dendrite formation are completed and neurons supported by glia cells.

The third aim of this thesis was to investigate the unexpected change of metabolism that developed after forebrain-specific Drp1 ablation. Monitoring physiological parameters of the initial Drp1-ablated mouse cohorts we found that the metabolic phenotype outweighed the neurological phenotype. Part of this work was to systematically survey various relevant metabolic parameters during phenotype progression, including blood hormone measurements as well as gene and protein expression level analyses in various tissues.

Additional Results

In order to monitor mitochondrial morphology after Drp1 ablation we electroporated primary hippocampal neurons derived from *Drp1*^{flxflx} E17 embryos with mYFP and Cre expression constructs. The expression of mitochondrially targeted YFP allowed us to monitor mitochondrial morphology while Cre expression would induce the knockout of the *drp1* gene. We found that following Drp1 ablation mitochondria would initially become superelongated and protrude into the dendrites in large tubular structures. However, three days after Drp1 ablation mitochondria would start forming mitochondrial blebs in the perikarya and after nine days the superelongated mitochondria were collapsed and only large spherical mitochondria around the nuclei were detectable (Figure 5A). This observation confirmed our hypothesis that the discrepancies between published neuronal mitochondrial phenotypes were caused by the time period between Drp1 ablation and visualization of mitochondria. Our data clearly show that mitochondrial morphology changes progressively with time after Drp1 ablation.

We wanted to see whether similar mitochondrial morphology phenotypes can be observed *in vivo*. Mice with loxP sites inserted in the *Drp1* gene (*Drp1*$^{flx/flx}$) (Ishihara et al., 2009) were crossed with mice expressing a Cre recombinase fusion protein that induces recombination only after tamoxifen binding (*Cre*$^{+}$) (Erdmann et al., 2007). The expression of the *Cre* transgene was under the control of the CamkIIα promoter limiting recombination primarily to cortex and hippocampus. At 8 weeks of age the offspring of these crossings were injected with tamoxifen and maximum depletion of Drp1 protein levels was observed in brain lysates as early as 10 days after tamoxifen administration (see Manuscript). We also visualized mitochondria by fluorescence microscopy of coronal cross sections of formalin-fixed paraffin-embedded (FFPE) mouse brains in hippocampal pyramidal neurons (Figure 5B). We were not able to pinpoint a hyperfused mitochondrial network as in neuronal cultures but observed that large spherical mitochondrial units started to form in the perikarya around ten days after Drp1 ablation. To test whether this change in mitochondrial morphology would alter neuronal resistance to apoptotic stimuli we subjected 4-week-Drp1-ablated mice and their wt counterparts to surgically induced focal ischemia which would induce small cortical infarcts (Figure 6A); we found that the infarct volume in *Drp1*$^{flx/flx}$ *Cre*$^{+}$ mice was greatly increased (infarct volume *Drp1*$^{flx/flx}$: 3.18 ±- 0.4 mm^3 versus *Drp1*$^{flx/flx}$ *Cre*$^{+}$ 5.29 ± 0.63 mm^3) (Figure 6B). We also induced status epilepticus in Drp1-ablated mice by microinjecting kainic acid onto the hypothalamus. This model was very efficient in inducing neuronal cell death as exemplified in Figure 6A. Cell death was induced in almost all pyramidal hippocampal neurons only sparing a small population in the CA2 region (Figure 6C). We compared neuronal cell death along the cornu ammonis between Drp1-ablated and wt animals and found that this excitotoxicity model induced cell death to equal extent in both groups (Figure 6D).

A

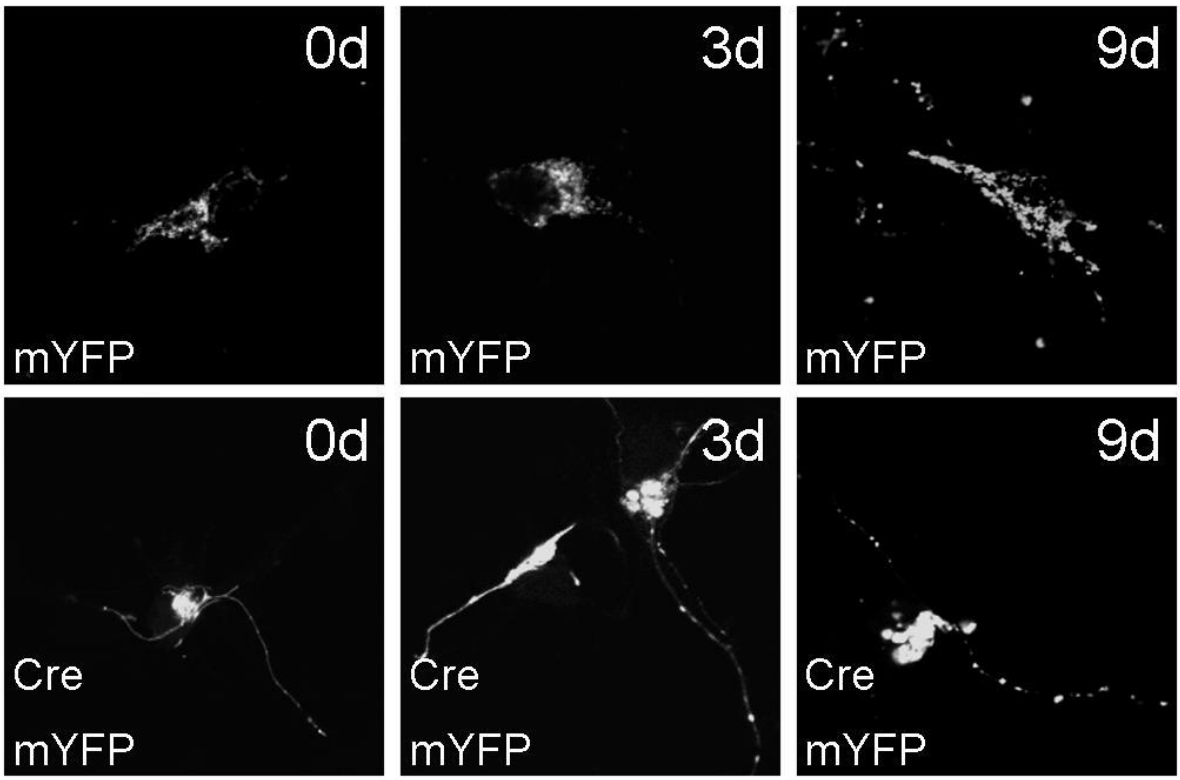
0d
3d
9d
mYFP
mYFP
mYFP
0d
3d
9d
Cre
mYFP
Cre
mYFP
Cre
mYFP

B

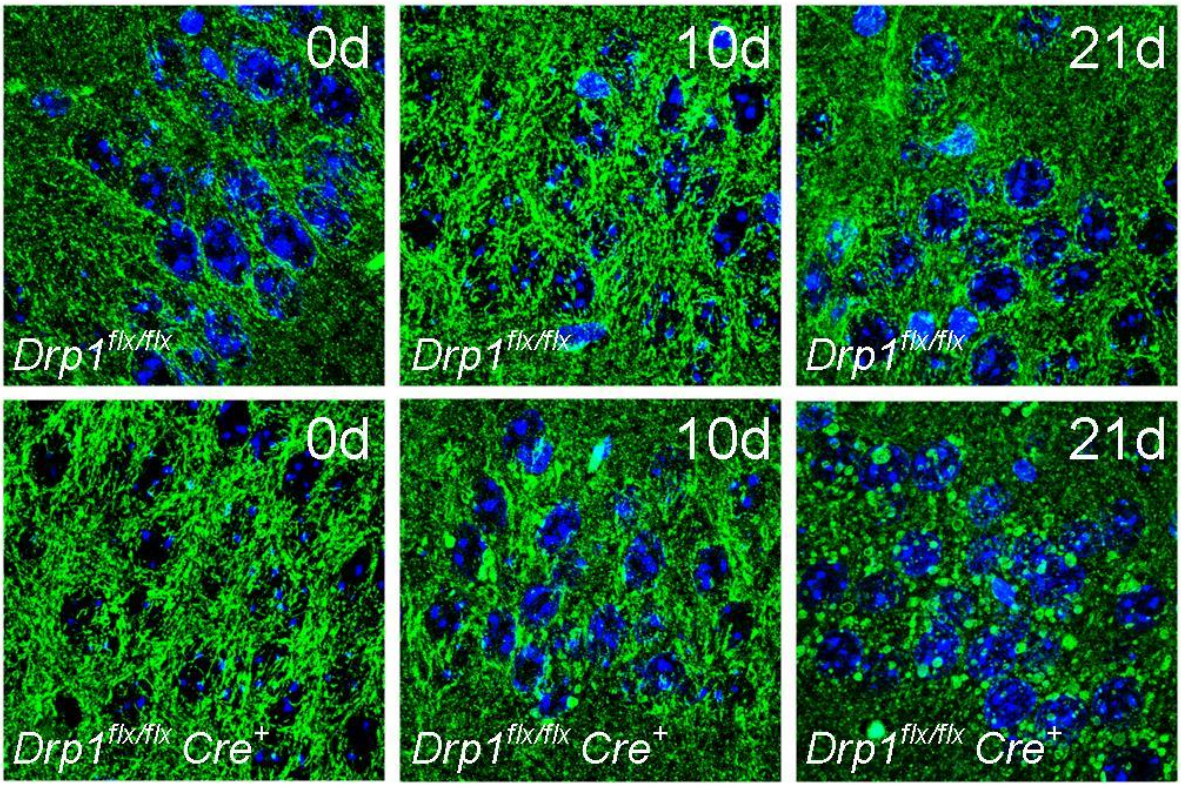
0d
10d
21d
Drp1flx/flx
Drp1flx/flx
Drp1flx/flx
0d
10d
21d
Drp1flx/flx Cre+
Drp1flx/flx Cre+
Drp1flx/flx Cre+

Figure 6 Effect of Drp1 ablation on neuronal mitochondrial morphology
(A) Primary cortical neurons isolated from *Drp1*$^{flx/flx}$ E17 embryos: prior to seeding they were co-electroporated with mYFP- and Cre-expression constructs. **(B)** 4-week-old *Drp1*$^{flx/flx}$ and *Drp1*$^{flx/flx}$ *Cre*$^{+}$ mice have been injected i.p. twice daily for 5 consecutive days with 1 mg of tamoxifen, and sacrificed 0-21 days after last injection. Coronal sections of formalin-fixed paraffin-embedded brains were immunostained for cytc oxidase subunit 1 (green) and with DAPI (blue). The images show pyramidal CA1 neurons. Similar abnormalities in mitochondria morphology were observed in dentage gyrus granule neurons.

Material and Methods

Permanent focal ischemia

Permanent focal ischemia was performed by electrocauterization of the middle cerebral artery (MCA) following craniotomy (Backhauss et al., 1992). Briefly, mice were deeply anesthetized by an i.p. injection of a ketamine/xylazil cocktail (10 mg/kg ketamine and 20 mg/kg xylazil). An incision in the scalp was made to expose the skull and the temporalis muscle. The m. temporalis was cut and a hole (diameter 5 mm) was drilled into the underlying skull to uncover the MCA, whose distal branches were subsequently electrocauterized. Three days post surgery anaesthetized mice were killed by transcardial perfusion with 20 ml of cold PBS followed by 20 ml of 4 % formaldehyde in PBS pH 7.4. Brains were dissected and post-fixed overnight. Following paraffin-embedding, 100-µm-spaced serial coronal cross sections were prepared and stained with cresyl violet. The infarct area of each section was measured and infarct volume calculated applying the Cavalieri principle.

Immunohistochemistry

Formalin-fixed, paraffin-embedded sections of the infarct area were deparaffinized and immersed in 95°C citrate buffer pH 6 for 15 min. Sections were blocked with 15% normal goat serum (NGS) for 1h and subsequently incubated with a primary antibody for cytochrome *c* oxidase subunit1a (abcam ab14705, 1:200) and the secondary antibody mouse AF488 (Molecular Probes A11029; 1:1000). Slides were mounted with Prolong Gold Antifade mounting solution containing DAPI (Life Technologies). Z-stacks were recorded with an inverted Zeiss Axiovert 200M LSM 510 Meta confocal microscope with a 100x/1.4 Oil DIC objective using Enterprise 405 nm and Argon 488 nm lasers. Z-stacks were projected onto a single plane using ImageJ.

Cell culture

Cortices of E17 *Drp1*$^{flx/flx}$ embryos were mechanically dissected and enzymatically dissociated in 0.25% trypsine (Life Technologies) for 10 min at 37°C. Neurons were plated on coverslips coated with 15 µg/ml poly-L-ornithine (Sigma) in Neurobasal medium (Life Technologies), 1.25 µM glutamine, 0.1 mM β-mercaptoethanol and 1x B27 (Life Technologies). After 48 h glia cell growth was inhibited with 5 µM Ara-C (Sigma). Prior to plating, neurons were co-electroporated using the Neon electroporation system (Life Technologies). The mYFP plasmid was previously described (de Brito and Scorrano, 2008; Cereghetti et al., 2008). pPGK-Cre was a kind gift from T. Langer (University of Cologne, Institute for Genetics, Department for Genetic Biochemistry, Germany).

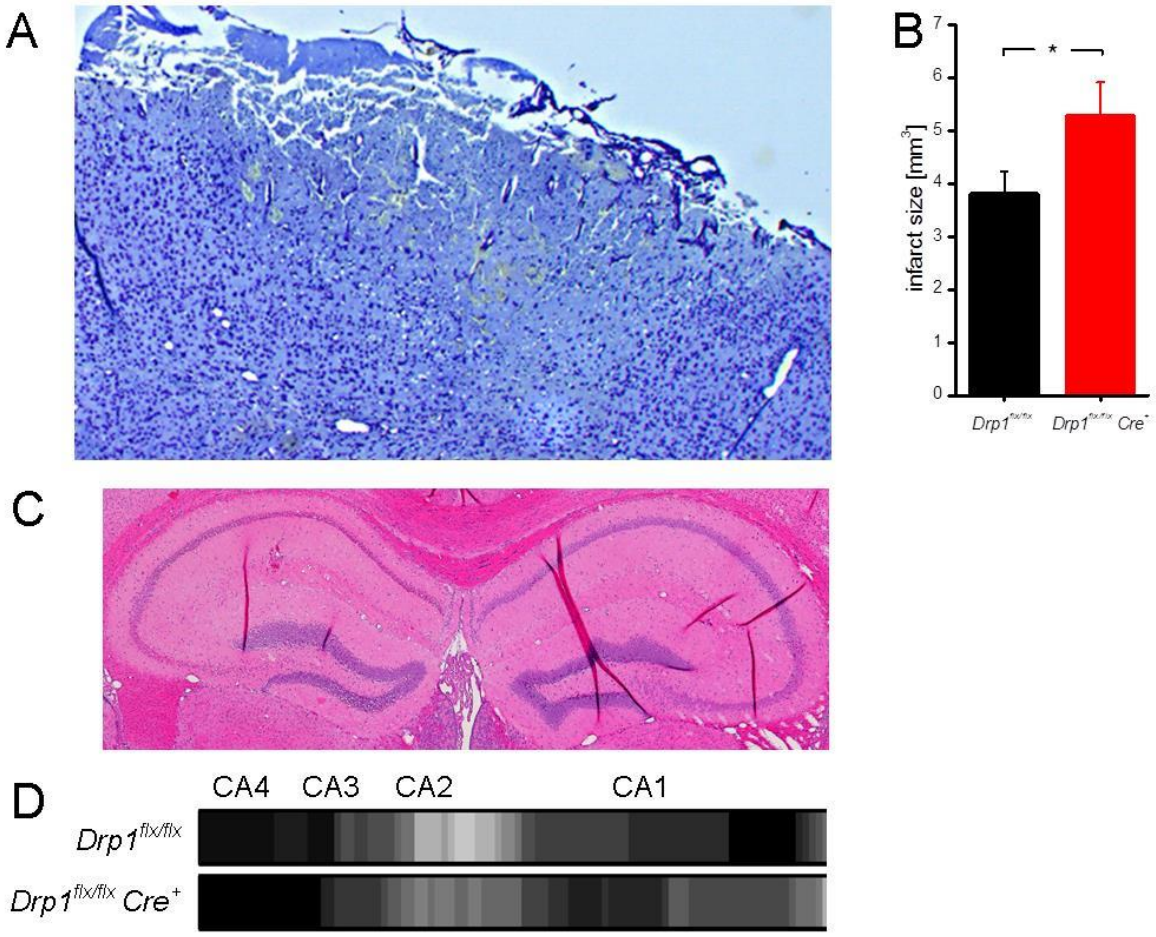

Figure 7 Drp1-ablated neurons are not protected against ischemic and excitotoxic insults

(A) 4 weeks after tamoxifen-treatment, *Drp1*$^{flx/flx}$ *Cre*$^{+}$ and control *Drp1*$^{flx/flx}$ mice were subjected to permanent ligation of the distal branches of the middle cerebral artery to induce focal cortical ischemia. Serial coronal sectioning was performed on formalin-fixed, paraffin-embedded brains to measure infarct areas. Cresyl stain demonstrating ischemic infarct area in the frontal cortex. **(B)** Quantification of infarct volumes reveals statistically significant differences. Data represent mean ± SEM of at least 12 animals (**C)** 4 weeks after tamoxifen-treatment, *Drp1*$^{flx/flx}$ *Cre*$^{+}$ and control (*Drp1*$^{flx/flx}$) mice were stereotaxically injected into the right hemisphere with 70nl of 20 mM kainic acid (-1.9 mm anterioposterior, -1.5 mm mediolateral, –2.0 mm dorsoventral, bregma used as reference) to induce status epilepticus. Mice were sacrificed 48h after injection, and formalin-fixed, paraffin-embedded brains were sectioned. H&E stain demonstrates extensive neuronal damage ipsilateral, extending over much of the pyramidal neurons of the cornu ammonis with the exception of the CA2 sector in some mice (in image left). Note the healthy appearance of neurons of the contralateral side (right) at the time of the experiment. **(D)** The ratio of apoptotic (condensed) versus non-apoptotic nuclei was calculated across the entire length of the cornu ammonis. The percentages were transferred into grey values, with the maximum grey value representing maximal damage. Data represents mean grey values of at least 5 animals.
The asterisk denote P-values of an unpaired, two-tailed Student`s t-test: *:P<0.05

Induction of status epilepticus

Status epilepticus was induced as previously described (Theofilas et al., 2009). Briefly, 4-week-Drp1-ablated and control mice were anesthetized by continuous isoflurane inhalation and their heads were placed inside a stereotaxic frame. Their scalp was opened by an incision and after drilling a small hole into the skull 70 nl of 20 mM kainic acid (SIGMA) were injected over the course of one minute with a 0.5 µl Hamilton syringe at the coordinates -1.9 mm (anterioposterior) -1.5 mm (mediolateral) using the bregma as a reference and -1.2 mm (dorsoventral) using the brain surface as a reference. The needle was left in place for 2 min and then slowly retracted over the course of another minute.

Two days post-surgery anaesthetized mice were killed by transcardial perfusion with 20 ml of cold PBS followed by 20 ml of 4 % formaldehyde in PBS pH 7.4. Brains were dissected and post-fixed overnight, dehydrated and embedded in paraffin. Coronal cross sections at the level of the injection site were H&E-stained and the number of surviving and apoptotic neurons determined along the cornu ammonis.

Manuscript: FGF21 mediates starvation-like response induced by the ablation of mitochondrial fission in the forebrain.

Authors/Affiliations

Björn Oettinghaus[1], Lisa Michelle Restelli[1], Maria Licci[1], Jan Schulz[2], Claudia Savoia[3], Karen Schmitt[4], Amandine Grimm[4], Anne Eckert[4], Lorenzo Morè[5], Patrizia D`Adamo[5], Paul Franken[6], Christoph Handschin[7], Jürgen Hench[1], Markus Tolnay[1], Naotada Ishihara[8], Katsuyoshi Mihara[8,9], Josef Bischofberger[2], Luca Scorrano[3,10*], and Stephan Frank[1*]

[1]Division of Neuropathology, Institute of Pathology; University Hospital Basel, Basel, 4031, Switzerland

[2]Division of Neurophysiology, Institute of Physiology, Department of Biomedicine; University Basel, Basel, 4056, Switzerland

[3]Division of Biochemistry, Department of Biology, University of Padua, Padua, 35121, Italy

[4]University Psychiatric Clinics, Basel, 4025, Switzerland

[5]Dulbecco Telethon Institute, San Raffaele Scientific Institute, Milan, 20132, Italy

[6]Faculty of Biology and Medicine, Center for Integrative Genomics, University of Lausanne, Lausanne, 1015, Switzerland

[7]Biozentrum, Division of Pharmacology/Neurobiology, University of Basel, Basel, 4056, Switzerland

[8]Department of Protein Biochemistry, Institute of Life Science, Kurume University, Kurume, 839-0864, Japan

[9]Department of Molecular Biology, Graduate School of Medical Science, Kyushu University, Fukuoka 812-8582, Japan

[10]Dulbecco-Telethon Institute, Venetian Institute of Molecular Medicine, Padua, 35129, Italy

Contact

*Correspondence: Luca.Scorrano@unipd.it; Stephan.Frank@usb.ch

Summary

Due to their high energy demand, their highly polarized nature and the sheer length of their processes, neurons - more than any other cell type - depend on a well-balanced dynamic mitochondrial network. Drp1, the only known mammalian mediator of mitochondrial fission, is essential for neuronal development. Apart from studies in Purkinje cells, not much is known about the role of Drp1 in the postnatal brain. Tamoxifen-inducible Drp1 ablation in the forebrain leads to a swollen, perinuclearly aggregated mitochondrial phenotype and mitochondrial depletion from synapses resulting in impaired synaptic transmission. In contrast to Drp1-ablated neuronal cultures however, dendritic morphology and synapse numbers are not affected. Forebrain-specific Drp1-ablated mice also develop a complex metabolic phenotype characterized by weight loss, increased lipolysis and elevated corticosterone levels. Investigating this catabolic shift we found evidence for the activation of the unfolded protein response pathway (UPR) and altered ER morphology in Drp1-ablated brain regions, culminating in the induction of the multifaceted metabolic cytokine Fgf21. Fgf21 is normally produced in liver, fat and skeletal muscle in response to metabolic stress as fasting or exercise. It increases insulin sensitivity, regulates lipolysis in adipocytes and stimulates corticosterone production via receptors in the hypothalamus, thus explaining essential aspects of the observed catabolic phenotype. In summary, our results show that brain tissue can signal metabolic stress via Fgf21 induction, which induces a systemic metabolic shift.

Highlights

- Loss of Drp1 in postmitotic hippocampal neurons causes impaired synaptic transmission *in vivo* while dendritic morphology and synapse numbers are retained.
- Genetic Drp1 ablation impinges on endoplasmic reticulum morphology and causes ER stress
- In Drp1-ablated brain tissue, activation of the unfolded protein response pathway locally induces the Fgf21 cytokine which, upon secretion, mediates a catabolic shift of systemic metabolism.

Introduction

Neurons have a particularly high energy demand and are heavily dependent on a functional mitochondrial network. Mitochondria constantly engage in membrane fusion and fission cycles, in which single organelles frequently bud off or merge with the mitochondrial syncytium. Single mitochondria sprouting from the network are transported along the cytoskeleton into dendrites, synapses and spines where they can contribute to local energy demands (Sheng, 2014). Mitochondrial fission is believed to be substantial for the sequestration of defective organelles and their removal from the network (McLelland et al., 2014; Twig et al., 2008), whereas. fusion is important for maintaining qualitative homogeneity of the syncytium through complementation (Chen et al., 2005). Mitochondrial fusion and fission are mediated by highly conserved dynamin-like proteins capable of self-assemble, GTP hydrolysis and of membrane remodeling (Bliek et al., 2013). Mitofusin 1 (Mfn1) and mitofusin 2 (Mfn2) are integral membrane proteins that are able to tether mitochondrial membranes by homo- or heterodimer formation thereby initiating mitochondrial fusion (Koshiba et al., 2004). Mfn1 is primarily expressed on the outer mitochondrial membrane (OMM) while Mfn2 is also

expressed on the endoplasmic reticulum (ER) establishing trans-organelle connections (de Brito and Scorrano, 2008). Optic atrophy 1 (Opa1) is a protein of the inner mitochondrial membrane (IMM) where it executes its pro-fusion activity. Mutations in Mfn2 and Opa1 are causally linked to neurodegenerative diseases highlighting the importance of a well-maintained mitochondrial network for neuronal health. Mfn2 is linked to an axonal peripheral neuropathy known as Charcot-Marie-Tooth disease type 2A whereas Opa1 mutations cause autosomal-dominant optic atrophy (Alexander et al., 2000; Delettre et al., 2000; Zuchner et al., 2004). The only known *bona fide* mammalian pro-fission protein of the dynamin superfamily is the cytosolic dynamin-related protein 1 (Drp1). It is activated by the phosphorylation of one or more residues and translocates to predefined mitochondrial fission sites where it binds to OMM-bound mitochondrial fission factor (Mff) (Otera et al., 2010). The exact molecular configuration of these fission sites is currently not fully understood. According to a currently favored model, Drp1 translocation is preceded by ER tubules wrapping around mitochondria to constrict the organelles (Friedman et al., 2011). A growing body of evidence suggests that this initial step of mitochondrial fission is driven by the constriction of actin and myosin filaments (DuBoff et al., 2012; Korobova et al., 2013, 2014; De Vos et al., 2005) to create a geometric hotspot for the assembly of multimeric Drp1 complexes which – upon GTP hydrolysis - constrict further to complete the mitochondrial fission process (Bui and Shaw, 2013). The involvement of an unidentified inner-mitochondrial fission machinery (similar to the FtsZ ring in chloroplastic and bacterial division) is currently being discussed (Friedman and Nunnari, 2014). Mutations of the *drp1* gene can occur sporadically in humans as exemplified by a lethal syndromic birth defect of an infant with a dominant negative mutation in *drp1* which displayed severe defects in brain development involving optic nerve atrophy and lactacidosis (Waterham et al., 2007). In mice, genetic knockout of *Drp1* pan-neurally or in midbrain and cerebellum also leads to neurodevelopmental defects and death at P0 (Ishihara et al., 2009; Wakabayashi et al., 2009). These neurodevelopmental deficiencies, possibly caused by inefficient transport of mitochondria to developing synapses and axonal growth cones (Morris and Hollenbeck, 1993; Verstreken et al., 2005), are in contrast to the neuroprotective effects of Drp1 ablation in primary neuronal cultures, and in animals treated with the pharmacological Drp1 inhibitor mdivi-1 (reviewed by Oettinghaus et al., 2012).

In this study we ablated Drp1 in postmitotic neurons of the adult mouse brain to bypass the critical role of Drp1 during brain development. Surprisingly, genetic Drp1 ablation from the forebrain of adult mice, resulted in a lethal metabolic phenotype. Here we show that a defect in mitochondrial fission in forebrain neurons impinges on the integrity of neuronal endoplasmic reticulum (ER) morphology, causing ER stress and activation of the unfolded protein response (UPR) pathway. As a direct result cortex and hippocampus, both of which not formally known to exert direct neuroendocrine functions, induce fibroblast growth factor 21 (Fgf21) - a stress-induced, catabolic cytokine that increases insulin sensitivity, regulates lipolysis in adipocytes and induces corticosterone production (Bookout et al., 2013; Kharitonenkov et al., 2005; Luo and McKeehan, 2013). These observations demonstrate that brain tissue can signal ER stress via UPR-induced Fgf21, inducing a profound metabolic shift at the systemic level.

Results

Inducible genetic ablation of Drp1 in the forebrain of adult mice

Mice with loxP sites inserted in the *Drp1* gene (*Drp1*$^{flx/flx}$) (Ishihara et al., 2009) were crossed with mice expressing a Cre recombinase fusion protein that induces recombination only after tamoxifen binding (*Cre*$^{+}$) (Erdmann et al., 2007). In these mice, *Cre* transgene expression is under the control of the CamKIIα promotor limiting recombination primarily to cortex and hippocampus. At 8 weeks of age the offspring of these crossings were injected i.p. with tamoxifen, yielding maximum depletion of Drp1 protein in the forebrain as early as 10 days after tamoxifen administration (Figure1A).

Drp1-ablated mice develop a lethal metabolic phenotype

Unexpectedly, starting already at week 4 after tamoxifen administration, *Drp1*$^{flx/flx}$ *Cre*$^{+}$ mice progressively lost body weight compared to littermate controls (Figure 1B). In addition, the animals appeared weak and their coordination and physical condition decreased as measured by the rotarod performance test (Figure 1C). At an average of approximately 11 weeks after Drp1 ablation their body temperature dropped to as low as 25°C and mice died (Figures 1D and 1E). When checked for cold resistance at 6 weeks after Drp1 ablation, i.e. at a time point when body temperature was normal, we found that *Drp1*$^{flx/flx}$ *Cre*$^{+}$ mice exposed for 4 hours to a 4°C environment showed a significantly reduced body temperature compared to control mice (*Drp1*$^{flx/flx}$: 31.4 ± 0.4°C (n=6) versus *Drp1*$^{flx/flx}$ *Cre*$^{+}$: 28.0 ± 0.9°C (n=8)) (Figure 1F). Thus, it appears that Drp1-ablated mice are impaired in regulating their body temperature already several weeks before the phenotype enters its terminal stage. In order to investigate whether this phenotype was associated with a neurological component we used an 8-radial arm maze to assess hippocampus-dependent working memory function by a spontaneous alternation task. Four weeks after tamoxifen treatment, *Drp1*$^{flx/flx}$ *Cre*$^{+}$ and *Drp1*$^{flx/flx}$ littermates were subjected to the task. When the percentage of correct alternations and total number of arm visits were scored, we noticed that *Drp1*$^{flx/flx}$ *Cre*$^{+}$ mice are significantly impaired in their short-term working memory (*Drp1*$^{flx/flx}$: 72.9 ± 2.3 % (n=7) versus *Drp1*$^{flx/flx}$ *Cre*$^{+}$:60.0 ± 3.6 % (n=10)) (Figure 1G). To verify that their compromised performance in the maze test was not due to impaired sensory perception, we confirmed that *Drp1*$^{flx/flx}$ *Cre*$^{+}$ mice have normal visual acuity and olfaction (Figures S1A and S1B). Collectively, from these experiments we conclude that forebrain-specific Drp1 ablation causes a profound, ultimately lethal metabolic phenotype, which is accompanied by deficits in hippocampus-dependent memory functions.

Mitochondria of Drp1-ablated neurons are greatly enlarged and show profound ultrastructural abnormalities

As an initial step to characterize this metabolic phenotype we visualized mitochondrial morphology in hippocampal neurons of Drp1-ablated mice by immunohistochemistry. At around day 10 after Drp1 ablation, we observed that enlarged spherical mitochondrial units started to aggregate in the neuronal perikarya (Figures 2A, S2A and S2B). Transmission electron microscopy (TEM) analysis (Figure 2B) revealed statistically significant differences in mitochondrial size as measured by the smallest radial diameter (*Drp1*$^{flx/flx}$: 472 ± 49 nm versus *Drp1*$^{flx/flx}$ *Cre*$^{+}$: 1180 ± 108 nm) (Figure 2C) and that the lumen

of roughly 40% of all Drp1-ablated mitochondria was at least partly devoid of cristae (*Drp1*$^{flx/flx}$: 9.1 ± 5.5% versus *Drp1*$^{flx/flx}$ *Cre*$^{+}$: 39.7 ± 8.6%) (Figure 2D). This set of experiments demonstrates that blocking mitochondrial fission through forebrain-specific Drp1 ablation severely impairs mitochondrial morphology and ultrastructure in hippocampal neurons.

Mitochondria of Drp1-ablated neurons have lower oxygen consumption rates but do not show increased oxidative stress

To check whether this abnormal mitochondrial phenotype was associated with functional defects of the organelle, we measured oxidative phosphorylation on isolated mitochondria of hippocampus (Figure 2E) and cortex (Figure S2C). In each case, we observed a significant decrease in mitochondrial ATP content in Drp1-ablated mice (Figure 2F and S2D), whereas no differences were noted in the mitochondrial membrane potential (Figure S2E, S2F and S2G). As Drp1 ablation in Purkinje neurons was recently reported to lead to increased oxidative stress (Kageyama et al., 2012), we measured the activity of reactive oxygen species (ROS) in Drp1-ablated brain tissue homogenates with fluorogenic detection probes but did not detect any significant changes in ROS production (Figure 2G and S2H). We also did not detect changes in the ratio of oxidized to reduced glutathione, nor significant differences in protein carbonylation or lipid peroxidation assays (Figure 2H-J and S2I-S2J). These results indicate that the changes in mitochondrial morphology and ultrastructure that occur at week 4 after Drp1 ablation are accompanied by significantly reduced respiratory capacity and ATP content of hippocampal mitochondria of *Drp1*$^{flx/flx}$ *Cre*$^{+}$ mice.

Drp1 ablation causes a dilation of rough ER cisternae and activates the UPR pathway

Analyzing TEM images of the hippocampus we noticed that in *Drp1*$^{flx/flx}$ *Cre*$^{+}$ animals the normally tubular architecture of the rough endoplasmic reticulum (rER) had changed into dramatically dilated and circular structures (Figure 3A and 3B). Hypothesizing that this change in ER morphology might represent a reflection of ER stress, we checked various parameters of the unfolded protein response. Indeed, analyzing forebrain protein lysates of 4-week-Drp1-ablated mice, we detected increased eIF2α phosphorylation in *Drp1*$^{flx/flx}$ *Cre*$^{+}$ mice compared to *Drp1*$^{flx/flx}$ controls (Figures 3C, 3D and S3A-S3D). In addition, already at 4 weeks after Drp1 ablation, we observed an increase in Chop mRNA levels (Figure 3G). With phenotype progression, we also find increased Bip/Grp78 as well as ATF4 levels at week 10 after Drp1 ablation (Figures 3C, 3E, 3F and S3A-S3C). In contrast, at no time point throughout phenotype progression did we find any evidence for the activation of the IRE1-intiated UPR subpathway, in particular no altered Xbp1 splicing (data not shown). Nevertheless, increased eIF2α phosphorylation, elevated protein levels of Bip/Grp78 and ATF4 as well as increased Chop mRNA levels in forebrain tissue of *Drp1*$^{flx/flx}$ *Cre*$^{+}$ mice collectively indicate that a block in mitochondrial fission is associated with profound morphological alterations of the rER activating an essential pathway of the unfolded protein response.

Drp1-ablated pyramidal CA1 neurons have a defect in synaptic transmission

To test how the severe mitochondrial deficiency in concert with altered ER morphology and UPR activation under conditions of Drp1 ablation affect neuronal health, we performed whole-cell patch-

clamp recordings of individual CA1 pyramidal neurons in acute hippocampal slices from animals at 4 weeks after tamoxifen treatment. Pyramidal CA1 neurons of *Drp1*$^{flx/flx}$ *Cre*$^{+}$ mice had normal basic electrophysiological properties and resting membrane potential (*Drp1*$^{flx/flx}$: -65.7 ± 1.4 mV (n=10) versus *Drp1*$^{flx/flx}$ *Cre*$^{+}$: -65.2 ± 2.4 mV (n= 7)) (Figure 4A). To test for differences in cellular excitability, current steps of increasing amplitude were injected. All evaluated parameters including action potential (AP) peak amplitude and half-width were not different between *Drp1*$^{flx/flx}$ *Cre*$^{+}$ and control mice (Figures 4B and 4C) indicating that the somatic generation of AP output was not affected by Drp1 ablation. Biocytin-filling of patch-clamped pyramidal cells did also not reveal any substantial changes in dendritic morphology (data not shown). To clarify whether the transport to the synapses of the grossly enlarged mitochondria of *Drp1*$^{flx/flx}$ *Cre*$^{+}$ mice was impaired, randomly selected synapses in TEM images of hippocampal neurons were checked for the presence of presynaptic mitochondria. Indeed, the percentage of synapses containing presynaptic mitochondria was greatly reduced in the hippocampi of *Drp1*$^{flx/flx}$ *Cre*$^{+}$ mice (*Drp1*$^{flx/flx}$: 35.7 ± 7.6 % (n=4) versus *Drp1*$^{flx/flx}$ *Cre*$^{+}$: 11 ± 4.1% (n=4)) (Figure 4D). Therefore, we decided to test whether this mitochondrial depletion from synaptic terminals would significantly hamper synaptic transmission using field potential recordings. Stimulation of Schaffer collateral inputs evoked field excitatory postsynaptic potentials (fEPSP) with normal pair-pulse facilitation (Δt= 10 and 100 ms), indicating normal release probability (Figure 4E). When synaptic transmission was challenged by application of 100 stimuli of either 10 or 100 Hz, under both conditions fEPSP facilitation was significantly reduced in brain slices from *Drp1*$^{flx/flx}$ *Cre*$^{+}$ mice (Figures 4F, 4G, S4A and S4B). This result is consistent with previous studies in *Drosophila* indicating that synaptic mitochondria are critical for reserve pool vesicle mobilization (Verstreken et al., 2005). Furthermore, this defect in synaptic transmission appears sufficiently pronounced to explain the memory impairment observed in the *Drp1*$^{flx/flx}$ *Cre*$^{+}$ mice.

Drp1-ablated mice develop hippocampal atrophy

Several previous studies indicate that Drp1 ablation *in vitro* causes a reduction in the number of dendrites, spines, and synapses (reviewed by Oettinghaus et al., 2012). Therefore, we performed Golgi silver impregnations on brain sections of Drp1-ablated mice. Upon Scholl analysis we verified that, while overall dendritic tree morphometry was unchanged, dendrites were significantly shorter in *Drp1*$^{flx/flx}$ *Cre*$^{+}$ mice at 10 weeks after Drp1 ablation (Figures 4H and 4I), which was associated with significantly decreased hippocampal volumes (*Drp1*$^{flx/flx}$: 2.65 ± 0.08 mm^3 (n=6) versus *Drp1*$^{flx/flx}$ *Cre*$^{+}$: 1.95 ± 0.33 mm^3 (n=5)) (Figure 4L). In contrast, cortical and midbrain volumes did not change (Figure 4M). To test whether this hippocampal atrophy was associated with a loss of spines, we quantified spine numbers on apical dendritic trees of pyramidal CA1 neurons, but did not find a difference (Figure 4J). Likewise, no reduction in synapse numbers, as assessed by co-localization of fluorescent stains for pre- (VGLUT2) and postsynaptic (PSD95) markers in laser confocal image zeta stacks, was found.(Figure 4K). Despite relatively subtle morphological changes influencing neuronal and especially hippocampal function, our analyses indicate that, *in vivo,* Drp1-ablated hippocampal CA1 neurons may be more resistant to mitochondrial and ER stress than neurons under *in vitro* conditions*,*

Metabolism of Drp1-ablated mice shifts towards lipolysis, associated, with significantly elevated corticosterone levels

As it is not immediately apparent how the neuronal phenotype with hippocampal atrophy and memory deficits, induced through a forebrain-specific defect in mitochondrial fission could be linked to weight loss and decreased body temperature, a number of metabolic tests was performed. Upon housing mice at four weeks after Drp1 ablation in metabolic cages, their respiratory exchange ratios were found to be significantly reduced (*Drp1*$^{flx/flx}$: 0.988 ± 0.011 (n=8) versus *Drp1*$^{flx/flx}$ *Cre*$^{+}$*:* 0.934 ± 0.012 (n=8)) (Figures 5A and 5F), indicative of a greater contribution of lipid β-oxidation towards ATP production in *Drp1*$^{flx/flx}$ *Cre*$^{+}$ animals. No changes in ambulatory activity, overall metabolic rates, and food or water intake were observed (Figures S5A-S5E). Corresponding to the results of respiratory exchange ratio measurements we also verified by EchoMRI a decrease in the percentage of body fat in Drp1-ablated mice (*Drp1*$^{flx/flx}$: 9.7 ± 0.01% (n=7) versus *Drp1*$^{flx/flx}$ *Cre*$^{+}$: 7.75 ± 0.62% (n=7)) (Figure 5B). In addition, histological analysis of white (WAT) and brown adipose tissue (BAT) revealed smaller WAT adipocytes and smaller fat vacuoles in BAT in Drp1-ablated mice (Figures 5C, D). Finally, at around 10 weeks after Drp1 ablation, levels of the thyroid hormone T4, involved in body temperature regulation, were found to drop,significantly (*Drp1*$^{flx/flx}$: 3.85 ± 0.25 µg/dl (n=9) versus *Drp1*$^{flx/flx}$ *Cre*$^{+}$: 2.74 ± 0.31 µg/dl (n=8)) (Figure 5E). Next, we tested whether hormonal dysregulation of appetite could have caused or contributed to the progressive body weight loss of Drp1-ablated mice. Plasma levels of leptin, an appetite-suppressing hormone secreted by adipocytes, were unchanged (*Drp1*$^{flx/flx}$: 418.7 ± 99.3 pg/ml (n=13) versus *Drp1*$^{flx/flx}$ *Cre*$^{+}$: 353.4 ± 103.6 pg/ml (n=16)) (Figure S5F). In contrast, plasma levels of active ghrelin, which signals appetite, were increased in *Drp1*$^{flx/flx}$ *Cre*$^{+}$ animals (*Drp1*$^{flx/flx}$: 336.3 ± 39 pg/ml (n=8) versus *Drp1*$^{flx/flx}$ *Cre*$^{+}$: 575.6 ± 152.5 pg/ml (n=4)) (Figure S5G), although these measurements did not reach statistical significance. Having established that a major hormonal suppressors (leptin) or stimulators of appetite (ghrelin) are unlikely to account for the observed weight loss in Drp1-ablated mice, long-term monitoring of food intake was performed. We found that Drp1-ablated mice periodically eat even more than their wildtype controls with their food intake declining only during the terminal stages of the phenotype (Figure 5E). We also subjected mice to glucose- and insulin-tolerance tests in order to exclude any difficulties in clearing glucose from blood. At 10 weeks after Drp1 ablation a general decrease in blood glucose was found, but glucose clearance in response to either high glucose levels or to insulin were unaffected (Figures S5H and S5I). Finally, to solve the so far explained discrepancy between weight loss and increased food intake in Drp1-ablated mice, we measured corticosterone (the major glucocorticoid in rodents) which drives gluconeogenesis, protein degradation, and lipolysis. Already at 6 weeks after Drp1 ablation corticosterone serum levels of Drp1-ablated mice were found to be significantly increased (*Drp1*$^{flx/flx}$: 111.5 ± 18.5 ng/ml (n=8) versus *Drp1*$^{flx/flx}$ *Cre*$^{+}$: 284.6 ± 33.7 ng/ml (n=4)) (Figure 5G), providing a first clue to the mechanisms underlying the profound shift in metabolism observed in forebrain-specific-Drp1-ablated mice.

Locally induced in Drp1-ablated brains via the UPR-pathway, the cytokine Fgf21 accumulates in the serum

Corticosterone levels are controlled by the hypothalamic-pituitary-adrenal axis, which can be stimulated by the catabolic cytokine Fgf21 (Bookout et al., 2013). By ELISA Fgf21 plasma levels were

found to be increased in *Drp1*$^{flx/flx}$ *Cre*$^{+}$ mice (Figure 5H). We also checked Fgf21 mRNA expression levels in the brain and other relevant tissues and found increased mRNA levels specifically in regions of Drp1 ablation (cortex, hippocampus), whereas no Fgf21 mRNA increases were observed in tissues where the cytokine is normally produced in response to metabolic stress (liver, skeletal muscle, WAT; Luo and McKeehan, 2013) (Figure 5I). With regard to our observation that Drp1 ablation in the brain activates the eIF2α/ATF4 signaling axis of the UPR, it is interesting to note that Fgf21 expression was previously shown to be induced by ATF4 *in vitro* (Muñoz et al., 2013). Therefore we checked whether Fgf21 activators other than ATF4 such as PPARα (Badman et al., 2007; Inagaki et al., 2007), PGC1α (Estall et al., 2009) and phospho-Akt (Tyynismaa et al., 2010) were also involved. By screening transcriptional levels of PPARα, PPARβ, PGC1α, PGC1β we did not find any increases in either of these mRNAs (Figure S5J); likewise, Western Blotting for phosphorylated Akt1 did not reveal any differences between *Drp1*$^{flx/flx}$ *Cre*$^{+}$ and control mice (Figures S5K, L). From these observations and taking into account our results represented by Figure 3 (including Figure S3), we conclude that Fgf21 induction in *Drp1*$^{flx/flx}$ *Cre*$^{+}$ mice most likely occurs through activation of the eIF2α/ATF4 signaling axis of the UPR.

Experimental procedures

Mice

Drp1$^{flx/flx}$ mice have been described previously (Ishihara et al., 2009). The CamKIIα CreERT2 (Cre^{+}) mouse was purchased from the European Mouse Mutant Archive (EMMA strain 02125) (Erdmann et al., 2007). At 8 weeks of age *Drp1*$^{flx/flx}$ *Cre*$^{+}$ mice were injected i.p. with 1 mg tamoxifen (10 mg/ml tamoxifen (Sigma) dissolved in a 9:1 ratio of sunflower seed oil to ethanol) twice per day on five consecutive days to induce recombination of the Drp1 locus.

Histology

Serial, coronal cross sections of formalin-fixed, paraffin-embedded (FFPE) mouse brains were prepared and sections representing the coordinates bregma (-1.34 mm) – (-2.46 mm) were selected and stained for COX subunit1a (Abcam). Z-stacks were recorded with an inverted Zeiss Axiovert 200M LSM 510 Meta confocal microscope with a 100x/1.4 Oil DIC objective using Enterprise 405 nm and Argon 488 nm lasers. Z-stacks were projected onto a single plane using ImageJ. Synapse numbers were quantified as described previously (Ippolito and Eroglu, 2010). Golgi staining was performed on PBS-perfused, unfixed brains using a commercial kit (FD Neurotechnologies).

Hippocampal volume was calculated from H&E stained 100-µm-spaced, serial, coronal cross sections applying the Cavalieri principle. For cortical and midbrain volume, only sections representing coordinates bregma 1.1 mm – (-1.2 mm) were considered, using the corpus callosum as reference.

Transmission electron microscopy

Semithin sections of osmium-stained hippocampi were prepared in order to identify hippocampal neurons, of which ultrathin sections were prepared. Imaging was done on a Phillips CM100 transmission electron microscope, and morphological analysis of ER and mitochondria was performed using ImageJ. The minimal radial diameter of a mitochondrion was calculated using a rotating calipers

algorithm and the roundness of rER structures was calculated using standard shape descriptors of ImageJ.

Electrophysiology

Transverse 350 to 400-μm-thick hippocampal brain slices were cut in a sucrose-based solution. During electrophysiological recordings, slices were continuously superfused with artificial cerebrospinal fluid (ACSF) maintained at 32-33ºC. During whole-cell patch-clamp recordings, hippocampal CA1 pyramidal neurons were filled with biocytin for subsequent morphological evaluation. Field excitatory postsynaptic potentials (fEPSP) were recorded with glass pipettes filled with 1 M NaCl placed in the stratum radiatum of the CA1 region. The stimulating electrode was placed ~500 μm away to stimulate Schaffer collaterals. Data analysis was performed offline using customized scripts written in python and Stimfit.

Isolated mitochondria

Mitochondria were isolated from cortex and hippocampus as previously described (Rhein et al., 2009). Oxygen consumption rate was measured in isolated mitochondria from cortex and hippocampus using a Seahorse Bioscience XF24Analyzer. ATP content from isolated mitochondria was determined using a bioluminescence assay (ViaLighTM HT; Cambrex Bio Science).

Behavior

Visual Performance was tested in the Morris Walter tank with a visible platform. Olfaction was checked using the cookie finding test. To score hippocampus-dependent working memory, the spontaneous alternation task was employed based on the spontaneous alternation paradigm (Ragozzino et al., 1996).

Metabolic measurements

Metabolic parameters (respiratory exchange ratio, motor activity, food and water intake) were measured using CLAMS equipment (Columbus Instruments). Mouse body composition was monitored with an EcoMRI-100 qNMR (EchoMRI Medical Systems).

Real-time PCR

RNA was isolated using commercial kits (Qiagen). Reverse-transcriptase PCR was performed using the High Capacity cDNA Reverse Transcription Kit (Invitrogen). Real-time PCR was performed using TaqMan assays (Life Technologies) on a 7900HT Real-Time PCR System (Applied Biosystems). Experimental details on these assays are specified in Supplemental Data.

Western Blot

Proteins of brain lysates were separated on 4-12% BisTris SDS-PAGE gels, blotted onto nitrocellulose membranes using the iBlot Dry Blotting System (Life Technologies), and probed with the indicated primary antibodies and isotype-matched secondary antibodies conjugated to horseradish peroxidase. Please refer to Supplemental Data for a complete list of the antibodies used. Signals were detected

using ECL (GE Healthcare). For the detection of carbonylated protein manufacturer`s instructions for the OxyBlot Protein Oxidation Detection Kit (Millipore) were followed.

ELISAs and colorimetric assays

Hormone levels were determined by ELISA on either serum or plasma and thiobarbituric acid reactive substances (TBARS) and glutathione levels were determined by colorimetric assays on brain homogenates. Blood was collected between 9 and 10 am by either tail vein or heart puncture. A complete list of all assays used is given in the Supplemental Data section.

Discussion

Dysregulated mitochondrial morphology has been implicated in a number of neurodegenerative diseases. In mouse models, the genetic knockout of essential mediators of mitochondrial fusion and fission results in early embryonic lethality, reflecting the physiological importance of properly regulated mitochondrial dynamics. While the constitutive knockout of the fission-mediating protein Drp1 is embryonically lethal between E17.5-18.5, brain-specific Drp1 ablation using a nestin promoter-driven knockout strategy is lethal around birth (Ishihara et al., 2009; Wakabayashi et al., 2009). In order to by-pass the neurodevelopmental defects due to Drp1 ablation, we employed a murine model that allowed us to ablate Drp1 *in vivo* in adult, postmitotic neurons of the forebrain. To this end, we crossed $Drp^{flx/flx}$ mice (Ishihara et al., 2009) with mice that express Cre recombinase under the control of a tamoxifen-inducible CamKIIα promoter.

Here we show that inducible Drp1 ablation in the adult mouse forebrain leads to mitochondrial aggregation in neuronal perikarya, accompanied by altered cristae morphology and lower oxygen consumption rates. While this does not immediately increase ROS formation, we do see an induction of various ER stress parameters. In particular, we find that the PERK-mediated UPR pathway is activated, and this is paralleled by a profoundly altered ER morphology.

In a model of angiotensin-II-induced chronic hypertension neuronal ER stress is associated with similar ER morphology changes reflecting that neuronal ER stress and ER shape are interconnected (Young et al., 2012). However, particularly in neurons, ER fragmentation seems to be a reversible phenomenon in response to insults not necessarily connected to ER stress (Kucharz et al., 2013), and thus it is possible that ER fragmentation *per se* is part of an general adaptive stress response. The origin of the stress in our Drp1 ablation model could also be due to mitochondrial stress caused by respiratory deficiency and associated changes in mitochondrial morphology. Alternatively, as we detect eIF2α phosphorylation prior to Bip upregulation, eIF2α could also be phosphorylated by the kinase GCN2, which gets activated during amino acid deprivation (Donnelly et al., 2013).

ER and mitochondrial network are tightly interconnected by membrane structures called mitochondria associated ER membranes (MAMs). Disruption of MAMs by mutant α-synuclein disrupts ER-mitochondria interorganellar connections, and induces Drp1-independent fragmentation of mitochondria (Guardia-Laguarta et al., 2014). Likewise, MAMs disruption by deletion of Mfn2, which interconnects ER and mitochondria, induces fragmentation of both organelles (de Brito and Scorrano, 2008). Hence, it seems very likely that profound morphological changes of one organelle inevitably impinge on the morphological integrity of the other. Mfn2-deficient cells also show UPR activation

(Muñoz et al., 2013), indicating that disruption of trans-organelle connections is sufficient to induce ER stress. It was previously shown that Drp1 also localizes to the ER where it can mediate ER morphological changes (Pitts et al., 1999; Wikstrom et al., 2013), indicating that Drp1 may directly regulate ER shape.

Neurons that have an aggregated mitochondrial phenotype show a reduction in dendritic and synaptic structures *in vitro* (reviewed in Oettinghaus et al., 2012). However, as discussed before, we could not show that in our *in vivo* model. Even though they have to cope with a decrease in oxidative phosphorylation and ER stress, Drp1 ablated pyramidal CA1 neurons have a regular dendritic tree morphology as well as regular synapse and spine numbers; in addition, no neurodegeneration is observed within 10 weeks of Drp1 ablation. In contrast, Drp1 ablated Purkinje neurons undergo neurodegeneration within 5 weeks after Drp1 ablation (Kageyama et al., 2012). As pointed out earlier, Drp1 is of particular importance for dendrite and synapse formation during neuronal development. In this context it is interesting to note that murine Purkinje neuron differentiation continues during the first three weeks after birth (Chizhikov and Millen, 2003), and that Drp1 ablation in the Purkinje cell model of Kageyama and co-workers (Kageyama et al., 2012) occurs at three weeks after birth. Therefore, one cannot exclude that Drp1 ablation overlaps with the final stages of Purkinje neuron differentiation, which might render them more susceptible to degeneration. In our model we can exclude neurodevelopmental defects caused by Drp1 ablation (tamoxifen knockout induction occurs at the age of 8 weeks), and our results show that dendritic and synaptic structures are largely unaffected by Drp1 ablation. We also find that basic functions are maintained in Drp1 ablated neurons: they generate APs, maintain their plasma membrane potential and are capable of synaptic transmission. However, numbers of presynaptic mitochondria are decreased and, when challenged by high frequency stimulation, synaptic transmission of Drp1 ablated neurons is impaired, indicating compromised neuronal function under certain conditions.

Interestingly, a similar electrophysiological phenotype with a similar mitochondrial morphology has been observed at neuromuscular junctions of Drp1 mutant flies (Verstreken et al., 2005). While this phenotype has been attributed to ATP-dependent effects on reserve pool vesicle recycling due to the lack of mitochondria at the bouton, it has been shown more recently in murine hippocampal neurons, that Drp1 is also directly involved in reserve pool vesicle formation (Li et al., 2013). Therefore, the defect in synaptic transmission in our model could well be sufficient to explain the impaired short-term spatial working memory verified during behavioral testing of our Drp1 ablated mice.

Finally, we observed a specific reduction in hippocampal volume which we believe is due to the nature of the metabolic phenotype characterized by increased circulating corticosterone. Hippocampal atrophy is a hallmark of post-traumatic stress disorder in which pathological stress hormone levels inhibit hippocampal neurogenesis (Bremner, 2006). We find that Drp1 ablation in the forebrain leads to a metabolic shift characterized by increased corticosterone levels. Corticosterone is the main glucocorticoid in rodents and has a variety of metabolic effects: it mobilizes energy stores by inducing lipolysis in fat tissue and by protein degradation in muscle, and it activates gluconeogenesis in the liver. Predominant in our mice was the effect on fatty acid metabolism. Despite normal feeding behavior, Drp1 ablated mice lost weight and had a decreased percentage of body fat. Corticosterone levels can be regulated via Fgf21 receptor binding in the hypothalamus (Bookout et al., 2013) and

accordingly, we find elevated Fgf21 plasma levels in forebrain-Drp1 ablated mice. We also find that Fgf21 mRNA expression is only increased in Drp1-ablated brain regions. Compellingly, forebrain-Drp1 ablated mice share a similar metabolic phenotype with Fgf21 overexpressing mice regarding weight development, lower glucose levels, fat tissue histology and corticosterone levels (Bookout et al., 2013; Kharitonenkov et al., 2005; Zhang et al., 2012). In contrast, however, mice overexpressing Fgf21 have extended life spans, similar to mice fed a calorie-restricted diet (Zhang et al., 2012). While we do not have a definitive explanation for this phenotypic discrepancy, the difference between those two models could potentially be attributed to functionally impaired Drp1 ablated neurons, and to a difference in the physiological distribution of Fgf21.

In our model the *CamKIIα* promoter that controls the CreERT2 transgene is also active in the paraventricular nucleus in the hypothalamus (Erdmann et al., 2007). It recently became apparent, that mitochondrial dynamics can also be involved in intraneuronal signal transduction. Changes of neuronal mitochondrial network morphology can be a specific reaction to hormone or metabolite sensing in certain highly-specialized hypothalamic neuronal subpopulations (Carneiro et al., 2012; Dietrich et al., 2013; Schneeberger et al., 2013). At this point, we cannot exclude that Drp1 ablation affects hormone or metabolite sensing in this subset of neurons, and that this also contributes to the observed metabolic phenotype. β-klotho – a substantial component of the Fgf21 receptor – expression, however, is limited to the suprachiasmatic nucleus where the Cre-regulating promoter in our model is not active (Bookout et al., 2013).

Fgf21 in our model is produced in close proximity to its hypothalamic receptor and induces corticosterone production as efficiently as systemic Fgf21 overexpression in mice which have a much higher Fgf21 levels. The physiological role of Fgf21 is perceived as a metabolic stress hormone mediating communication between stressed organ and adipose tissue, thereby inducing a beneficial metabolic shift (Luo and McKeehan, 2013). It is thus very likely, that Fgf21 production in Drp1 ablated brain is in fact beneficial to the organism and initiates a metabolic shift that supports Drp1 deficient brain regions and maintains their functionality.

Fgf21 has recently also been identified as biomarker for mitochondrial myopathies (Suomalainen et al., 2011). It therefore seems an attractive hypothesis that Fgf21 signaling may play a role in neurodegenerative diseases where defects in mitochondrial morphology and function as well as ER stress are known to occur. In fact, altered mitochondrial morphology (Wang et al., 2009) and increased levels of phosphorylated eIF2α (Chang et al., 2002) in AD brains have been reported.

In summary, we conclude that Drp1 function is pivotal in postmitotic neurons which display a remarkable resilience and are able to adapt to blocked mitochondrial fission caused by Drp1 ablation. Most surprisingly, these intraneuronal adaptations are communicated to the organism via the catabolic cytokine Fgf21 which induces a profound metabolic shift (Figures 6A and 6B). The results presented in this work provide a new perspective on the interplay of mitochondria with the endoplasmic reticulum and will hopefully inspire a new direction of research in the scientific mitochondrial community.

Author Contributions

B.O., L.M.R., M.L., J.S., C.S., A.G., L.M. performed experiments. J.B., A.E., P. D`A., P.F., C.H., J.H. and M.T. analyzed and interpreted experimental data. N.I. and K.M. generated $Drp^{flx/flx}$ mice. L.S. and S.F. conceived the project, coordinated and supervised research. B.O., L.M.R., L.S. and S.F. wrote the manuscript.

Acknowledgements

This work was supported by Swiss National Science Foundation grant 31003A_127308 and the Novartis Foundation for Medical-Biological Research. The authors would like to thank S. Berger for his helpful scientific advice, the Neuropathology Lab (Institute of Pathology, Basel University) and M. Beer, C. Lautenschlager and A. Rufle for their advice and help with experimental procedures.

References

Alexander, C., Votruba, M., Pesch, U.E., Thiselton, D.L., Mayer, S., Moore, A., Rodriguez, M., Kellner, U., Leo-Kottler, B., Auburger, G., et al. (2000). OPA1, encoding a dynamin-related GTPase, is mutated in autosomal dominant optic atrophy linked to chromosome 3q28. Nat Genet *26*, 211–215.

Badman, M.K., Pissios, P., Kennedy, A.R., Koukos, G., Flier, J.S., and Maratos-Flier, E. (2007). Hepatic Fibroblast Growth Factor 21 Is Regulated by PPARα and Is a Key Mediator of Hepatic Lipid Metabolism in Ketotic States. Cell Metab. *5*, 426–437.

Bliek, A.M. van der, Shen, Q., and Kawajiri, S. (2013). Mechanisms of Mitochondrial Fission and Fusion. Cold Spring Harb. Perspect. Biol. *5*, a011072.

Bookout, A.L., de Groot, M.H.M., Owen, B.M., Lee, S., Gautron, L., Lawrence, H.L., Ding, X., Elmquist, J.K., Takahashi, J.S., Mangelsdorf, D.J., et al. (2013). FGF21 regulates metabolism and circadian behavior by acting on the nervous system. Nat. Med. *19*, 1147–1152.

Bremner, J.D. (2006). Stress and Brain Atrophy. CNS Neurol. Disord. Drug Targets *5*, 503–512.

De Brito, O.M., and Scorrano, L. (2008). Mitofusin 2 tethers endoplasmic reticulum to mitochondria. Nature *456*, 605–610.

Bui, H.T., and Shaw, J.M. (2013). Dynamin Assembly Strategies and Adaptor Proteins in Mitochondrial Fission. Curr. Biol. *23*, R891–R899.

Carneiro, L., Allard, C., Guissard, C., Fioramonti, X., Tourrel-Cuzin, C., Bailbé, D., Barreau, C., Offer, G., Nédelec, E., Salin, B., et al. (2012). Importance of Mitochondrial Dynamin-Related Protein 1 in Hypothalamic Glucose Sensitivity in Rats. Antioxid. Redox Signal. *17*, 433–444.

Chang, R.C.C. 1, Wong, A.K.Y., Ng, H.-K., and Hugon, J. 1 2 (2002). Phosphorylation of eukaryotic initiation factor-2[alpha] (eIF2[alpha]) is associated with neuronal degeneration in Alzheimer's disease. [Miscellaneous Article]. Neuroreport Dec. 20 2002 *13*, 2429–2432.

Chen, H., Chomyn, A., and Chan, D.C. (2005). Disruption of Fusion Results in Mitochondrial Heterogeneity and Dysfunction. J. Biol. Chem. *280*, 26185–26192.

Chizhikov, V., and Millen, K.J. (2003). Development and malformations of the cerebellum in mice. Mol. Genet. Metab. *80*, 54–65.

Delettre, C., Lenaers, G., Griffoin, J.M., Gigarel, N., Lorenzo, C., Belenguer, P., Pelloquin, L., Grosgeorge, J., Turc-Carel, C., Perret, E., et al. (2000). Nuclear gene OPA1, encoding a mitochondrial dynamin-related protein, is mutated in dominant optic atrophy. Nat Genet *26*, 207–210.

Dietrich, M.O., Liu, Z.-W., and Horvath, T.L. (2013). Mitochondrial Dynamics Controlled by Mitofusins Regulate Agrp Neuronal Activity and Diet-Induced Obesity. Cell *155*, 188–199.

Donnelly, N., Gorman, A.M., Gupta, S., and Samali, A. (2013). The eIF2α kinases: their structures and functions. Cell. Mol. Life Sci. *70*, 3493–3511.

DuBoff, B., Götz, J., and Feany, M.B. (2012). Tau Promotes Neurodegeneration via DRP1 Mislocalization In Vivo. Neuron *75*, 618–632.

Erdmann, G., Schutz, G., and Berger, S. (2007). Inducible gene inactivation in neurons of the adult mouse forebrain. BMC Neurosci *8*, 63.

Estall, J.L., Ruas, J.L., Choi, C.S., Laznik, D., Badman, M., Maratos-Flier, E., Shulman, G.I., and Spiegelman, B.M. (2009). PGC-1α negatively regulates hepatic FGF21 expression by modulating the heme/Rev-Erbα axis. Proc. Natl. Acad. Sci. *106*, 22510–22515.

Friedman, J.R., and Nunnari, J. (2014). Mitochondrial form and function. Nature *505*, 335–343.

Friedman, J.R., Lackner, L.L., West, M., DiBenedetto, J.R., Nunnari, J., and Voeltz, G.K. (2011). ER tubules mark sites of mitochondrial division. Science *334*, 358–362.

Guardia-Laguarta, C., Area-Gomez, E., Rüb, C., Liu, Y., Magrané, J., Becker, D., Voos, W., Schon, E.A., and Przedborski, S. (2014). α-Synuclein Is Localized to Mitochondria-Associated ER Membranes. J. Neurosci. *34*, 249–259.

Hsuchou, H., Pan, W., and Kastin, A.J. (2007). The fasting polypeptide FGF21 can enter brain from blood. Peptides *28*, 2382–2386.

Inagaki, T., Dutchak, P., Zhao, G., Ding, X., Gautron, L., Parameswara, V., Li, Y., Goetz, R., Mohammadi, M., Esser, V., et al. (2007). Endocrine Regulation of the Fasting Response by PPARα-Mediated Induction of Fibroblast Growth Factor 21. Cell Metab. *5*, 415–425.

Ippolito, D.M., and Eroglu, C. (2010). Quantifying Synapses: an Immunocytochemistry-based Assay to Quantify Synapse Number. J. Vis. Exp.

Ishihara, N., Nomura, M., Jofuku, A., Kato, H., Suzuki, S.O., Masuda, K., Otera, H., Nakanishi, Y., Nonaka, I., Goto, Y., et al. (2009). Mitochondrial fission factor Drp1 is essential for embryonic development and synapse formation in mice. Nat Cell Biol *11*, 958–966.

Kageyama, Y., Zhang, Z., Roda, R., Fukaya, M., Wakabayashi, J., Wakabayashi, N., Kensler, T.W., Reddy, P.H., Iijima, M., and Sesaki, H. (2012). Mitochondrial division ensures the survival of postmitotic neurons by suppressing oxidative damage. J. Cell Biol. *197*, 535–551.

Kharitonenkov, A., Shiyanova, T.L., Koester, A., Ford, A.M., Micanovic, R., Galbreath, E.J., Sandusky, G.E., Hammond, L.J., Moyers, J.S., Owens, R.A., et al. (2005). FGF-21 as a novel metabolic regulator. J. Clin. Invest. *115*, 1627–1635.

Korobova, F., Ramabhadran, V., and Higgs, H.N. (2013). An Actin-Dependent Step in Mitochondrial Fission Mediated by the ER-Associated Formin INF2. Science *339*, 464–467.

Korobova, F., Gauvin, T.J., and Higgs, H.N. (2014). A Role for Myosin II in Mammalian Mitochondrial Fission. Curr. Biol. *24*, 409–414.

Koshiba, T., Detmer, S.A., Kaiser, J.T., Chen, H., McCaffery, J.M., and Chan, D.C. (2004). Structural Basis of Mitochondrial Tethering by Mitofusin Complexes. Science *305*, 858–862.

Kucharz, K., Wieloch, T., and Toresson, H. (2013). Fission and fusion of the neuronal endoplasmic reticulum. Transl. Stroke Res. *4*, 652–662.

Li, H., Alavian, K.N., Lazrove, E., Mehta, N., Jones, A., Zhang, P., Licznerski, P., Graham, M., Uo, T., Guo, J., et al. (2013). A Bcl-xL–Drp1 complex regulates synaptic vesicle membrane dynamics during endocytosis. Nat. Cell Biol. *15*, 773–785.

Luo, Y., and McKeehan, W.L. (2013). Stressed liver and muscle call on adipocytes with FGF21. Cell. Endocrinol. *4*, 194.

McLelland, G.-L., Soubannier, V., Chen, C.X., McBride, H.M., and Fon, E.A. (2014). Parkin and PINK1 function in a vesicular trafficking pathway regulating mitochondrial quality control. EMBO J.

Morris, R.L., and Hollenbeck, P.J. (1993). The regulation of bidirectional mitochondrial transport is coordinated with axonal outgrowth. J Cell Sci *104 (Pt 3)*, 917–927.

Muñoz, J.P., Ivanova, S., Sánchez-Wandelmer, J., Martínez-Cristóbal, P., Noguera, E., Sancho, A., Díaz-Ramos, A., Hernández-Alvarez, M.I., Sebastián, D., Mauvezin, C., et al. (2013). Mfn2 modulates the UPR and mitochondrial function via repression of PERK. EMBO J. *32*, 2348–2361.

Oettinghaus, B., Licci, M., Scorrano, L., and Frank, S. (2012). Less than perfect divorces: dysregulated mitochondrial fission and neurodegeneration. Acta Neuropathol *123*, 189–203.

Otera, H., Wang, C., Cleland, M.M., Setoguchi, K., Yokota, S., Youle, R.J., and Mihara, K. (2010). Mff is an essential factor for mitochondrial recruitment of Drp1 during mitochondrial fission in mammalian cells. J Cell Biol *191*, 1141–1158.

Pitts, K.R., Yoon, Y., Krueger, E.W., and McNiven, M.A. (1999). The dynamin-like protein DLP1 is essential for normal distribution and morphology of the endoplasmic reticulum and mitochondria in mammalian cells. Mol. Biol. Cell *10*, 4403–4417.

Ragozzino, M.E., Unick, K.E., and Gold, P.E. (1996). Hippocampal acetylcholine release during memory testing in rats: augmentation by glucose. Proc. Natl. Acad. Sci. U. S. A. *93*, 4693–4698.

Rhein, V., Song, X., Wiesner, A., Ittner, L.M., Baysang, G., Meier, F., Ozmen, L., Bluethmann, H., Dröse, S., Brandt, U., et al. (2009). Amyloid-β and tau synergistically impair the oxidative phosphorylation system in triple transgenic Alzheimer's disease mice. Proc. Natl. Acad. Sci. *106*, 20057–20062.

Schneeberger, M., Dietrich, M.O., Sebastián, D., Imbernón, M., Castaño, C., Garcia, A., Esteban, Y., Gonzalez-Franquesa, A., Rodríguez, I.C., Bortolozzi, A., et al. (2013). Mitofusin 2 in POMC Neurons Connects ER Stress with Leptin Resistance and Energy Imbalance. Cell *155*, 172–187.

Sheng, Z.-H. (2014). Mitochondrial trafficking and anchoring in neurons: New insight and implications. J. Cell Biol. *204*, 1087–1098.

Suomalainen, A., Elo, J.M., Pietiläinen, K.H., Hakonen, A.H., Sevastianova, K., Korpela, M., Isohanni, P., Marjavaara, S.K., Tyni, T., Kiuru-Enari, S., et al. (2011). FGF-21 as a biomarker for muscle-

manifesting mitochondrial respiratory chain deficiencies: a diagnostic study. Lancet Neurol. *10*, 806–818.

Twig, G., Elorza, A., Molina, A.J., Mohamed, H., Wikstrom, J.D., Walzer, G., Stiles, L., Haigh, S.E., Katz, S., Las, G., et al. (2008). Fission and selective fusion govern mitochondrial segregation and elimination by autophagy. Embo J *27*, 433–446.

Tyynismaa, H., Carroll, C.J., Raimundo, N., Ahola-Erkkilä, S., Wenz, T., Ruhanen, H., Guse, K., Hemminki, A., Peltola-Mjøsund, K.E., Tulkki, V., et al. (2010). Mitochondrial myopathy induces a starvation-like response. Hum. Mol. Genet. *19*, 3948–3958.

Verstreken, P., Ly, C.V., Venken, K.J., Koh, T.W., Zhou, Y., and Bellen, H.J. (2005). Synaptic mitochondria are critical for mobilization of reserve pool vesicles at *Drosophila* neuromuscular junctions. Neuron *47*, 365–378.

De Vos, K.J., Allan, V.J., Grierson, A.J., and Sheetz, M.P. (2005). Mitochondrial function and actin regulate dynamin-related protein 1-dependent mitochondrial fission. Curr Biol *15*, 678–683.

Wakabayashi, J., Zhang, Z., Wakabayashi, N., Tamura, Y., Fukaya, M., Kensler, T.W., Iijima, M., and Sesaki, H. (2009). The dynamin-related GTPase Drp1 is required for embryonic and brain development in mice. J Cell Biol *186*, 805–816.

Wang, X., Su, B., Lee, H.G., Li, X., Perry, G., Smith, M.A., and Zhu, X. (2009). Impaired balance of mitochondrial fission and fusion in Alzheimer's disease. J Neurosci *29*, 9090–9103.

Waterham, H.R., Koster, J., van Roermund, C.W., Mooyer, P.A., Wanders, R.J., and Leonard, J.V. (2007). A lethal defect of mitochondrial and peroxisomal fission. N Engl J Med *356*, 1736–1741.

Wikstrom, J.D., Israeli, T., Bachar-Wikstrom, E., Swisa, A., Ariav, Y., Waiss, M., Kaganovich, D., Dor, Y., Cerasi, E., and Leibowitz, G. (2013). AMPK Regulates ER Morphology and Function in Stressed Pancreatic β-Cells via Phosphorylation of DRP1. Mol. Endocrinol. *27*, 1706–1723.

Young, C.N., Cao, X., Guruju, M.R., Pierce, J.P., Morgan, D.A., Wang, G., Iadecola, C., Mark, A.L., and Davisson, R.L. (2012). ER stress in the brain subfornical organ mediates angiotensin-dependent hypertension. J. Clin. Invest. *122*, 3960–3964.

Zhang, Y., Xie, Y., Berglund, E.D., Coate, K.C., He, T.T., Katafuchi, T., Xiao, G., Potthoff, M.J., Wei, W., Wan, Y., et al. (2012). The starvation hormone, fibroblast growth factor-21, extends lifespan in mice. eLife *1*, e00065.

Zuchner, S., Mersiyanova, I.V., Muglia, M., Bissar-Tadmouri, N., Rochelle, J., Dadali, E.L., Zappia, M., Nelis, E., Patitucci, A., Senderek, J., et al. (2004). Mutations in the mitochondrial GTPase mitofusin 2 cause Charcot-Marie-Tooth neuropathy type 2A. Nat Genet *36*, 449–451.

Figure Legends

Figure 1 Drp1-ablated mice display a lethal metabolic phenotype

(A) 4 week-old *Drp1*$^{flx/flx}$ and *Drp1*$^{flx/flx}$ *Cre*$^{+}$ mice were injected i.p. twice daily for 5 consecutive days with 1mg of tamoxifen, and sacrificed at the indicated time after the last injection. Hippocampal lysates were separated by SDS-PAGE and immunoblotted using the indicated antibodies.

(B) Body weight of Drp1-ablated and control mice. Data represent average ±SEM of at least 4 animals.

(C) Rotarod performance of Drp1-ablated and control mice. Data represent average ±SEM of at least 8 animals.

(D) Body temperature of Drp1-ablated animals plotted as a function of days to death. Data represent average ±SEM of at least 8 animals.

(E) Kaplan Meier Plot of Drp1-ablated and control animals. Each group is represented by at least 15 animals.

(F) Drp1-ablated and control animals were exposed to a 4°C cold environment for the indicated time and body temperature was recorded. Data represent average ±SEM of at least 6 animals.

(G) Drp1-ablated and control animals were placed in an 8-arm, radial maze which they had to systematically explore. Correct alternation of arm visits was scored. Data represent average ±SEM of at least 7 animals.

The asterisks denote P-values of an unpaired, two-tailed Student`s t-test: *:P<0.05, **:P<0.01, ***:P<0.001. See also Figure S1

Figure 2 Parameters of Drp1-ablated mitochondria

(A) Coronal sections of FFPE brains of 4-week-Drp1-ablated and control mice were immunostained for cytochrome *c* oxidase subunit 1 (green) and with DAPI (blue). Images show CA1 pyramidal neurons. White scale bar represents 10 µm.

(B) Representative TEM images of mitochondria of hippocampal neurons of 4-week-Drp1-ablated and control animals. “N” indicates the nucleus and “M” indicates mitochondria. Black scale bar represents 1 µm.

(C) Smallest radial diameter of 4-week-Drp1-ablated and control mitochondria measured on TEM images. Data represent average ±SEM of at least 4 animals of which the mitochondria of at least 80 neurons were measured.

(D) Percentage of mitochondria with abnormal cristae of 4-week-Drp1-ablated and control mitochondria measured on TEM images. At least one third of the mitochondrial lumen of the counted mitochondria was devoid of cristae. Data represent average ±SEM of at least 4 animals of which at least 100 mitochondria were scored.

(E) Oxygen consumption rate of isolated, hippocampal mitochondria of 4-week-Drp1-ablated and control mice was measured with a Seahorse Bioscience XF24 Analyzer. Substances were injected at the indicated time points. Data represent average ±SEM of at least 4 animals whose hippocampi were pooled and the measurements were performed with at least 6 replicates.

(F) ATP content of isolated, hippocampal mitochondria of 4-week-Drp1-ablated and control mice was measured with a bioluminescence assay. Data represent average ±SEM of at least 4 animals whose hippocampi were pooled and the measurements were performed with at least 8 replicates.

(G) Oxidative stress levels represented by DHR and MitoSox fluorescence in hippocampal tissue homogenate of 4-week-Drp1-ablated and control mice. Data represent average ±SEM of at least 4 animals whose hippocampi were pooled and the measurements were performed with at least 4 replicates.

(H+I) Ratio of oxidized to reduced glutathione and thiobarbituric acid reactive substance (TBARS) levels (representing lipid peroxidation) in hippocampal lysates of 4-week-Drp1-ablated and control mice were measured by commercial colorimetric kits. Data represent average ±SEM of at least 6 animals.

(J) Hippocampal lysates of 4-week-Drp1-ablated and control mice were separated by SDS-PAGE and immunoblotted using an antibody for carbonylated protein of a commercial oxyblot kit. Data represent average ±SEM of at least 4 animals.

The asterisks denote P-values of an unpaired, two-tailed Student`s t-test: *:P<0.05, **:P<0.01, ***:P<0.001. See also Figure S2

Figure 3 Drp1 ablation induces morphological ER alterations and ER stress

(A) Representative TEM images of the rER of hippocampal neurons of 4-week-Drp1-ablated and control animals. Black scale bar represents 1 µm.

(B) rER circularity (4π x Area/ $Perimeter^2$, a value of 1 represents a full circle) of rER structures of Drp1-ablated and control hippocampal neurons as measured on TEM images. Data represent average ±SEM of at least 4 animals of which rER structures of at least 80 neurons were measured.

(C) Representative Western blot of Drp1-ablated and control hippocampal lysates which were separated by SDS-PAGE and immunoblotted using the indicated antibodies.

(D) Quantification of phosphorylated eIF2α band intensity normalized to total eIF2α. Data represent average ±SEM of at least 4 animals.

(E+F) Quantification of ATF4 and Bip band intensity normalized to actin. Data represent average ±SEM of at least 4 animals.

(G) RNA was isolated from different mouse brain regions at indicated time points after tamoxifen-induced Drp1 ablation. RNA was retrotranscribed into cDNA and a qRT-PCR performed using the TaqMan system. Chop mRNA ct values were normalized against 18S rRNA ct values. Data represent average ±SEM of at least 4 animals.

The asterisks denote P-values of an unpaired, two-tailed Student`s t-test: *:P<0.05, **:P<0.01, ***:P<0.001. See also Figure S3

Figure 4 Drp1 ablation does not lead to neurodegeneration but leads to impaired synaptic transmission

(A) Hippocampal slice cultures of 4-week-Drp1-ablated and control animals were prepared and pyramidal CA1 neurons were patch clamped and resting membrane potential was measured. Data represent average ±SEM of at least 7 neurons.

(B+C) One-second-long current steps of increasing amplitude were injected to induce action potentials and maximal amplitude and half width were plotted. Data represent average ±SEM of at least 7 neurons.

(D) Synapses in TEM images of 4-week-Drp1-ablated and control hippocampi were screened for the presence of presynaptic mitochondria. Data represent average ±SEM of at least 4 animals of which at least 100 synapses were screened.

(E) Representative field excitatory postsynaptic potentials (fEPSP) before and after 10s of 10Hz stimulation. fEPSPs were recorded in the CA1 stratum radiatum in 4-week-Drp1-ablated and control hippocampal slice cultures after stimulating the Schaffer collaterals.

(F) Mean slope of fEPSPs during the time course of a 10s 10Hz stimulation. Data represent average ±SEM of at least 6 neurons.

(G) Maximal mean fEPSP slope after 10s 10Hz stimulation. Data represent average ±SEM of at least 6 neurons.

(H) Representative camera lucida drawing of Golgi stained 10-week-Drp1-ablated and control CA1 pyramidal neurons.

(I) Scholl – analysis of Golgi stained 10-week-Drp1-ablated and control CA1 pyramidal neurons. Each data point represents the number of intersections of the dendritic tree with concentric rings that were drawn with increasing diameter around the soma. Data represent average ±SEM of at least 100 neurons.

(J) Number of spines per µm on dendrites of the apical dendritic tree of CA1 pyramidal neurons.

(K) Coronal cross sections of 10-week-Drp1-ablated and control brains were stained with the presynaptic marker VGLUT2 (green) and the postsynaptic marker PSD95 (red). A 150 µm x 150 µm x 5 µm confocal image stack in the CA1 stratum radiatum was recorded and the number of overlapping punctae was determined. Data represent average ±SEM of at least 5 animals of which 4 stacks each were recorded. White scale bar represents 5 µm.

(L+M) Hippocampal Volume was recorded on H&E-stained, serial, coronal cross sections of 8-week-Drp1-ablated animals applying the Cavalieri principle. For cortical and midbrain volume only sections representing the coordinates bregma 1.1 mm – (-1.2 mm) were considered. Data represent average ±SEM of at least 5 animals.

The asterisks denote P-values of an unpaired, two-tailed Student`s t-test: *:P<0.05, **:P<0.01, ***:P<0.001. See also Figure S4

Figure 5 Drp1 ablation in the forebrain induces metabolic shift transmitted by Fgf21

(A) 4-week-Drp1-ablated and control animals were housed individually in metabolic cages and their respiratory gas exchange was monitored. Data represent average ±SEM of at least 8 animals.

(B) Body fat composition of 4-week-Drp1-ablated and control animals was measured via EchoMRI. Data represent average ±SEM of at least 8 animals.

(C+D) H&E staining of FFPE white and brown adipose tissue sections of mice was performed 10 weeks after Drp1 ablation. White adipose tissue was blindedly classified by three operators by cell size and brown adipose tissue by vacuole size. Chi-square test for trend analysis revealed a significant difference in frequency distribution for white (P:0.0075) and brown adipose tissue (P:0.0249) when comparing Drp1-ablated and control mice

(E) Food intake of Drp1-ablated and control animals was monitored. Data represent average ±SEM of at least 4 animals.

(F+G) T4 and corticosterone serum levels in tail vein blood of Drp1-ablated and control animals were determined by ELISA. Data represent average ±SEM of at least 4 animals.

(H) FGF21 plasma levels in cardiac blood of Drp1-ablated and control animals were determined by ELISA. Data represent average ±SEM of at least 3 animals.

(I) RNA was isolated from different mouse brain regions at indicated time points after tamoxifen-induced Drp1 ablation. RNA was retrotranscribed into cDNA and a qRT-PCR performed using the TaqMan system. FGF21 mRNA ct values were normalised against 18S rRNA ct values. Data represent average ±SEM of at least 4 animals.

The asterisks denote P-values of an unpaired, two-tailed Student`s t-test: *:P<0.05, **:P<0.01, ***:P<0.001. See also Figure S5

Figure 6 Graphic Abstract

(A) Drp1 ablation in the brain leads to mitochondrial and ER stress and morphological changes in these organelles which leads to Fgf21 induction via unfolded protein response pathway signaling via receptor binding in the hypothalamus Fgf21 produced in the brain induces corticosterone in the suprarenal glands.

(B) Chronically elevated Fgf21 and corticosterone levels induce various effects on peripheral metabolic organs, resulting in a systemic catabolic shift.

Figures

Figure 1 Drp1-ablated mice display a lethal metabolic phenotype

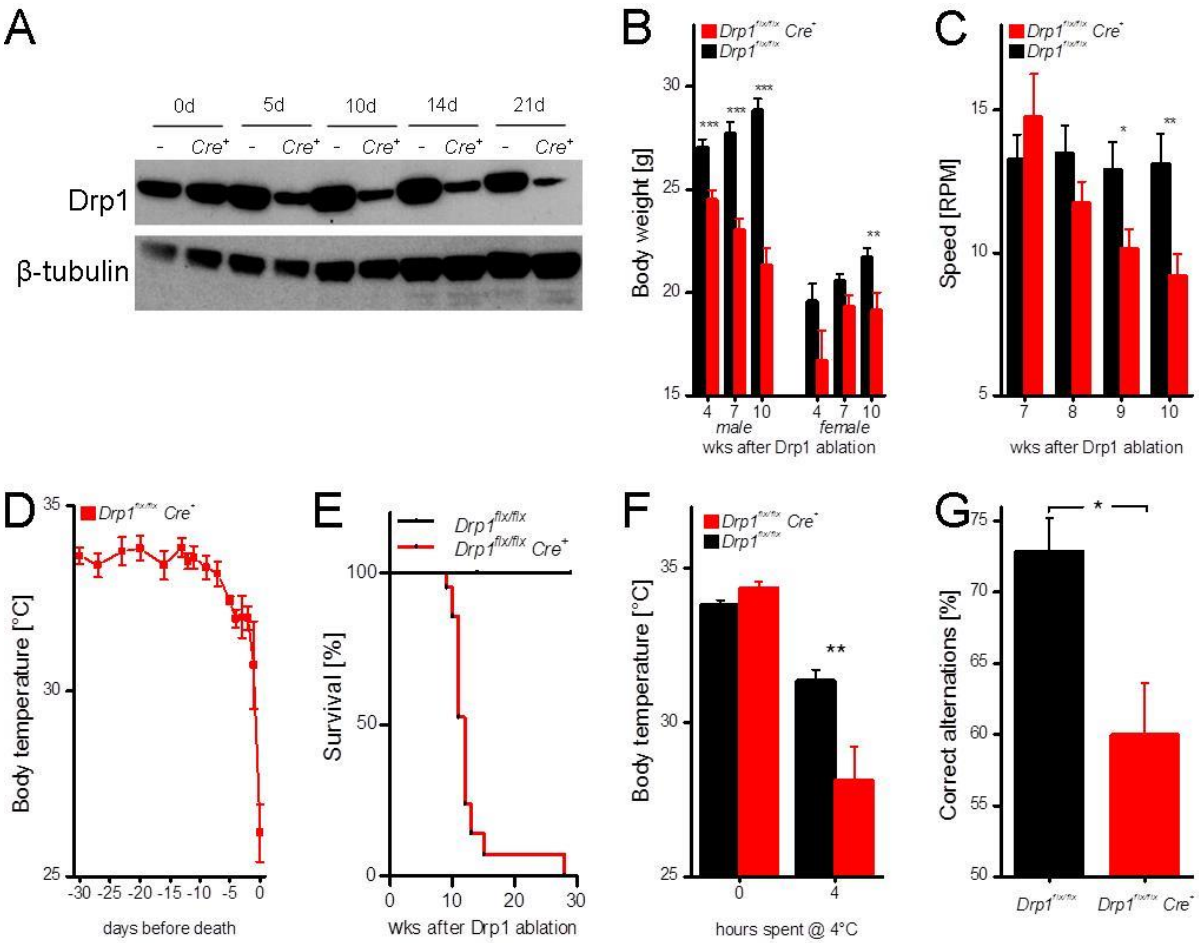

Figure 2 Parameters of Drp1-ablated mitochondria

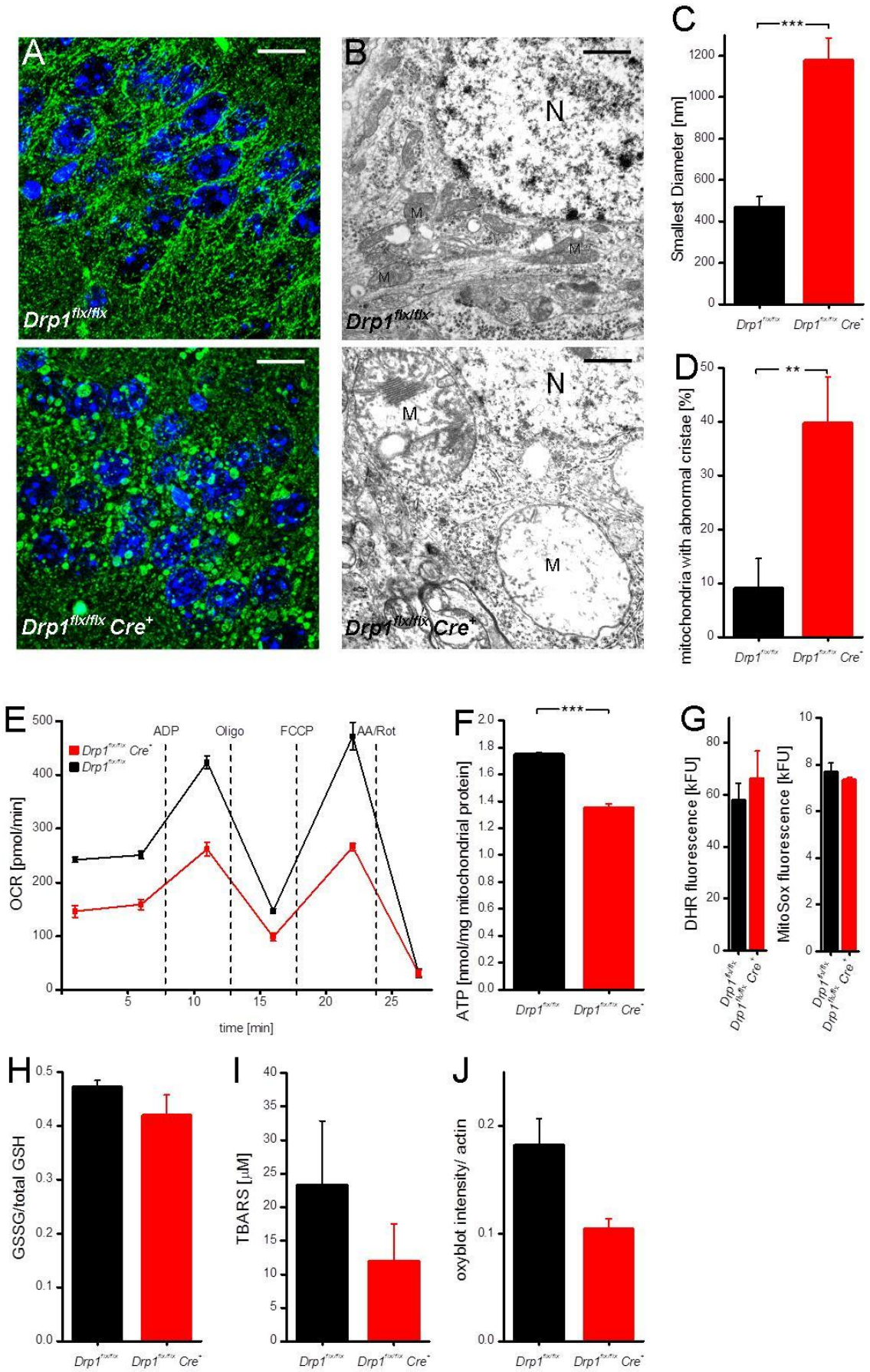

Figure 3 Drp1 ablation induces morphological ER alterations and ER stress

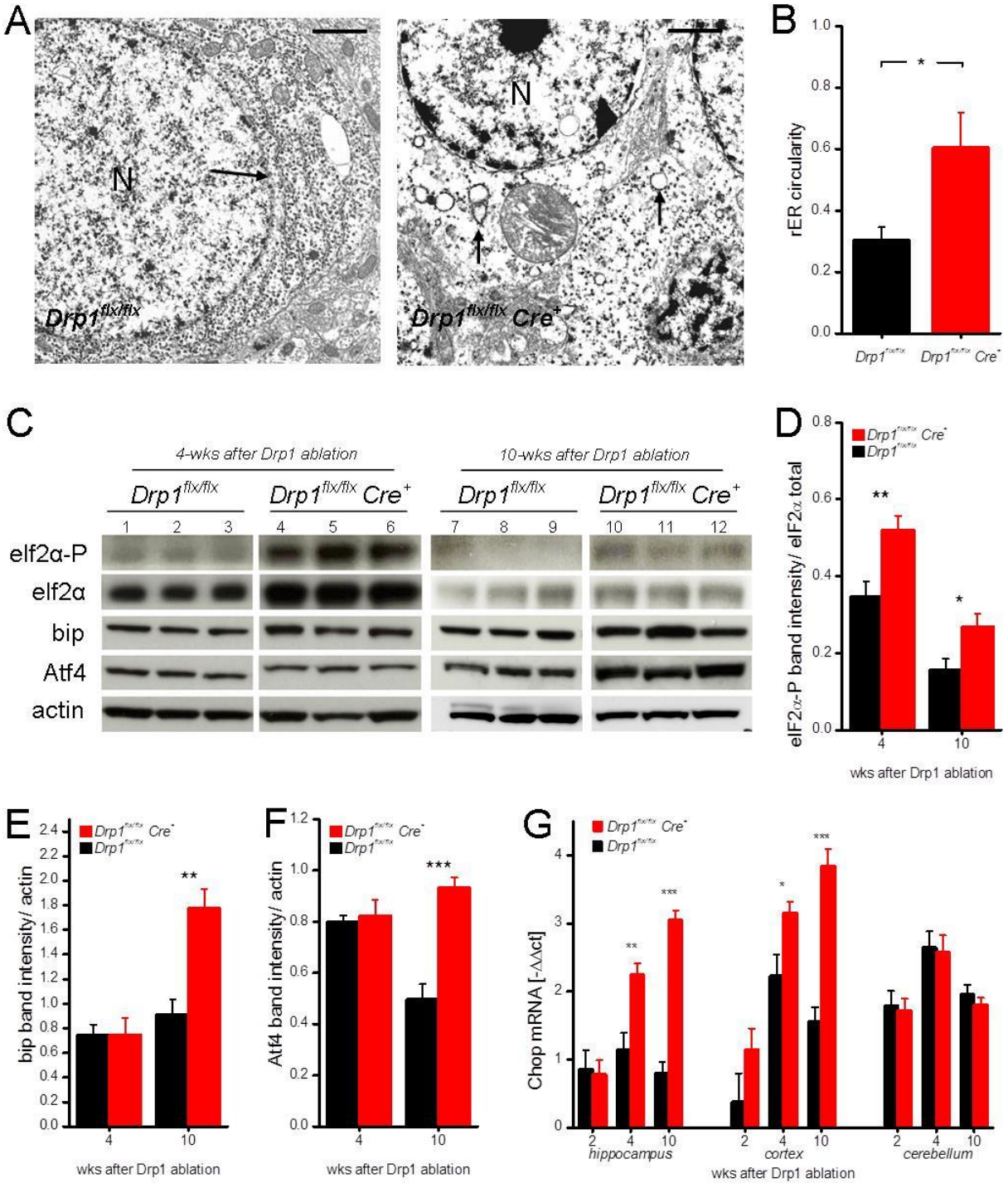

Figure 4 Drp1 ablation does not lead to neurodegeneration but leads to impaired synaptic transmission

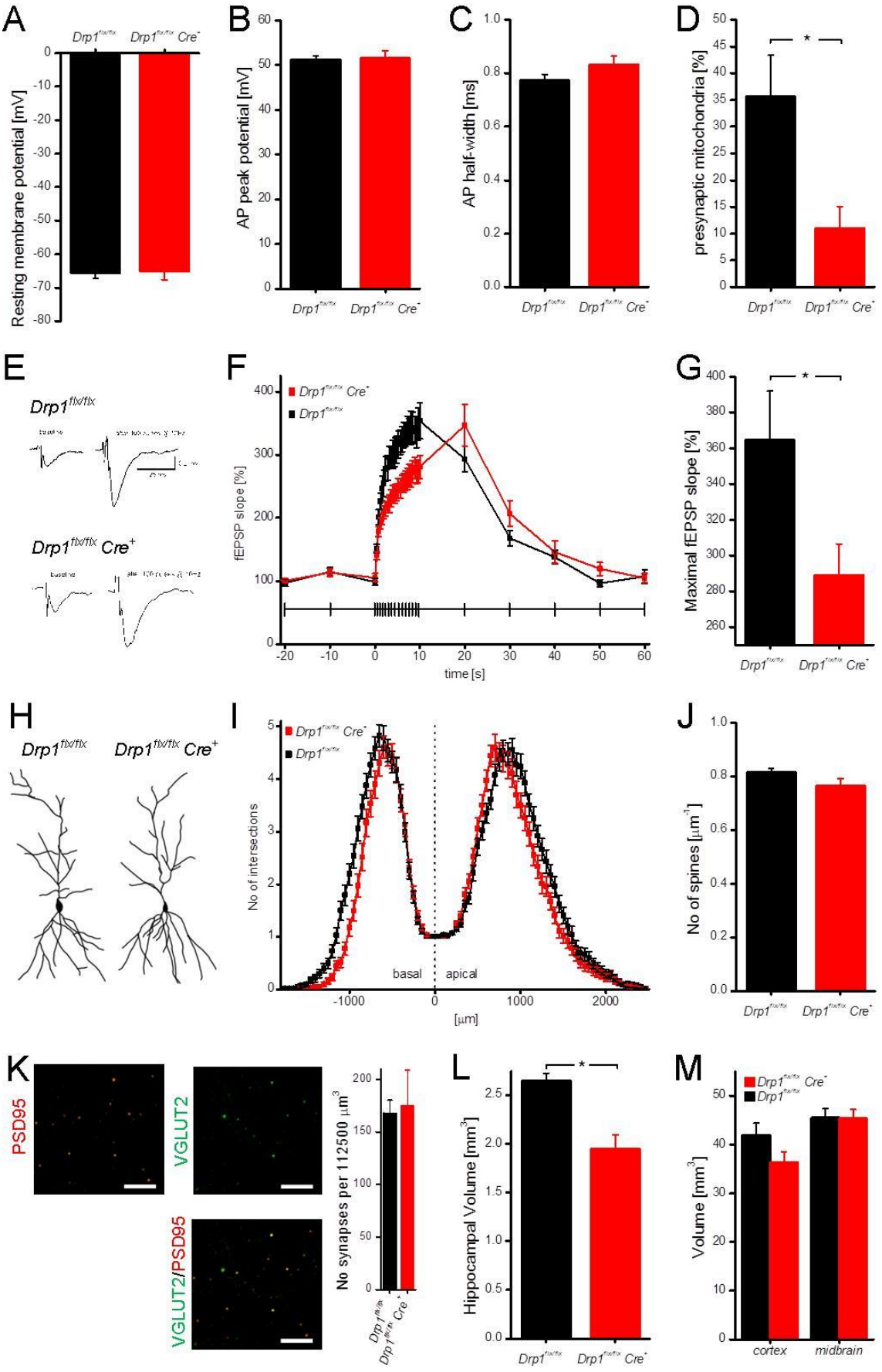

Figure 5 Drp1 ablation in the forebrain induces metabolic shift transmitted by Fgf21

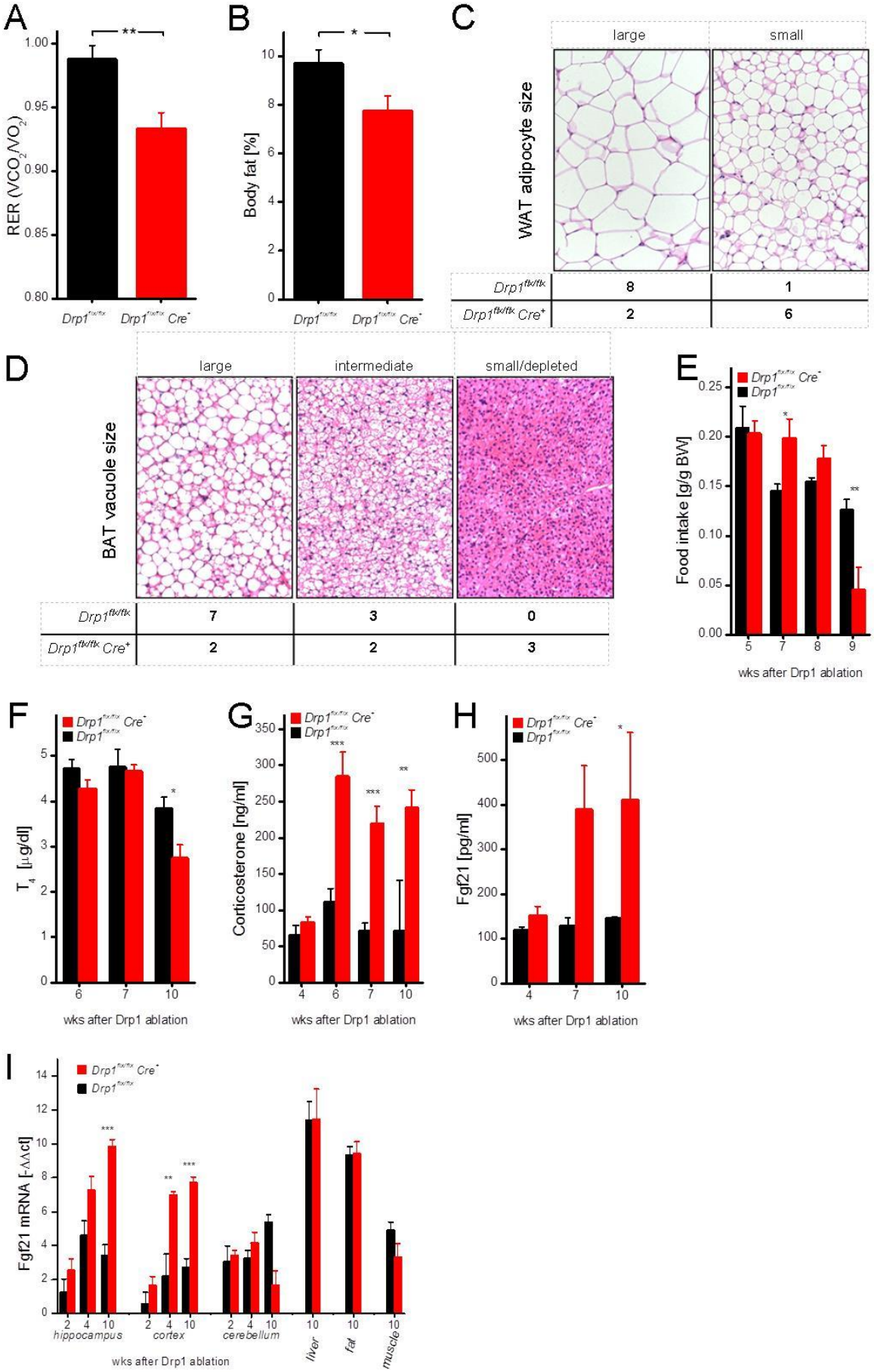

Figure 6 Graphic Abstract

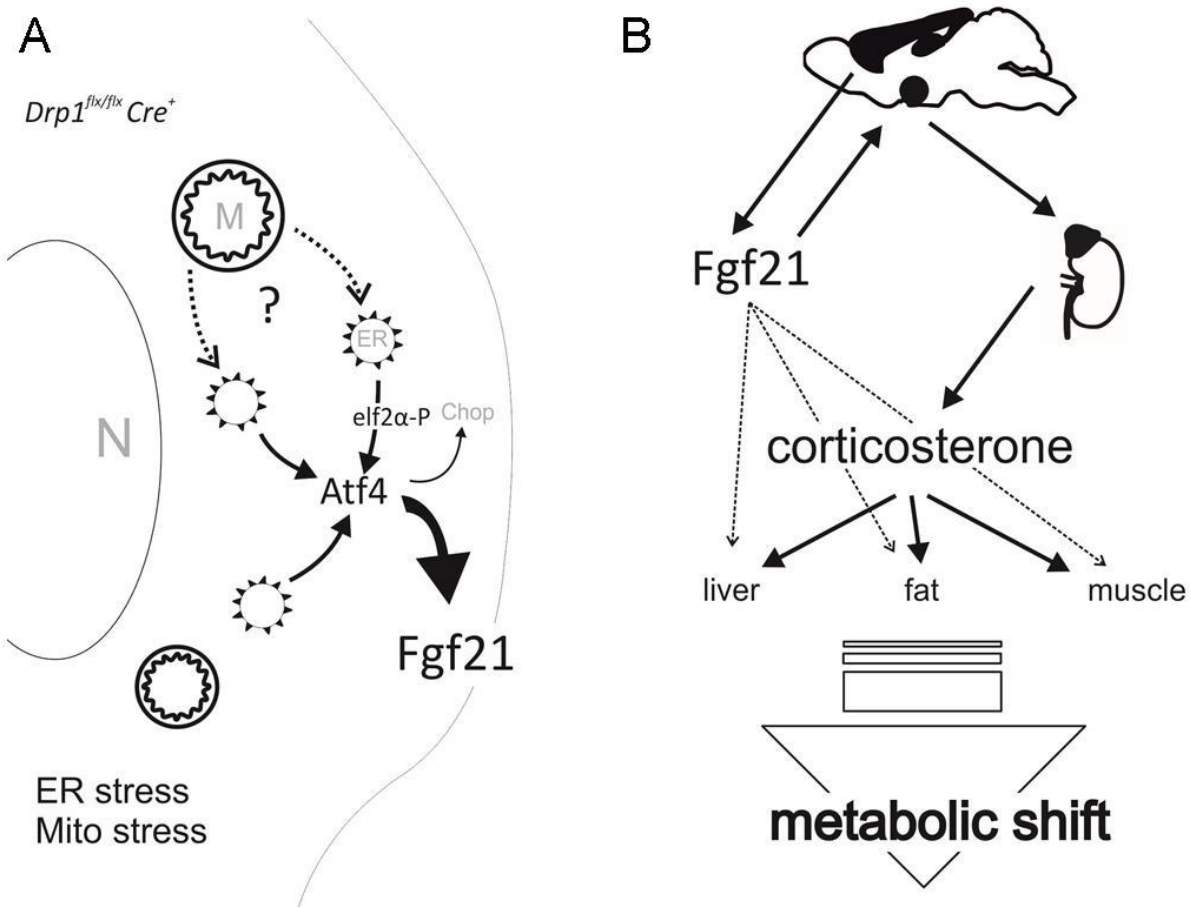

Supplemental Information

Supplemental Experimental Procedures

Mice

Drp1$^{flx/flx}$ mice were a gift from Katsujoshi Mihara (Ishihara et al., 2009). The *CamKIIalpha CreERT2* mouse was purchased from the European Mouse Mutant Archive (EMMA strain 02125) (Erdmann et al., 2007). At 8 weeks of age mice were injected i.p. with 1 mg Tamoxifen (10 mg/ml Tamoxifen, Sigma T5648 in 9:1 sunflower seed oil to ethanol) twice per day on five consecutive days to induce Drp1 locus recombination. Experiments were performed in compliance with protocols approved by the local Basel Committee for Animal Care and Animal Use. Mice were terminally anaesthetized with an intraperitoneal injection of 10 mg/kg ketamine and 20 mg/kg xylazil followed by 250 mg/kg tiopenthal.

Behavior

For all of the following behavioral tests mice were brought into a separated testing room with dim illumination and left to habituate for 2 h before any procedure began. Visual Performance was tested in the Morris Walter tank with a visible platform. Each mouse was placed on a flagged squared platform (15 cm wide) located in the centre of the South-east quadrant into the water-tank (150 cm diameter) and let to observe the environment for two minutes. The tank was filled with water kept at 28°C. Thirty minutes later each mouse was released from four different starting points: south, west, north and east in that order. Latencies to reach the visible platform were scored. Cut-off time was two minutes. Olfaction was tested using the cookie finding test. Each mouse was temporary taken away from his home cage and a food pellet of 0.8-1.0 grams was buried under the sawdust layer, invisible to the naked eye. The position of the pellet was at the centre of the southern part of the cage, away from corners. Then each mouse was returned to his home cage and the latency to find the pellet was scored. To score hippocampus-dependent working memory the spontaneous alternation task was employed based on the spontaneous alternation paradigm (Ragozzino et al., 1996). A standard 8-arm, radial maze for mice was employed. Four out of the eight arms were kept open only, in the way to form a cross. Each mouse was singly released in the central hub and left free to explore for 10 minutes. Arm-entry number and sequence were scored (arms were named as A, B, C and D). A correct alternation was considered when mice made one-repetition only over five entries (A, B, D, C, D is correct while A, B, C, B, A is not).

Histology and immunohistochemistry

Anaesthetized mice were killed by transcardial perfusion with 20 ml of cold PBS followed by 20 ml of 4 % Formaldehyde in PBS ph 7.4. Brain and interscapular white and brown adipose tissue were dissected and post-fixed overnight. Following paraffin embedding 10-μm, coronal cross sections were prepared. A haematoxylin and eosin staining (H&E) was performed for the morphological analysis of the adipose tissue. Brain sections were deparaffinized and immersed in 95°C citrate buffer ph 6 for 15 min. Sections were blocked with 15% normal goat serum (NGS) for 1h and subsequently incubated with cytochrome *c* oxidase subunit1a antibody (abcam ab14705, 1:200) at 4°C overnight and mouse

AF488 (Molecular Probes A11029; 1:1000). Slides were mounted with Prolong Gold antifade mounting solution containing DAPI (Life Technologies). Cross sections representing the coordinates bregma (-1.34) – (-2.46) were selected and z-stacks were recorded with an inverted Zeiss Axiovert 200M LSM 510 Meta confocal microscope with a 100x/1.4 Oil DIC objective using Enterprise 405 nm and Argon 488 lasers. Z-stacks were projected onto a single plane using ImageJ.

Golgi staining was performed on PBS-perfused, unfixed brains using a commercial kit (Rapid GolgiStain Kit; FD Neurotechnologies; PK401). Camera lucida drawings were analysed with the Sholl Analysis tool of ImageJ.

Synapse number was quantified as described in (Ippolito and Eroglu, 2010), shortly we stained coronal cross sections of mouse brains with a presynaptic marker VGLUT2 (Millipore; AB2251; 1:1000) and a postsynaptic marker PSD95 (Novex; 51-6900; 1:100). The corresponding secondary antibodies were anti guinea pig AF488 (Molecular Probes; A-11073; 1:1000) and anti-rabbit AF594 (Molecular Probes; A-11012; 1:1000): The number of colocalizing punctae within a 150 µm x 150 µm x 5 µm confocal image stack (for microscope configuration see above) was analyzed using ImageJ. Four of these image stacks were recorded per animal within the coordinates bregma (-1.34) - -(2.46). An imaginary vertical line was drawn along the open end of the arrow shaped structure of the granule nuclei of the dentate gyrus towards the stratum radiatum where a z-stack was recorded.

Hippocampal volume was calculated from H&E stained 100 µm-spaced, serial, coronal cross sections applying the Cavalieri principle. For the Cortical and the midbrain volume we only considered the sections representing coordinates bregma 1.1 – (-1.2) using the corpus callosum as a reference.

Transmission Electron Microscopy

Anaesthetized mice were killed by transcardial perfusion with 20 ml of cold PBS followed by 20 ml of 1 % Gluteraldehyde in 0.1 M Cacodylate buffer ph 7.4. The hippocampus was dissected and post fixed for 1 week. Hippocampi were then stained with OsO_4 and embedded in epoxide resin. Semithin sections were prepared to localize the nuclear bands of the hippocampus of which ultrathin sections were prepared that were collected onto a mesh grid and imaged with a Phillips CM100 transmission electron microscope. Morphological analysis of ER and mitochondria was performed using ImageJ. The minimal radial diameter of a mitochondrion was calculated using the rotating calipers algorithm (http://doube.org/files/RotatingCalipers.txt) and the roundness of rER structures was calculated using the standard shape descriptors of ImageJ. The mitochondria and ER structures in the perikarya of in average 80 hippocampal neurons were analyzed per animal. Criteria for the identification of synapses were a postsynaptic electron dense area and presynaptic vesicles.

Electrophysiology

Twelve-week-old *Drp1*$^{flx/flx}$ *Cre*$^{+}$ and control mice (4 weeks after tamoxifen treatment) were anaesthetized with isoflurane (4% in O_2, Vapor, Draeger) and killed by decapitation. In order to increase cell viability, animals were exposed to oxygen-enriched atmosphere for 10 min prior to decapitation. Transverse 350 to 400-µm-thick hippocampal brain slices were cut using a Leica VT1200 Vibratome (Bischofberger et al., 2006; Geiger et al., 2002). For cutting and storage, a sucrose-based solution was used, containing (in mM): 87 NaCl, 25 $NaHCO_3$, 2.5 KCl, 1.25 NaH_2PO_4, 75 sucrose, 0.5

$CaCl_2$, 7 $MgCl_2$ and 10 glucose (equilibrated with 95% O_2/ 5% CO_2). Slices were kept at 35°C for 30 min after slicing and subsequently stored at room temperature until experiments were performed. During electrophysiological recordings, slices were continuously superfused with artificial cerebrospinal fluid (ACSF) containing (in mM: 125 NaCl, 25 $NaHCO_3$, 25 glucose, 3 KCl, 1 NaH_2PO_4, 2 $CaCl_2$, and 1 $MgCl_2$; equilibrated with 95% O_2/ 5% CO_2) at 32-33 ºC.

Whole-cell, patch-clamp recordings were obtained from hippocampal CA1 pyramidal neurons using patch pipettes (resistance of 3-6 MΩ) pulled from borosilicate glass tubing with 2.0 mm outer diameter and 0.5 mm wall thickness (Hilgenberg, Malsfeld, Germany; Flaming-Brown P-97 puller, Sutter Instruments, Novato, USA). Patch-pipettes were filled with a solution containing (in mM): 135 K gluconate, 20 KCl, 10 HEPES, 2 $MgCl_2$, 2 Na_2ATP, 0.3 NaGTP, 0.1 EGTA, and 0.2% biocytin adjusted to pH 7.3-7.4 with NaOH. To evaluate cellular properties and excitability 1-s-long current steps of increasing amplitude (steps of 25 pA) were injected.

Field excitatory postsynaptic potentials (fEPSP) were recorded with glass pipettes filled with 1 M NaCl (resistance of 3-5 MΩ) placed in the stratum radiatum of the CA1 region. The bipolar tungsten stimulating electrode (Stereotrodes, World Precision Instruments, Inc.) was placed ~500 µm away to stimulate the Schaffer collaterals (SC; 200-400 µA). To restrict the fEPSP to AMPA receptor-mediated currents, 25 µM of the NMDA receptor antagonist AP5 (D-(-)-2-amino-5-phosphonopentanoic acid) were added to the bath solution. SC inputs were evoked at 0.1 Hz. To challenge synaptic transmission 100 stimuli were applied either at 10 or at 100 Hz.

Voltage signals were measured with a Multiclamp 700A amplifier (Molecular Devices, Palo Alto, CA, USA), low-pass filtered with cut-off frequencies of 10 kHz for whole-cell patch-clamp and 2 kHz for fEPSP recordings, respectively, and digitized at 20 kHz using a CED Power 1401 interface (Cambridge Electronic Design, Cambridge, UK). Bridge balance was used to compensate the series resistance (R_S = 10-30 MΩ) in current clamp recordings. Data acquisition was controlled by custom software (FPulse, U. Fröbe, Physiological Institute Freiburg) running under IGOR Pro 6.31 (WaveMetrics, Lake Oswego, Oregon).

During the recording, neurons were filled with biocytin. At the end of the recording, the pipette was carefully removed from the neuron to avoid rupture of the membrane. Following the successful pipette removal, indicated by the formation of an outside-out patch, the brain slice was stored another 30 min in ACSF to allow for sufficient time for the diffusion of biocytin. Brain slices were fixed overnight in 4% paraformaldehyde and then incubated overnight with 0.3% triton X-100 and avidin, Fluorescein conjugate (1:500; Invitrogen). After washing, the slices were embedded in Prolong Gold (Invitrogen). Fluorescence labeling was analyzed with a confocal laser scanning microscope (LSM 700, Zeiss).

Data analysis was performed offline using customized scripts written in python and the open source analysis software Stimfit (http://code.google.com/p/stimfit C. Schmidt-Hieber, University College London). To evaluate the facilitation of fEPSPs during high-frequency stimulation, four subsequent waveforms were averaged and the strength of synaptic transmission was measured as the fEPSP slope. A linear fit to the fEPSP was calculated for a window of 1-ms length sliding over the ascending phase of the fEPSP after the initial fiber volley and the maximal value was recorded.

Preparation of isolated mitochondria.

Cortex and hippocampus were quickly dissected on ice and washed in an ice-cold buffer (210 mM mannitol, 70mM sucrose, 10 mM HEPES, 1 mM EDTA, 0.45% BSA, 0.5 mM DTT, and Complete Protease Inhibitor mixture tablets (RocheDiagnostics). The tissue samples were homogenized in 2 ml of buffer with a glass homogenizer (10–15 strokes, 400 rpm). 10 µl of the suspension was used for protein determination. All cortex and hippocampus homogenate samples were normalized on 1.5 mg/ml before ROS measurement.

Mitochondria were isolated from cortex and hippocampus as previously described (Rhein et al., 2009). Briefly, mice were killed by decapitation, and cortex and hippocampus were quickly dissected on ice and washed in an ice cold buffer (210 mM mannitol, 70mM sucrose, 10 mM Hepes, 1 mM EDTA, 0.45 % BSA, 0.5 mM DTT, and Complete Protease Inhibitor mixture tablets (RocheDiagnostics). The tissue sample was homogenized in 2 ml of buffer with a glass homogenizer (10–15 strokes, 400 rpm), and the resulting homogenate was centrifuged at 1400 x *g* for 7 min at 4 °C to remove nuclei and tissue particles. The low-speed centrifugation step was repeated once with the supernatant. Then, the supernatant fraction was centrifuged at 10000 x *g* for 5 min at 4 °C to pellet mitochondria. The resulting pellet was resuspended in 1 ml of ice cold buffer and centrifuged again at 1400 x *g* for 3 min at 4 °C. Finally, the mitochondria-enriched supernatant was centrifuged at 10000 x *g* for 5 min at 4 °C to obtain a mitochondrial fraction. This fraction was resuspended in 300 ul of PBS and kept at 4 °C until use. 10µl of the suspension were used for protein determination. All isolated mitochondria samples were normalized on 1mg/ml of protein before ATP content determination and 5ug / 50 µl before oxygen consumption rate (OCR) measurements.

ATP measurement

ATP content from isolated mitochondria was determined using a bioluminescence assay (ViaLighTM HT; Cambrex Bio Science) according to the manufacturer's instructions. The enzyme luciferase, which catalyzes the formation of light from ATP and luciferin was used. The emitted light is linearly related to the ATP concentration and is measured using the luminometer VictorX5 (Perkin Elmer).

Oxygen consumption rate measurements

Oxygen consumption rate was measured in isolated mitochondria from cortex and hippocampus using a Seahorse Bioscience XF24Analyzer, following the recommendation of the company. Briefly, mitochondria were first diluted 10X in cold 1X Mitochondrial Assay Solution (MAS; 70 mM sucrose, 220 mM mannitol, 10 mM KH_2PO_4,5 mM $MgCl_2$, 2 mM HEPES, 1 mM EGTA and 0.2% (w/v) fatty acid-free BSA, pH 7.2 at 37°C) containing 10 mM Succinate, 2 mM Malate and 10 mM Pyruvate. 50 µL of mitochondrial suspension was delivered to each well of a XF Cell Culture microplate (except for background correction wells) and centrifuged at 2000 x g for 20 minutes at 4°C. After centrifugation, 450 µL of pre-warmed (37°C) 1X MAS + substrate was added to each well and the plate was incubated 5 min at 37°C in a CO_2-free incubator prior to the experiment. The plate containing isolated mitochondria was placed in a XF24 Analyzer and oxygen consumption rate was evaluated under different respiratory states. The experiment started in a coupled state in the presence of succinate, pyruvate and malate. State 3 was initiated following the injection of 55 µl of 40 mM ADP (4 mM final).

State 4o was induced with the addition of 62 µl of 25 µg/ml oligomycin (2.5 µg/ml final) and State 3 uncoupled (3u) was assessed after injection of 68 µl 40 µM FCCP (4 µM final) before shutting down mitochondrial respiration by injecting 76 µl of 40 µM and 20 µM (4 µM and 2 µM final) of antimycin A and rotenone respectively.

Metabolic measurements

Metabolic parameters were measured by CLAMS (Columbus Instruments). After a 48 h acclimatization 4-week-Drp1-ablated and control mice were monitored for 72 h. Mouse body compostion was monitored with an EcoMRI-100 qNMR (EchoMRI Medical Systems). For the i.p. glucose tolerance test mice (10 weeks post tamoxifen injection) were starved overnight and 2g/kg glucose was injected i.p. Blood glucose was monitored in tail vein blood using Accu Check Aviva test strips (Roche). For the insulin tolerance test we injected 7.5 U/kg insulin (Actrapid Human Insulin A10AB01 100U/ml) i.p. and monitored tail vein blood glucose concentration accordingly.

Real-time PCR

Organs were collected from PBS perfused mice and RNA was isolated using Qiagen kits (RNeasy Lipid Tissue Kit for adipose tissue; 74804, RNeasy Fibrous Tissue kit for muscle; 74704 and RNeasy kit for other organs 74104). Reverse-Transcriptase PCR was performed using the High Capacity cDNA Reverse Transcription Kit (Invitrogen; 4368814). Real-time PCR was performed using TaqMan assays (Life Technologies) on a 7900HT Real-Time PCR System (Applied Biosystems). The following TaqMan assays were used: FGF21 (Mm00840165_g1), 18S (Mm03928990_g1), Chop (Mm01135937_g1), PPARα (m00440939_m1), PPARδ (Mm00803184_m1), PGC-1α (Mm01208835_m1), PGC-1β (Mm00504720_m1), ATF4 (Mm00515325_g1), Akt1 (Mm01331626_m1), PI3K (Mm00803160_m1). Cross-threshold (Ct) values were normalized to 18S Ct values.

Western Blot

Brains of perfused mice were dissected and lysates were prepared in RIPA Buffer (150mM NaCl; 1 % IGEPAL; 0.5 % sodium deoxycholate acid; 0.1 % sodium dodecyl sulfate; 50 mM Tris pH8) containing a protease inhibitor cocktail (Sigma; P83450) and phosphatase inhibitor (Roche; 04906837001). Brain extracts were run on 4-12 % BisTris SDS-PAGE gels and blotted onto nitrocellulose membranes using the iBlot Dry Blotting System (Life Technologies). Membranes were probed with the following antibodies: Drp1 (BD Biosciences, 611112), ATF4 (Santa Cruz, sc-200), Bip (BD Biosciences, 610978), Akt1 (Cell Signaling, 9272), Akt1-P S473 (Cell Signaling, 4060), actin (Thermo Scientific; MA1-91399). The secondary antibodies were anti mouse-HRP (GE Healthcare; NA931) and anti rabbit (GE Healthcare; NA934) and for signal detection Amersham ECL Prime Western Blotting Detection Reagent (GE Healthcare; RPN2232) was used in conjunction with Amersham Hyperfilm (GE Healthcare; 28-9068-44). For the detection of carbonylated protein the guidelines of the OxyBlot Protein Oxidation Detection Kit (Millipore; S7150) were followed.

ELISAs and colorimetric assays

Blood was collected between 9 and 10 am and hormone levels were detected by ELISA from either serum: Corticosterone (Arbor Assays; K014-H1), T4 (Callbiotech; t4044T-100), or plasma: Leptin (BioVendor, RD291001200R), Ghrelin (Millipore, EZRGRA-90K), FGF21 (BioVendor; RD291108200R).

Brains were dissected from PBS perfused mice and homogenates were prepared according to the protocols of the following kits: TBARS (Cayman Chemicals; 10009055-96), Glutathione (Cayman Chemicals; 703002-96)

Fluorescent ROS probes

The formation of mitochondrial reactive oxygen species (ROS) and superoxide anion radicals in cortical and hippocampal homogenates was measured using the fluorescent probes dihydrorhodamine-123 (DHR) (Sigma) and the Red Mitochondrial Superoxide Indicator MitoSOX (Molecular probes) respectively. Sample homogenates were loaded for 15 min with 10 µM DHR or 75 min with 5 µM MitoSOX at room temperature in the dark on an orbital shaker. After washing twice with HBSS (Sigma), DHR, which is oxidized to cationic rhodamine 123 localized within the mitochondria and exhibits a green fluorescence, was detected using the VictorX5 multilabel reader (PerkinElmer) at Ex: 485 nm / Em: 535 nm. MitoSOX, which is specifically oxidized by mitochondrial superoxide and exhibits a red fluorescence, was detected at Ex: 535 nm / Em: 595 nm. The intensity of fluorescence was proportional to the level of reactive oxygen species.

Supplemental References

Bischofberger, J., Engel, D., Li, L., Geiger, J.R., and Jonas, P. (2006). Patch-clamp recording from mossy fiber terminals in hippocampal slices. Nat. Protoc. *1*, 2075–2081.

Erdmann, G., Schutz, G., and Berger, S. (2007). Inducible gene inactivation in neurons of the adult mouse forebrain. BMC Neurosci *8*, 63.

Geiger, J.R.P., Bischofberger, J., Vida, I., Fröbe, U., Pfitzinger, S., Weber, H.J., Haverkampf, K., and Jonas, P. (2002). Patch-clamp recording in brain slices with improved slicer technology. Pflüg. Arch. Eur. J. Physiol. *443*, 491–501.

Ippolito, D.M., and Eroglu, C. (2010). Quantifying Synapses: an Immunocytochemistry-based Assay to Quantify Synapse Number. J. Vis. Exp.

Ragozzino, M.E., Unick, K.E., and Gold, P.E. (1996). Hippocampal acetylcholine release during memory testing in rats: augmentation by glucose. Proc. Natl. Acad. Sci. U. S. A. *93*, 4693–4698.

Rhein, V., Song, X., Wiesner, A., Ittner, L.M., Baysang, G., Meier, F., Ozmen, L., Bluethmann, H., Dröse, S., Brandt, U., et al. (2009). Amyloid-β and tau synergistically impair the oxidative phosphorylation system in triple transgenic Alzheimer's disease mice. Proc. Natl. Acad. Sci. *106*, 20057–20062.

Supplemental Figure Legends

Figure S1 Drp1-ablated mice display a lethal metabolic phenotype

(A) Visual performance of 4-week-Drp1-ablated and control mice was tested in the Morris Walter tank with a visible platform. Data represent average ±SEM of at least 7 animals.

(B) Olfaction of 4-week-Drp1-ablated and control mice was tested using the cookie finding test. A cookie was placed inside the mouse`s cage and the time until the cookie was found was measured. Data represent average ±SEM of at least 7 animals.

Figure S2 Parameters of Drp1-ablated mitochondria

(A+B) 4-week-Drp1-ablated and control mice were injected i.p. twice daily for 5 consecutive days with 1mg of tamoxifen, and sacrificed 4 weeks after the last tamoxifen injection. Coronal sections of formalin-fixed paraffin-embedded (FFPE) brains were immuno-stained for cytochrome *c* oxidase subunit 1 (green) and with DAPI (blue). Images show CA4 pyramidal neurons (A) and granule cell neurons of the dentate gyrus (B). White scale bar represents 10 µm.

(C) Oxygen consumption rate of isolated, cortical mitochondria of 4-week-Drp1-ablated and control mice was measured with a Seahorse Bioscience XF24 Analyzer. Substances were injected at the indicated time points. Data represent average ±SEM of at least 4 animals whose cortices were pooled and the measurements were performed with at least 6 replicates.

(D) ATP content of isolated, cortical mitochondria of 4-week-Drp1-ablated and control mice was measured with a bioluminescence assay. Data represent average ±SEM of at least 4 animals whose cortices were pooled and the measurements were performed with at least 8 replicates.

(E+F+G) Mitochondrial membrane potential of isolated, cortical mitochondria of 4-week-Drp1-ablated and control mice was measured by the increase of the fluorescence caused by the accumulation of the indicated dyes. Data represent average ±SEM of at least 4 animals whose cortices were pooled and the measurements were performed with at least 4 replicates.

(H) Oxidative stress levels represented by DHR and MitoSox fluorescence in cortical tissue homogenate of 4-week-Drp1-ablated and control mice. Data represent average ±SEM of at least 4 animals whose cortices were pooled and the measurements were performed with at least 4 replicates.

(I) Thiobarbituric acid reactive substances (TBARS) levels - representing lipid peroxidation - in 4-week-Drp1-ablated and control cortical lysates were measured by commercial fluorescence kits. Data represent average ±SEM of at least 6 animals.

(J) 4-week-Drp1-ablated and control cortical lysates were separated by SDS-PAGE and immunoblotted using an antibody for carbonylated protein of a commercial oxyblot kit. Data represent average ±SEM of at least 4 animals.

Asterisks denote P-values of an unpaired, two-tailed Student`s t-test: *:P<0.05, **:P<0.01, ***:P<0.001.

Figure S3 Drp1 ablation induces morphological ER alterations and ER stress

(A) Representative Western blot of Drp1-ablated and control cortical lysates which were separated by SDS-PAGE and immunoblotted using the indicated antibodies.

(B+C) Quantification of ATF4 and Bip band intensity normalized to actin. Data represent average ±SEM of at least 4 animals.

(D) Quantification of phosphorylated eIF2α band intensity normalized to total eIF2α. Data represent average ±SEM of at least 4 animals.

Asterisks denote P-values of an unpaired, two-tailed Student`s t-test: *:P<0.05, **:P<0.01, ***:P<0.001.

Figure S4 Drp1 ablation does not lead to neurodegeneration but leads to impaired synaptic transmission

(A) fEPSPs were recorded in the CA1 stratum radiatum in 4-week-Drp1-ablated and control hippocampal slice cultures after stimulating the Schaffer collaterals. Mean slope of fEPSPs during the time course of a 100Hz stimulation. Data represent average ±SEM of at least 6 neurons.

(B) Maximal mean fEPSP slope after 100 Hz stimulation. Data represent average ±SEM of at least 6 neurons.

Asterisks denote P-values of an unpaired, two-tailed Student`s t-test: *:P<0.05, **:P<0.01, ***:P<0.001.

Figure S5 Drp1 ablation in the forebrain induces metabolic shift transmitted by Fgf21

(A+B+C+D+E) 4-week-Drp1-ablated and control animals were housed in metabolic cages and their ambulatory activity, drinking, food intake and their respiratory gas exchange was monitored. The latter was used to calculate metabolic rate and respiratory exchange ratio. Data represent average ±SEM of at least 8 animals.

(F+G) Leptin and active ghrelin plasma levels in cardiac blood of 10-week-Drp1-ablated and control animals were determined by ELISA. Data represent average ±SEM of at least 5 animals

(H) Glucose tolerance test in 10-week-Drp1-ablated and control animals. Animals were starved overnight and injected with 2g/kg glucose and their glucose blood levels were monitored for the indicated time points. Data represent average ±SEM of at least 7 animals.

(I) Insulin tolerance test in 10-week-Drp1-ablated and control animals. Animals were starved overnight and injected with 7.5 U/kg insulin and their glucose blood levels were monitored for the indicated time points. Data represent average ±SEM of at least 5 animals.

(J) RNA was isolated from hippocampus from 10-week-Drp1-ablated and control animals. RNA was retrotranscribed into cDNA and a qRT-PCR performed using the TaqMan system. Indicated mRNA ct values were normalized against 18S rRNA ct values. Data represent average ±SEM of at least 4 animals.

(K) Representative Western blot of 10-week-Drp1-ablated and control hippocampal lysates which were separated by SDS-PAGE and immunoblotted using the indicated antibodies.

(L) Quantification of phosphorylated S473 Akt1 band intensity normalized to total Akt1. Data represent average ±SEM of at least 4 animals.

Asterisks denote P-values of an unpaired, two-tailed Student`s t-test: *:P<0.05, **:P<0.01, ***:P<0.001

Supplementary Figures

Figure S1 Drp1-ablated mice display a lethal metabolic phenotype

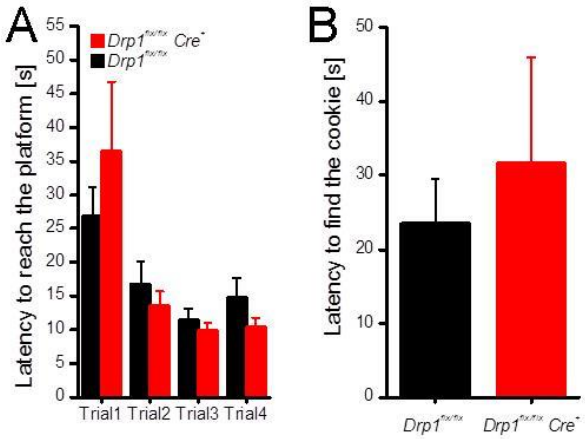

Figure S2 Parameters of Drp1-ablated mitochondria

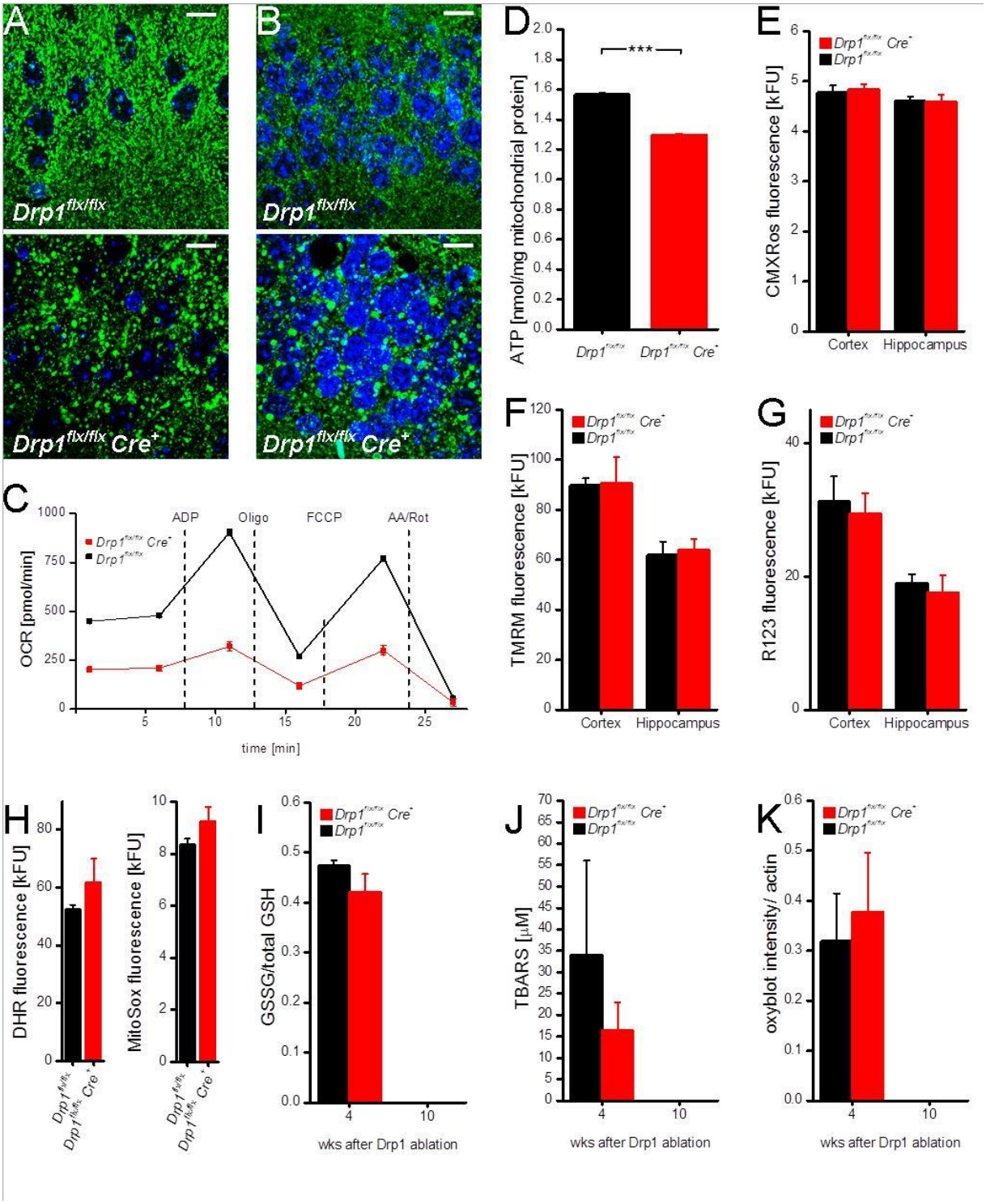

Figure S3 Drp1 ablation induces morphological ER alterations and ER stress

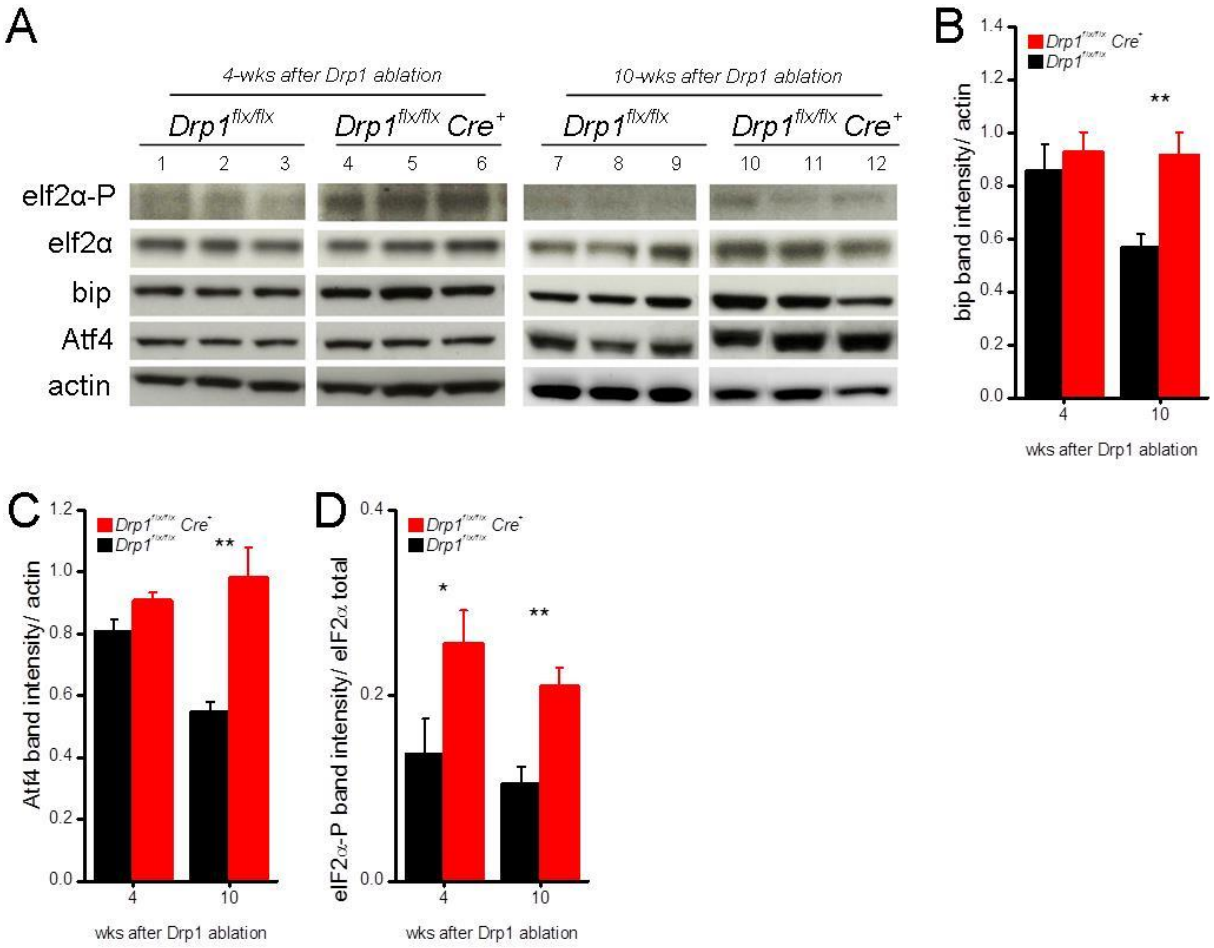

Figure S4 Drp1 ablation does not lead to neurodegeneration but leads to impaired synaptic transmission

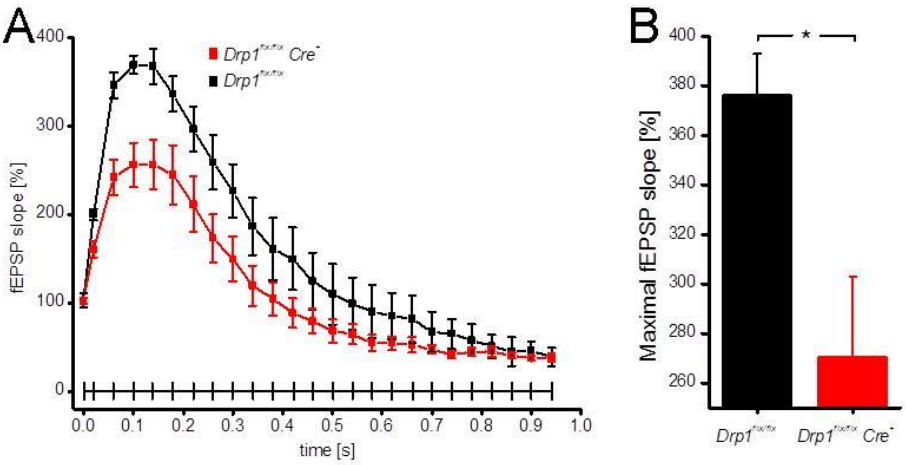

Figure S5 Drp1 blation in the forebrain induces metabolic shift transmitted by Fgf21

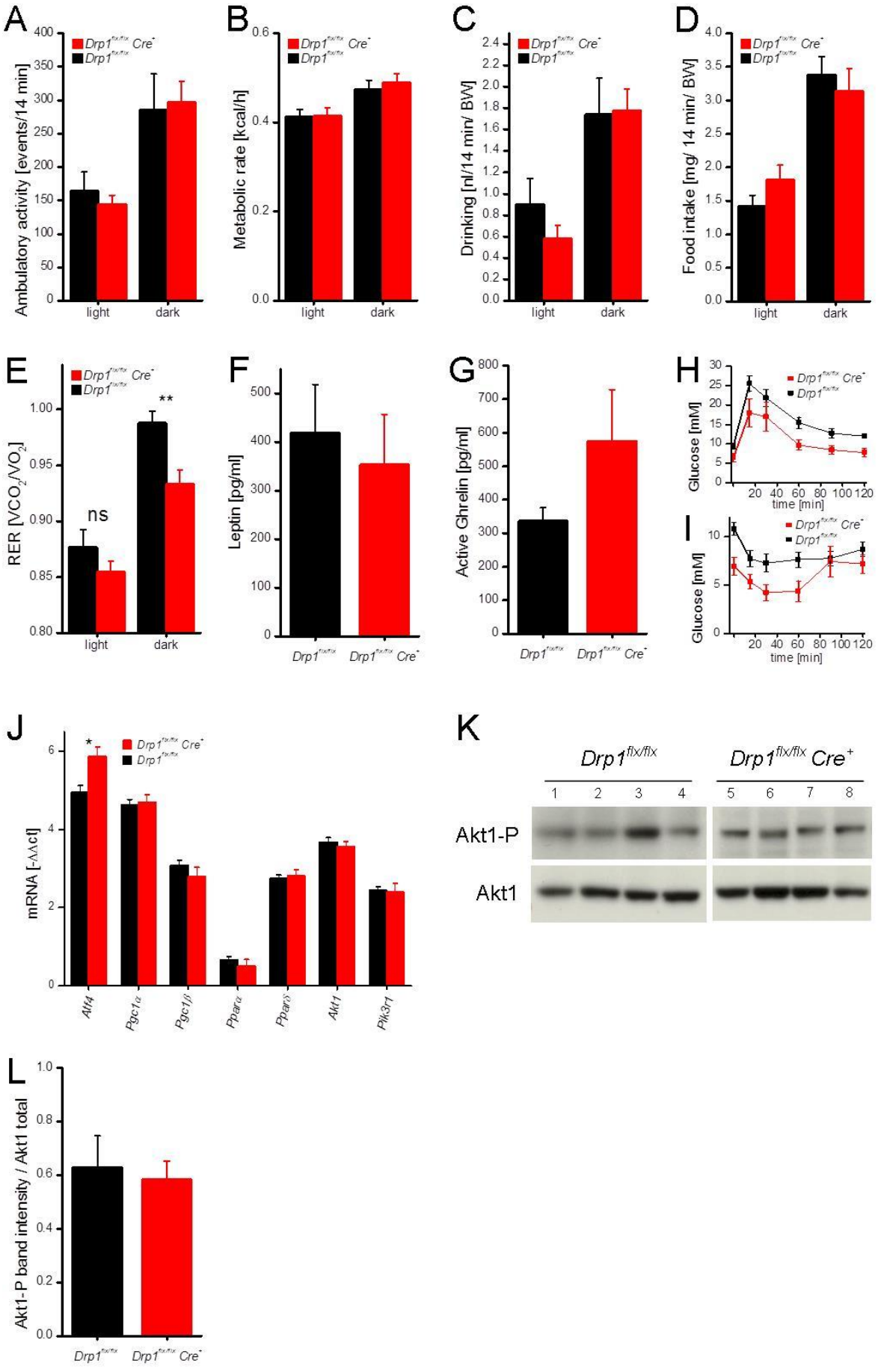

General Discussion

Dysregulated mitochondrial morphology has been implicated in a number of neurodegenerative diseases. In mouse models, the genetic knockout of essential mediators of mitochondrial fusion and fission results in early embryonic lethality, reflecting the physiological importance of properly regulated mitochondrial dynamics. The fission-mediating protein Drp1 is known as a double-edged sword. It can actively drive neurodegeneration under some conditions, and - at the same time - be essential for neuronal development and neuronal stability. Ablation of Drp1 is reported to lead either to a neuroprotective superelongated (Figure 3B) (Barsoum et al., 2006; Cheung et al., 2007; Costa et al., 2010; Dagda et al., 2008; Meuer et al., 2007; Tian et al., 2009; Young et al., 2010; Yuan et al., 2007) or an aggregated mitochondondrial phenotype (Figure 3C) promoting neurodegeneration (Ishihara et al., 2009; Li et al., 2004; Uo et al., 2009; Wakabayashi et al., 2009; Wang et al., 2009). From previously published models it had remained unclear in how far Drp1-induced neurodegeneration might be caused by a defect during neuronal differentiation due to the absence of Drp1. In order to by-pass neuronal defects caused by Drp1 ablation we developed a model that allowed us to ablate Drp1 in adult, postmitotic neurons *in vivo*. The first aim of this thesis was to dissect the role of Drp1 during neurodevelopment from its role in regulating health and death of adult neurons.

In vitro, in primary cortical neurons we could demonstrate that the two types of neuronal mitochondrial morphology reported in the literature represent two sequential stages. The initial phase (1-3 days after Drp1 ablation), characterized by a superelongated mitochondrial network, is transitory and gives way to the final stage where Drp1 ablation results in the collapse of the organelles into large spheres that aggregate in the neuronal perikarya (6-9 days after Drp1 ablation).

However, *in vivo,* we could recapitulate only this second aggregated organellar morphology but failed to observe clearly superelongated mitochondria. This superelongated phenotype was reported in Purkinje neurons *in vivo* at one week after Drp1 ablation (Kageyama et al., 2012) and in CA1 pyramidal neurons expressing mutant tau, which disrupts actin and subsequently causes Drp1 translocation to mitochondrial fission sites (DuBoff et al., 2013). It thus appears that the superelongated mitochondrial phenotype may occur *in vivo*, and our *in vitro* results suggest that mitochondrial aggregation should be preceded by elongation of the organelles. We think that this discrepancy is based on experimental reasons: in our mice, mitochondria around the nuclei of wildtype pyramidal neurons are already quite long, and in order to convincingly pinpoint a superelongated phenotype one would need to be able to trace single mitochondria reaching into the dendrites. However, due to the nature of the staining, it is impossible to accurately measure mitochondrial length in the soma and to trace single dendritic mitochondria. Given the time of maximum reduction of Drp1 protein levels (10 d) and the occurrence of the first mitochondrial blebs (also 10 d), we would expect mitochondria to pass the superelongated stage at an earlier timepoint after Drp1 ablation. In future experiments, we will therefore address this question by crossing our mouse line with a reporter strain that we recently obtained and which expresses a Cre recombinase-activatable mYFP. Titrating the dose of tamoxifen would allow us to induce a mosaic pattern of Cre activity in the forebrain which should allow tracing mitochondria of single neurons (Bersell et al., 2013). Another approach might be

to co-stain coronal brain sections for mitochondria and β-tubulin. β-tubulin staining would aid in identifying dendrites with the same orientation as the tissue section cutting plane, and only mitochondria associated with dendritic structures would be measured (Kopeikina et al., 2011).

A number of recent publications have shown that treatment with the Drp1 inhibitor mdivi-1 reduces the infarct area in various models of ischemia (Grohm et al., 2012; Park et al., 2011; Zhang et al., 2013). However, off-target effects of this (and other published) Drp1 inhibitors cannot be excluded. For example, mdivi-1 inhibits Bax-stimulated cytochrome *c* release from isolated mitochondria that cannot undergo fission (Cassidy-Stone et al., 2008). It is also likely that those inhibitors do not suppress all Drp1 functions: Inhibitor-bound Drp1 might, for instance, still be able to translocate to mitochondria or other cellular membranes and be subjected to posttranslational modifications. Also, no survival problems have been reported for mice treated continuously for three months with a Drp1 inhibitor, while our mice die within the same time period after Drp1 ablation (Guo et al., 2013b). In order to answer the question whether the beneficial effects of Drp1 inhibitors under ischemic conditions really result from Drp1 inactivation, we will have to repeat our MCA-O experiments one week after Drp1 ablation, when we expect the mitochondria to be elongated. We will additionally try to dose Drp1 levels by heterozygously deleting Drp1, which is well tolerated and has no apparent phenotype (Manczak et al., 2012).

The second aim of the thesis was to test the effect of long-term Drp1 ablation on neuronal function.

Our experiments revealed that mitochondria in long-term Drp1 ablated neurons are not only much larger than in wildtype neurons but also loose part of their cristae structure. Curiously, Drp1 inhibition has been shown to inhibit cristae remodeling in certain apoptotic settings (Costa et al., 2010; Germain et al., 2005), while Drp1 ablation-induced aggregation of mtDNA nucleoids is characterized by empty inner mitochondrial–space (Ban-Ishihara et al., 2013). We assume that the observed disruption of cristae structures at least partly results from nucleoid aggregation; but we also observed a large amount of mitochondrial cross sections entirely devoid of cristae, which is different from the TEM images published by Ban-Ishihara and co-workers (Ban-Ishihara et al., 2013). Thus, most likely, additional mechanisms regulating mitochondrial ultrastructure are affected by Drp1 loss. Not surprisingly, Drp1 ablated mitochondria have a less sufficient respiratory capacity and accumulate less ATP than control mitochondria. Based on enzyme-histochemical stainings of respiratory complexes, similar observations have been made by Kageyama et al. in Drp1 ablated Purkinje neurons (Kageyama et al., 2012). Kageyama and coworkers observe that within 5 weeks after Drp1 ablation the number of Purkinje cells is decreased, which can partially be rescued by antioxidant treatment. Of note, at 4 weeks after Drp1 ablation, we were not able to detect any ROS formation or neurodegeneration in our model. Nevertheless (and quite unexpectedly) our mice died around 12 weeks after Drp1 ablation for reasons that will be discussed further below. At this point, we cannot exclude that oxidative stress and neurodegeneration could in fact be detected in our model at later timepoints if our mice lived longer.

While we did not detect any ROS stress during the first 4 weeks following Drp1 ablation, we did find substantial evidence for ER stress. During ER stress the chaperone Bip detects unfolded proteins inside the ER lumen and activates of a number of subpathways. One of them is initiated by the autophosphorylation of the integral ER membrane protein pancreatic eIF2α kinase (PERK). PERK

phosphorylates eukaryotic initiation factor 2α (eIF2α) which induces activating transcription factor 4 (ATF4). ATF4, in turn, activates the transcription of a myriad of genes, among them *DNA damage inducible transcript 3* (*Ddit3*). The translation product of *Ddit3*, also known as Chop, acts as a dominant dimerization protein for transcription factors of the C/EBP family and promotes apoptosis. On mRNA as well as protein level, we find ample evidence for the activation of the PERK-mediated ER stress pathway which is paralleled by substantial changes in ER morphology in Drp1-ablated neurons.

In a model of angiotensin-II-induced chronic hypertension neuronal ER stress is associated with similar ER morphology changes reflecting that neuronal ER stress and ER shape are interconnected (Young et al., 2012). However, particularly in neurons, ER fragmentation seems to be a reversible phenomenon in response to insults not necessarily connected to ER stress (Kucharz et al., 2013), and thus it is possible that ER fragmentation *per se* is part of an general adaptive stress response. The origin of the stress in our Drp1 ablation model could also be due to mitochondrial stress caused by respiratory deficiency and associated changes in mitochondrial morphology. Alternatively, as we detect eIF2α phosphorylation prior to Bip upregulation, eIF2α could also get phosphorylated by the kinase GCN2, which is activate during amino acid deprivation (Donnelly et al., 2013).

ER and mitochondrial network are tightly interconnected by membrane structures called mitochondria associated ER membranes (MAMs). Disruption of MAMs by mutant α-synuclein disrupts ER-mitochondria interorganellar connections, and induces Drp1-independent fragmentation of mitochondria (Guardia-Laguarta et al., 2014). Likewise, MAMs disruption by deletion of Mfn2, which interconnects ER and mitochondria, induces fragmentation of both organelles (de Brito and Scorrano, 2008). Hence, it seems very likely that profound morphological changes of one organelle inevitably impinge on the morphological integrity of the other. Mfn2-deficient cells also show UPR activation (Muñoz et al., 2013), indicating that disruption of trans-organelle connections is sufficient to induce ER stress. It was previously shown that Drp1 also localizes to the ER and can mediate ER morphological changes (Pitts et al., 1999; Wikstrom et al., 2013) indicating that Drp1 may directly regulate ER shape.

Neurons that have an aggregated mitochondrial phenotype show a reduction in dendritic and synaptic structures *in vitro* (reviewed in Oettinghaus et al., 2012). However, as discussed before, we could not show that in our *in vivo* model. Even though they have to cope with decreased oxidative phosphorylation, ER stress, and are more sensitive to ischemia, Drp1 ablated pyramidal CA1 neurons have a regular dendritic tree morphology as well as regular synapse and spine numbers; in addition, no neurodegeneration is observed within 10 weeks of Drp1 ablation. In contrast, Drp1 ablated Purkinje neurons undergo neurodegeneration within 5 weeks after Drp1 ablation (Kageyama et al., 2012). As pointed out earlier, Drp1 is of particular importance for dendrite and synapse formation during neuronal development. In this context, it is interesting to note that murine Purkinje neuron differentiation continues during the first three weeks after birth (Chizhikov and Millen, 2003), and that the onset of Drp1 ablation in the Purkinje cell model of Kageyama and co-workers occurs at three weeks after birth. Therefore, one cannot exclude that Drp1 ablation overlaps with the final stages of Purkinje neuron differentiation, which might render them more susceptible to degeneration. In our model we can exclude neurodevelopmental defects caused by Drp1 ablation (tamoxifen knockout induction occurs at the age of 8 weeks), and our results show that dendritic and synaptic structures are largely unaffected by Drp1 ablation. We also find that basic functions are maintained in Drp1

ablated neurons: they generate action potentials, maintain their plasma membrane potential and are capable of synaptic transmission. However, numbers of presynaptic mitochondria are decreased and, when challenged by high frequency stimulation, synaptic transmission of Drp1 ablated neurons is impaired, indicating compromised neuronal function under certain conditions.

Interestingly, a similar electrophysiological phenotype with a similar mitochondrial morphology has been observed at the neuromuscular junction of Drp1 mutant flies (Verstreken et al., 2005). While this phenotype has been attributed to ATP-dependent effects on reserve pool vesicle recycling due to the lack of mitochondria at the bouton, it has been shown more recently in murine hippocampal neurons, that Drp1 is also directly involved in reserve pool vesicle formation (Li et al., 2013). We think that the defect in synaptic transmission observed in our model is sufficient to explain the decrease in short-term spatial working memory verified during behavioral testing of our Drp1 ablated mice.

Finally, we observed a specific reduction in hippocampal volume which we believe is due to the nature of the metabolic phenotype characterized by increased circulating corticosterone. Hippocampal atrophy is a hallmark of post-traumatic stress disorder in which pathological stress hormone levels inhibit hippocampal neurogenesis (Bremner, 2006); therefore, testing whether Drp1 ablation effects hippocampal neurogenesis appears as a tempting hypothesis to be addressed by future experimentation.

Our investigation of the long-term effects of Drp1 ablation on neuronal function was limited by the profound metabolic phenotype, invariably resulting in death of the animals within three months of Drp1 ablation. In addition, we were also limited in all electrophysiological measurements because after the age of 3 months it becomes exceedingly difficult to prepare murine hippocampal slice cultures suitable for respective analyses. In particular, we cannot exclude that Drp1 ablation for longer than three months causes neurodegeneration. In order to address this, we will use *Drp1*$^{flx/flx}$ mice expressing Cre-activatable mYFP, and via tamoxifen titration induce Cre activity in only a few neurons, which might not be sufficient to cause the full-blown lethal phenotype. In these mice, the fate of mYFP expressing Drp1 ablated neurons can be monitored over time.

We have not determined whether forebrain-Drp1 ablated mice also have a decrease in long-term memory. Long-term memory requires *de novo* spine formation in existing neuronal circuits, a process that is highly reliant on protein synthesis. Phosphorylation of eIF2α, however, reduces the rates of mRNA translation, greatly impairing memory and contributing also to the cognitive impairment in AD (Costa-Mattioli et al., 2007; Ma et al., 2013). It thus appears likely, that the mice in our model also suffer from long-term memory impairment. In addition to extending our behavior experiments to test for long-term memory deficiency, we will therefore isolate polysomal fractions from Drp1 ablated brain tissue to check whether neurons in our model are subjected to translational arrest (Del Prete et al., 2007).

Our results also raise the question of whether Drp1 is directly involved in shaping the neuronal ER. As already discussed, Drp1 not only serves to induce mitochondrial fission but also interacts with a number of other cellular membranes including the ER. In the future, we will address this question by deriving neurons from *Drp1*$^{flx/flx}$ mice expressing Cre-activatable mYFP, and co-electroporate them with

Cre and ERdsRed2 expression constructs to visualize the ER after Drp1 ablation. In addition, we will induce ER fragmentation via NMDA receptor activation as previously reported (Kucharz et al., 2009).

Even though the ER shape of *drp1* knockout embryonic fibroblasts (MEFs) was reported to be normal (Ishihara et al., 2009), unpublished results from our lab show that ER morphology changes after transfection of *Drp1*$^{flx/flx}$ MEFs with Cre. We will generate *Drp1*$^{flx/flx}$ MEFs stably expressing mYFP and ERdsRed2 to monitor mitochondrial and ER morphology after Drp1 ablation and under conditions of ER stress. Furthermore, we will generate a CFP-Drp1 fusion construct including versions with dominant-negative and phosphomimetic Drp1 mutations. This will allow us to directly monitor Drp1 translocation to mitochondria and ER simultaneously in live cells. If possible, we will make use of superresolution microscopy to obtain precise colocalization imaging. We will also try to inhibit translocation of Drp1 to mitochondria by downregulating INF2 (Korobova et al., 2013) and by expressing P301L mutant tau (DuBoff et al., 2012). Once we have established a baseline of results and can genetically separate Drp1 translocation to ER and mitochondria, we will test whether treatment with the small molecule Drp1 inhibitor mdivi-1 blocks Drp1 function on ER and mitochondria, respectively.

We also plan to recapitulate all of our findings in MEFs in primary neuronal cultures. To limit animal use, we have already derived a line of neural stem/progenitor cells (NSC) from WT mice. These cells can be propagated as progenitors and expanded, and then differentiated with appropriate stimuli and culture conditions to pure neuronal cultures. We will make use of this model to reduce animal numbers and to create neural stem progenitors stably expressing the above described constructs.

Mice in which Drp1 translocation to mitochondria is inhibited by mutant tau can maintain a superelongated mitochondrial phenotype for up to seven months (DuBoff et al., 2012). We will purchase mice expressing transgenic P301L tau from the Jackson laboratory (stock No: 024854) to derive primary neuronal cultures in order to monitor ER and mitochondrial shape. Furthermore, we will cross these animals with *Drp1*$^{flx/flx}$ Cre^{+} mice expressing Cre-activatable mYFP to see how additional deletion of Drp1 influences mitochondrial and ER shape.

The third aim of this study was to investigate the metabolism of our mouse model. We find that Drp1 ablation in the forebrain leads to a metabolic shift characterized by an increase in corticosterone levels. Corticosterone is the main glucocorticoid in rodents and has a variety of metabolic effects: it mobilizes energy stores by inducing lipolysis in fat tissue and by protein degradation in muscle, and it activates gluconeogenesis in the liver. Predominant in our mice was the effect on fatty acid metabolism. Despite normal feeding behavior, Drp1 ablated mice lost weight and had a decreased percentage of body fat.

Corticosterone levels can be regulated via Fgf21 receptor binding in the hypothalamus (Bookout et al., 2013) and accordingly, we find elevated Fgf21 plasma levels in forebrain-Drp1 ablated mice. We also find that Fgf21 mRNA expression is only increased in brain regions in which we ablated Drp1. Compellingly, forebrain-Drp1 ablated mice share a similar metabolic phenotype with Fgf21 overexpressing mice regarding weight development, lower glucose levels, fat tissue histology and corticosterone levels (Bookout et al., 2013; Kharitonenkov et al., 2005; Zhang et al., 2012). In contrast,

however, mice overexpressing Fgf21 do not die but in fact have an extended life span, similar to mice fed a calorie-restricted diet (Zhang et al., 2012). While we do not have a definitive explanation for this phenotypic discrepancy, the difference between those two models could potentially be attributed to functionally impaired Drp1 ablated neurons, and to a difference in the physiological distribution of Fgf21.

In our model the *CamKIIα* promoter that controls the CreERT2 transgene is also active in the paraventricular nucleus in the hypothalamus (Erdmann et al., 2007). It recently became apparent, that mitochondrial dynamics can also be involved in intraneuronal signal transduction. Changes of the morphology of the neuronal mitochondrial network can be a specific reaction to hormone or metabolite sensing in certain highly-specialized hypothalamic neuronal subpopulations (Carneiro et al., 2012; Dietrich et al., 2013; Schneeberger et al., 2013). At this point, we cannot exclude that Drp1 ablation affects hormone or metabolite sensing in this subset of neurons, and that this also contributes to the observed metabolic phenotype. β-klotho – a substantial component of the Fgf21 receptor – expression, however, is limited to the suprachiasmatic nucleus where the Cre-regulating promoter in our model is not active (Bookout et al., 2013).

Fgf21 in our model is produced in close proximity to its hypothalamic receptor and induces corticosterone production as efficiently as systemic Fgf21 overexpression in mice which have a much higher Fgf21 levels. Fgf21 can cross the blood brain barrier via diffusion; however, degradation of Fgf21 in brain is 2-fold higher than in the serum (Hsuchou et al., 2007), indicating that some of the Fgf21 produced in brain might not reach Fgf21 receptors in the periphery. The activation of Fgf21 receptors in adipose tissue is essential for the pharmacologically induced antidiabetic effects of Fgf21, in particular in lowering glucose concentrations and body weight (Luo and McKeehan, 2013). Transgenic mice with a respiratory deficiency in muscle tissue also induce Fgf21 to reach serum concentrations comparable to our model (Kim et al., 2013; Tyynismaa et al., 2010); however, the authors don`t state whether the Fgf21 produced in the periphery at these concentrations is sufficient to induce corticosterone production. The physiological role of Fgf21 is perceived as a metabolic stress hormone mediating inter-organ communication between stressed organ and adipose tissue, which induces a beneficial metabolic shift (Luo and McKeehan, 2013). It is thus very likely, that Fgf21 production in Drp1 ablated brain is in fact beneficial to the organism and initiates a metabolic shift that supports Drp1 ablated brain regions and maintains their functionality.

Collectively, through our work, we have characterized the basic mechanisms underlying the metabolic shift caused by forebrain-specific Drp1 ablation. Nevertheless, it remains unclear how Drp1 ablated neurons survive *in vivo* and how their metabolism changes due to the respiratory deficiency. The non-glucose metabolites that can be used by neurons - lactate and ketone bodies - require oxidative phosphorylation, and it thus appears likely that Drp1 ablated neurons primarily rely on glycolysis. With this hypothesis in mind, we will perform future gene expression assays on glycolytic genes to verify our assumption.

We also have not yet determined, how increased corticosterone and Fgf21 levels change metabolism in muscle and liver, where corticosterone could induce protein degradation (skeletal muscle) and gluconeogenesis (liver), respectively. We will therefore systemically measure skeletal muscle fiber size in various hindlimb muscles, as well as serum alanine concentration. In addition, we are going to

measure hepatic mRNA expression levels of genes regulating gluconeogenesis: PGC1α, pyruvate-carboxylase and phosphoenolpyruvate-carboxykinase.

The major novelty of this thesis work is that cortex and hippocampus can exert neuroendocrinological functions, signaling mitochondrial deficits via the UPR pathway to the periphery. To verify this hypothesis *in vivo,* we will treat Drp1 ablated mice and littermate controls with the FDA-approved chemical chaperone tauroursodeoxycholic acid (TUDCA), which reduces ER stress. We expect that this treatment will reduce eIF2α phosphorylation and thus Fgf21 levels, and will investigate whether this treatment is sufficient to normalize corticosterone levels and to rescue mitochondrial morphology. If indeed neuronal UPR signaling causes the metabolic shift in our mice, TUDCA treatment will either aggravate or ameliorate the metabolic phenotype depending on whether the Fgf21-induced change in metabolism is beneficial or harmful to the organsim.

Fgf21 has recently been identified as biomarker for mitochondrial myopathies (Suomalainen et al., 2011). It therefore seems a plausible hypothesis that Fgf21 signaling plays a role in neurodegenerative diseases where defects in mitochondrial morphology and function as well as ER stress are known to occur. In this context, for instance, it is interesting to note that in AD brains altered mitochondrial morphology (Wang et al., 2009) and increased levels of phosphorylated eIF2α (Chang et al., 2002) have been reported. In a continuation of our project, we therefore plan to obtain blood and CSF samples from AD patients (ethical approval pending) to measure Fgf21 serum levels and to correlate those with mitochondrial morphology as well as with the levels of phosphorylated eIF2α protein and Fgf21 mRNA.

In summary, we conclude that Drp1 function is pivotal in postmitotic neurons which, however, display a remarkable resilience and are able to adapt to blocked mitochondrial fission caused by Drp1 ablation. Most surprisingly, these intraneuronal adaptations are communicated to the organism via the catabolic cytokine Fgf21 which induces a profound metabolic shift. This work also provides a number of suggestions on how to further test and verify our model, and how this could be of clinical relevance. The presented results provide a new perspective on the interplay of mitochondria and ER in the course of neurodegenerative disease, and will hopefully inspire a new direction of research in the scientific mitochondrial community.

References

Anglade, P., Vyas, S., Javoy-Agid, F., Herrero, M.T., Michel, P.P., Marquez, J., Mouatt-Prigent, A., Ruberg, M., Hirsch, E.C., and Agid, Y. (1997). Apoptosis and autophagy in nigral neurons of patients with Parkinson's disease. Histol Histopathol *12*, 25–31.

Arnoult, D., Rismanchi, N., Grodet, A., Roberts, R.G., Seeburg, D.P., Estaquier, J., Sheng, M., and Blackstone, C. (2005). Bax/Bak-dependent release of DDP/TIMM8a promotes Drp1-mediated mitochondrial fission and mitoptosis during programmed cell death. Curr Biol *15*, 2112–2118.

Ashrafi, G., and Schwarz, T.L. (2013). The pathways of mitophagy for quality control and clearance of mitochondria. Cell Death Differ. *20*, 31–42.

Backhauss, C., Karkoutly, C., Welsch, M., and Krieglstein, J. (1992). A mouse model of focal cerebral ischemia for screening neuroprotective drug effects. J. Pharmacol. Toxicol. Methods *27*, 27–32.

Barsoum, M.J., Yuan, H., Gerencser, A.A., Liot, G., Kushnareva, Y., Graber, S., Kovacs, I., Lee, W.D., Waggoner, J., Cui, J., et al. (2006). Nitric oxide-induced mitochondrial fission is regulated by dynamin-related GTPases in neurons. Embo J *25*, 3900–3911.

Belgard, T.G., Marques, A.C., Oliver, P.L., Abaan, H.O., Sirey, T.M., Hoerder-Suabedissen, A., Garcia-Moreno, F., Molnar, Z., Margulies, E.H., and Ponting, C.P. (2011). A transcriptomic atlas of mouse neocortical layers. Neuron *71*, 605–616.

Bernardi, P., and Azzone, G.F. (1981). Cytochrome c as an electron shuttle between the outer and inner mitochondrial membranes. J Biol Chem *256*, 7187–7192.

Bersell, K., Choudhury, S., Mollova, M., Polizzotti, B.D., Ganapathy, B., Walsh, S., Wadugu, B., Arab, S., and Kuhn, B. (2013). Moderate and high amounts of tamoxifen in αMHC-MerCreMer mice induce a DNA damage response, leading to heart failure and death. Dis. Model. Mech. *6*, 1459–1469.

Bliek, A.M. van der, Shen, Q., and Kawajiri, S. (2013). Mechanisms of Mitochondrial Fission and Fusion. Cold Spring Harb. Perspect. Biol. *5*, a011072.

Van der Bliek, A.M. (1999). Functional diversity in the dynamin family. Trends Cell Biol *9*, 96–102.

Boland, B., Kumar, A., Lee, S., Platt, F.M., Wegiel, J., Yu, W.H., and Nixon, R.A. (2008). Autophagy Induction and Autophagosome Clearance in Neurons: Relationship to Autophagic Pathology in Alzheimer's Disease. J. Neurosci. *28*, 6926–6937.

Bonekamp, N.A., Vormund, K., Jacob, R., and Schrader, M. (2010). Dynamin-like protein 1 at the Golgi complex: A novel component of the sorting/targeting machinery en route to the plasma membrane. Exp. Cell Res. *316*, 3454–3467.

Bookout, A.L., de Groot, M.H.M., Owen, B.M., Lee, S., Gautron, L., Lawrence, H.L., Ding, X., Elmquist, J.K., Takahashi, J.S., Mangelsdorf, D.J., et al. (2013). FGF21 regulates metabolism and circadian behavior by acting on the nervous system. Nat. Med. *19*, 1147–1152.

Braschi, E., Zunino, R., and McBride, H.M. (2009). MAPL is a new mitochondrial SUMO E3 ligase that regulates mitochondrial fission. EMBO Rep *10*, 748–754.

Bremner, J.D. (2006). Stress and Brain Atrophy. CNS Neurol. Disord. Drug Targets *5*, 503–512.

De Brito, O.M., and Scorrano, L. (2008). Mitofusin 2 tethers endoplasmic reticulum to mitochondria. Nature *456*, 605–610.

Brooks, C., Wei, Q., Cho, S.G., and Dong, Z. (2009). Regulation of mitochondrial dynamics in acute kidney injury in cell culture and rodent models. J Clin Invest *119*, 1275–1285.

Broughton, B.R., Reutens, D.C., and Sobey, C.G. (2009). Apoptotic mechanisms after cerebral ischemia. Stroke *40*, e331–9.

Brouillet, E., Guyot, M.-C., Mittoux, V., Altairac, S., Condé, F., Palfi, S., and Hantraye, P. (1998). Partial Inhibition of Brain Succinate Dehydrogenase by 3-Nitropropionic Acid Is Sufficient to Initiate Striatal Degeneration in Rat. J. Neurochem. *70*, 794–805.

Bui, H.T., and Shaw, J.M. (2013). Dynamin Assembly Strategies and Adaptor Proteins in Mitochondrial Fission. Curr. Biol. *23*, R891–R899.

Cai, Q., Zakaria, H.M., Simone, A., and Sheng, Z.-H. (2012). Spatial Parkin Translocation and Degradation of Damaged Mitochondria via Mitophagy in Live Cortical Neurons. Curr. Biol. *22*, 545–552.

Von Campenhausen, S., Bornschein, B., Wick, R., Botzel, K., Sampaio, C., Poewe, W., Oertel, W., Siebert, U., Berger, K., and Dodel, R. (2005). Prevalence and incidence of Parkinson's disease in Europe. Eur Neuropsychopharmacol *15*, 473–490.

Carneiro, L., Allard, C., Guissard, C., Fioramonti, X., Tourrel-Cuzin, C., Bailbé, D., Barreau, C., Offer, G., Nédelec, E., Salin, B., et al. (2012). Importance of Mitochondrial Dynamin-Related Protein 1 in Hypothalamic Glucose Sensitivity in Rats. Antioxid. Redox Signal. *17*, 433–444.

Cassidy-Stone, A., Chipuk, J.E., Ingerman, E., Song, C., Yoo, C., Kuwana, T., Kurth, M.J., Shaw, J.T., Hinshaw, J.E., Green, D.R., et al. (2008). Chemical inhibition of the mitochondrial division dynamin reveals its role in Bax/Bak-dependent mitochondrial outer membrane permeabilization. Dev Cell *14*, 193–204.

Cereghetti, G.M., Stangherlin, A., Martins de Brito, O., Chang, C.R., Blackstone, C., Bernardi, P., and Scorrano, L. (2008). Dephosphorylation by calcineurin regulates translocation of Drp1 to mitochondria. Proc Natl Acad Sci U A *105*, 15803–15808.

Chang, C.R., and Blackstone, C. (2007). Cyclic AMP-dependent protein kinase phosphorylation of Drp1 regulates its GTPase activity and mitochondrial morphology. J Biol Chem *282*, 21583–21587.

Chang, R.C.C. 1, Wong, A.K.Y., Ng, H.-K., and Hugon, J. 1 2 (2002). Phosphorylation of eukaryotic initiation factor-2[alpha] (eIF2[alpha]) is associated with neuronal degeneration in Alzheimer's disease. [Miscellaneous Article]. Neuroreport Dec. 20 2002 *13*, 2429–2432.

Chen, H., Detmer, S.A., Ewald, A.J., Griffin, E.E., Fraser, S.E., and Chan, D.C. (2003). Mitofusins Mfn1 and Mfn2 coordinately regulate mitochondrial fusion and are essential for embryonic development. J Cell Biol *160*, 189–200.

Chen, H., Chomyn, A., and Chan, D.C. (2005). Disruption of Fusion Results in Mitochondrial Heterogeneity and Dysfunction. J. Biol. Chem. *280*, 26185–26192.

Chen, H., Vermulst, M., Wang, Y.E., Chomyn, A., Prolla, T.A., McCaffery, J.M., and Chan, D.C. (2010). Mitochondrial fusion is required for mtDNA stability in skeletal muscle and tolerance of mtDNA mutations. Cell *141*, 280–289.

Cheung, E.C., McBride, H.M., and Slack, R.S. (2007). Mitochondrial dynamics in the regulation of neuronal cell death. Apoptosis *12*, 979–992.

Chizhikov, V., and Millen, K.J. (2003). Development and malformations of the cerebellum in mice. Mol. Genet. Metab. *80*, 54–65.

Cipolat, S., Rudka, T., Hartmann, D., Costa, V., Serneels, L., Craessaerts, K., Metzger, K., Frezza, C., Annaert, W., D'Adamio, L., et al. (2006). Mitochondrial rhomboid PARL regulates cytochrome c release during apoptosis via OPA1-dependent cristae remodeling. Cell *126*, 163–175.

Clark, I.E., Dodson, M.W., Jiang, C., Cao, J.H., Huh, J.R., Seol, J.H., Yoo, S.J., Hay, B.A., and Guo, M. (2006). Drosophila pink1 is required for mitochondrial function and interacts genetically with parkin. Nature *441*, 1162–1166.

Cocucci, E., Aguet, F., Boulant, S., and Kirchhausen, T. (2012). The First Five Seconds in the Life of a Clathrin-Coated Pit. Cell *150*, 495–507.

Costa, V., Giacomello, M., Hudec, R., Lopreiato, R., Ermak, G., Lim, D., Malorni, W., Davies, K.J., Carafoli, E., and Scorrano, L. (2010). Mitochondrial fission and cristae disruption increase the response of cell models of Huntington's disease to apoptotic stimuli. EMBO Mol Med *2*, 490–503.

Costa-Mattioli, M., Gobert, D., Stern, E., Gamache, K., Colina, R., Cuello, C., Sossin, W., Kaufman, R., Pelletier, J., Rosenblum, K., et al. (2007). eIF2α Phosphorylation Bidirectionally Regulates the Switch from Short- to Long-Term Synaptic Plasticity and Memory. Cell *129*, 195–206.

Cribbs, J.T., and Strack, S. (2007). Reversible phosphorylation of Drp1 by cyclic AMP-dependent protein kinase and calcineurin regulates mitochondrial fission and cell death. EMBO Rep *8*, 939–944.

Dagda, R.K., Merrill, R.A., Cribbs, J.T., Chen, Y., Hell, J.W., Usachev, Y.M., and Strack, S. (2008). The spinocerebellar ataxia 12 gene product and protein phosphatase 2A regulatory subunit Bbeta2 antagonizes neuronal survival by promoting mitochondrial fission. J Biol Chem *283*, 36241–36248.

Dagda, R.K., Gusdon, A.M., Pien, I., Strack, S., Green, S., Li, C., Van Houten, B., Cherra, S.J., 3rd, and Chu, C.T. (2011). Mitochondrially localized PKA reverses mitochondrial pathology and dysfunction in a cellular model of Parkinson's disease. Cell Death Differ *18*, 1914–1923.

Delille, H.K., and Schrader, M. (2008). Targeting of hFis1 to Peroxisomes Is Mediated by Pex19p. J. Biol. Chem. *283*, 31107–31115.

Dietrich, M.O., Liu, Z.-W., and Horvath, T.L. (2013). Mitochondrial Dynamics Controlled by Mitofusins Regulate Agrp Neuronal Activity and Diet-Induced Obesity. Cell *155*, 188–199.

Donnelly, N., Gorman, A.M., Gupta, S., and Samali, A. (2013). The eIF2α kinases: their structures and functions. Cell. Mol. Life Sci. *70*, 3493–3511.

DuBoff, B., Götz, J., and Feany, M.B. (2012). Tau Promotes Neurodegeneration via DRP1 Mislocalization In Vivo. Neuron *75*, 618–632.

DuBoff, B., Feany, M., and Götz, J. (2013). Why size matters – balancing mitochondrial dynamics in Alzheimer's disease. Trends Neurosci. *36*, 325–335.

Ehringer, H., and Hornykiewicz, O. (1960). [Distribution of noradrenaline and dopamine (3-hydroxytyramine) in the human brain and their behavior in diseases of the extrapyramidal system]. Klin Wochenschr *38*, 1236–1239.

English, A.R., and Voeltz, G.K. (2013). Rab10 GTPase regulates ER dynamics and morphology. Nat. Cell Biol. *15*, 169–178.

Erdmann, G., Schutz, G., and Berger, S. (2007). Inducible gene inactivation in neurons of the adult mouse forebrain. BMC Neurosci *8*, 63.

Fearnley, J.M., and Lees, A.J. (1991). Ageing and Parkinson's disease: substantia nigra regional selectivity. Brain J. Neurol. *114 (Pt 5)*, 2283–2301.

Ferraro, E., Pesaresi, M.G., De Zio, D., Cencioni, M.T., Gortat, A., Cozzolino, M., Berghella, L., Salvatore, A.M., Oettinghaus, B., Scorrano, L., et al. (2011). Apaf1 plays a pro-survival role by regulating centrosome morphology and function. J Cell Sci *124*, 3450–3463.

Figueroa-Romero, C., Iniguez-Lluhi, J.A., Stadler, J., Chang, C.R., Arnoult, D., Keller, P.J., Hong, Y., Blackstone, C., and Feldman, E.L. (2009). SUMOylation of the mitochondrial fission protein Drp1 occurs at multiple nonconsensus sites within the B domain and is linked to its activity cycle. Faseb J *23*, 3917–3927.

Frank, S., Gaume, B., Bergmann-Leitner, E.S., Leitner, W.W., Robert, E.G., Catez, F., Smith, C.L., and Youle, R.J. (2001). The role of dynamin-related protein 1, a mediator of mitochondrial fission, in apoptosis. Dev Cell *1*, 515–525.

Frezza, C., Cipolat, S., Martins de Brito, O., Micaroni, M., Beznoussenko, G.V., Rudka, T., Bartoli, D., Polishuck, R.S., Danial, N.N., De Strooper, B., et al. (2006). OPA1 controls apoptotic cristae remodeling independently from mitochondrial fusion. Cell *126*, 177–189.

Friedman, J.R., Lackner, L.L., West, M., DiBenedetto, J.R., Nunnari, J., and Voeltz, G.K. (2011). ER tubules mark sites of mitochondrial division. Science *334*, 358–362.

Gandre-Babbe, S., and Bliek, A.M. van der (2008). The Novel Tail-anchored Membrane Protein Mff Controls Mitochondrial and Peroxisomal Fission in Mammalian Cells. Mol. Biol. Cell *19*, 2402–2412.

Gawlowski, T., Suarez, J., Scott, B., Torres-Gonzalez, M., Wang, H., Schwappacher, R., Han, X., Yates, J.R., Hoshijima, M., and Dillmann, W. (2012). Modulation of Dynamin-related Protein 1 (DRP1) Function by Increased O-linked-β-N-acetylglucosamine Modification (O-GlcNAc) in Cardiac Myocytes. J. Biol. Chem. *287*, 30024–30034.

Germain, M., Mathai, J.P., McBride, H.M., and Shore, G.C. (2005). Endoplasmic reticulum BIK initiates DRP1-regulated remodelling of mitochondrial cristae during apoptosis. Embo J *24*, 1546–1556.

Glotzer, M. (2005). The Molecular Requirements for Cytokinesis. Science *307*, 1735–1739.

Gomes, L.C., and Scorrano, L. (2008). High levels of Fis1, a pro-fission mitochondrial protein, trigger autophagy. Biochim Biophys Acta *1777*, 860–866.

Gomes, L.C., Di Benedetto, G., and Scorrano, L. (2011). During autophagy mitochondria elongate, are spared from degradation and sustain cell viability. Nat Cell Biol *13*, 589–598.

Greene, J.C., Whitworth, A.J., Kuo, I., Andrews, L.A., Feany, M.B., and Pallanck, L.J. (2003). Mitochondrial pathology and apoptotic muscle degeneration in Drosophila parkin mutants. Proc Natl Acad Sci U A *100*, 4078–4083.

Grohm, J., Kim, S.-W., Mamrak, U., Tobaben, S., Cassidy-Stone, A., Nunnari, J., Plesnila, N., and Culmsee, C. (2012). Inhibition of Drp1 provides neuroprotection in vitro and in vivo. Cell Death Differ. *19*, 1446–1458.

Guardia-Laguarta, C., Area-Gomez, E., Rüb, C., Liu, Y., Magrané, J., Becker, D., Voos, W., Schon, E.A., and Przedborski, S. (2014). α-Synuclein Is Localized to Mitochondria-Associated ER Membranes. J. Neurosci. *34*, 249–259.

Guo, C., Hildick, K.L., Luo, J., Dearden, L., Wilkinson, K.A., and Henley, J.M. (2013a). SENP3-mediated deSUMOylation of dynamin-related protein 1 promotes cell death following ischaemia. EMBO J. *32*, 1514–1528.

Guo, X., Disatnik, M.-H., Monbureau, M., Shamloo, M., Mochly-Rosen, D., and Qi, X. (2013b). Inhibition of mitochondrial fragmentation diminishes Huntington's disease–associated neurodegeneration. J. Clin. Invest. *123*, 5371–5388.

Han, X.J., Lu, Y.F., Li, S.A., Kaitsuka, T., Sato, Y., Tomizawa, K., Nairn, A.C., Takei, K., Matsui, H., and Matsushita, M. (2008). CaM kinase Ialpha-induced phosphorylation of Drp1 regulates mitochondrial morphology. J Cell Biol *182*, 573–585.

Harder, Z., Zunino, R., and McBride, H. (2004). Sumo1 conjugates mitochondrial substrates and participates in mitochondrial fission. Curr Biol *14*, 340–345.

Higuchi, M., Tomioka, M., Takano, J., Shirotani, K., Iwata, N., Masumoto, H., Maki, M., Itohara, S., and Saido, T.C. (2005). Distinct mechanistic roles of calpain and caspase activation in neurodegeneration as revealed in mice overexpressing their specific inhibitors. J Biol Chem *280*, 15229–15237.

Hsuchou, H., Pan, W., and Kastin, A.J. (2007). The fasting polypeptide FGF21 can enter brain from blood. Peptides *28*, 2382–2386.

Ingerman, E., Perkins, E.M., Marino, M., Mears, J.A., McCaffery, J.M., Hinshaw, J.E., and Nunnari, J. (2005). Dnm1 forms spirals that are structurally tailored to fit mitochondria. J Cell Biol *170*, 1021–1027.

Ishihara, N., Nomura, M., Jofuku, A., Kato, H., Suzuki, S.O., Masuda, K., Otera, H., Nakanishi, Y., Nonaka, I., Goto, Y., et al. (2009). Mitochondrial fission factor Drp1 is essential for embryonic development and synapse formation in mice. Nat Cell Biol *11*, 958–966.

Ban-Ishihara, R., Ishihara, T., Sasaki, N., Mihara, K., and Ishihara, N. (2013). Dynamics of nucleoid structure regulated by mitochondrial fission contributes to cristae reformation and release of cytochrome c. Proc. Natl. Acad. Sci. *110*, 11863–11868.

Jahani-Asl, A., Pilon-Larose, K., Xu, W., MacLaurin, J.G., Park, D.S., McBride, H.M., and Slack, R.S. (2011). The mitochondrial inner membrane GTPase, optic atrophy 1 (Opa1), restores mitochondrial morphology and promotes neuronal survival following excitotoxicity. J Biol Chem *286*, 4772–4782.

Kageyama, Y., Zhang, Z., Roda, R., Fukaya, M., Wakabayashi, J., Wakabayashi, N., Kensler, T.W., Reddy, P.H., Iijima, M., and Sesaki, H. (2012). Mitochondrial division ensures the survival of postmitotic neurons by suppressing oxidative damage. J. Cell Biol. *197*, 535–551.

Karbowski, M., and Youle, R.J. (2011). Regulating mitochondrial outer membrane proteins by ubiquitination and proteasomal degradation. Curr. Opin. Cell Biol. *23*, 476–482.

Karbowski, M., Lee, Y.-J., Gaume, B., Jeong, S.-Y., Frank, S., Nechushtan, A., Santel, A., Fuller, M., Smith, C.L., and Youle, R.J. (2002). Spatial and temporal association of Bax with mitochondrial fission sites, Drp1, and Mfn2 during apoptosis. J. Cell Biol. *159*, 931–938.

Karbowski, M., Neutzner, A., and Youle, R.J. (2007). The mitochondrial E3 ubiquitin ligase MARCH5 is required for Drp1 dependent mitochondrial division. J Cell Biol *178*, 71–84.

Kashatus, D.F., Lim, K.H., Brady, D.C., Pershing, N.L., Cox, A.D., and Counter, C.M. (2011). RALA and RALBP1 regulate mitochondrial fission at mitosis. Nat Cell Biol *13*, 1108–1115.

Kharitonenkov, A., Shiyanova, T.L., Koester, A., Ford, A.M., Micanovic, R., Galbreath, E.J., Sandusky, G.E., Hammond, L.J., Moyers, J.S., Owens, R.A., et al. (2005). FGF-21 as a novel metabolic regulator. J. Clin. Invest. *115*, 1627–1635.

Kim, K.H., Jeong, Y.T., Oh, H., Kim, S.H., Cho, J.M., Kim, Y.-N., Kim, S.S., Kim, D.H., Hur, K.Y., Kim, H.K., et al. (2013). Autophagy deficiency leads to protection from obesity and insulin resistance by inducing Fgf21 as a mitokine. Nat. Med. *19*, 83–92.

Kitada, T., Pisani, A., Porter, D.R., Yamaguchi, H., Tscherter, A., Martella, G., Bonsi, P., Zhang, C., Pothos, E.N., and Shen, J. (2007). From the Cover: Impaired dopamine release and synaptic plasticity in the striatum of PINK1-deficient mice. Proc Natl Acad Sci U A *104*, 11441–11446.

Koch, A., Thiemann, M., Grabenbauer, M., Yoon, Y., McNiven, M.A., and Schrader, M. (2003). Dynamin-like protein 1 is involved in peroxisomal fission. J Biol Chem *278*, 8597–8605.

Koch, A., Yoon, Y., Bonekamp, N.A., McNiven, M.A., and Schrader, M. (2005). A Role for Fis1 in Both Mitochondrial and Peroxisomal Fission in Mammalian Cells. Mol. Biol. Cell *16*, 5077–5086.

Koirala, S., Guo, Q., Kalia, R., Bui, H.T., Eckert, D.M., Frost, A., and Shaw, J.M. (2013). Interchangeable adaptors regulate mitochondrial dynamin assembly for membrane scission. Proc. Natl. Acad. Sci. *110*, E1342–E1351.

Kopeikina, K.J., Carlson, G.A., Pitstick, R., Ludvigson, A.E., Peters, A., Luebke, J.I., Koffie, R.M., Frosch, M.P., Hyman, B.T., and Spires-Jones, T.L. (2011). Tau accumulation causes mitochondrial distribution deficits in neurons in a mouse model of tauopathy and in human Alzheimer's disease brain. Am J Pathol *179*, 2071–2082.

Korobova, F., Ramabhadran, V., and Higgs, H.N. (2013). An Actin-Dependent Step in Mitochondrial Fission Mediated by the ER-Associated Formin INF2. Science *339*, 464–467.

Korobova, F., Gauvin, T.J., and Higgs, H.N. (2014). A Role for Myosin II in Mammalian Mitochondrial Fission. Curr. Biol. *24*, 409–414.

Koshiba, T., Detmer, S.A., Kaiser, J.T., Chen, H., McCaffery, J.M., and Chan, D.C. (2004). Structural Basis of Mitochondrial Tethering by Mitofusin Complexes. Science *305*, 858–862.

Kucharz, K., Krogh, M., Ng, A.N., and Toresson, H. (2009). NMDA Receptor Stimulation Induces Reversible Fission of the Neuronal Endoplasmic Reticulum. PLoS ONE *4*.

Kucharz, K., Wieloch, T., and Toresson, H. (2013). Fission and fusion of the neuronal endoplasmic reticulum. Transl. Stroke Res. *4*, 652–662.

Laar, V.S.V., Arnold, B., Cassady, S.J., Chu, C.T., Burton, E.A., and Berman, S.B. (2011). Bioenergetics of neurons inhibit the translocation response of Parkin following rapid mitochondrial depolarization. Hum. Mol. Genet. *20*, 927–940.

Lackner, L.L., Horner, J.S., and Nunnari, J. (2009). Mechanistic analysis of a dynamin effector. Science *325*, 874–877.

Langer, T., Kaser, M., Klanner, C., and Leonhard, K. (2001). AAA proteases of mitochondria: quality control of membrane proteins and regulatory functions during mitochondrial biogenesis. Biochem Soc Trans *29*, 431–436.

Langston, J.W., Ballard, P., Tetrud, J.W., and Irwin, I. (1983). Chronic Parkinsonism in humans due to a product of meperidine-analog synthesis. Science *219*, 979–980.

Lewis, M.R., and Lewis, W.H. (1914). Mitochondria in Tissue Culture. Science *39*, 330–333.

Li, H., Alavian, K.N., Lazrove, E., Mehta, N., Jones, A., Zhang, P., Licznerski, P., Graham, M., Uo, T., Guo, J., et al. (2013). A Bcl-xL–Drp1 complex regulates synaptic vesicle membrane dynamics during endocytosis. Nat. Cell Biol. *15*, 773–785.

Li, Z., Okamoto, K., Hayashi, Y., and Sheng, M. (2004). The importance of dendritic mitochondria in the morphogenesis and plasticity of spines and synapses. Cell *119*, 873–887.

Lipsky, N.G., and Pedersen, P.L. (1981). Mitochondrial turnover in animal cells. Half-lives of mitochondria and mitochondrial subfractions of rat liver based on [14C]bicarbonate incorporation. J. Biol. Chem. *256*, 8652–8657.

Liu, X., Weaver, D., Shirihai, O., and Hajnoczky, G. (2009). Mitochondrial "kiss-and-run": interplay between mitochondrial motility and fusion-fission dynamics. Embo J *28*, 3074–3089.

Lopes, J.P., and Agostinho, P. (2011). Cdk5: multitasking between physiological and pathological conditions. Prog Neurobiol *94*, 49–63.

Losón, O.C., Song, Z., Chen, H., and Chan, D.C. (2013). Fis1, Mff, MiD49, and MiD51 mediate Drp1 recruitment in mitochondrial fission. Mol. Biol. Cell *24*, 659–667.

Luo, Y., and McKeehan, W.L. (2013). Stressed liver and muscle call on adipocytes with FGF21. Cell. Endocrinol. *4*, 194.

Ma, T., Trinh, M.A., Wexler, A.J., Bourbon, C., Gatti, E., Pierre, P., Cavener, D.R., and Klann, E. (2013). Suppression of eIF2α kinases alleviates Alzheimer's disease-related plasticity and memory deficits. Nat. Neurosci. *16*, 1299–1305.

Manczak, M., and Reddy, P.H. (2012). Abnormal interaction between the mitochondrial fission protein Drp1 and hyperphosphorylated tau in Alzheimer's disease neurons: implications for mitochondrial dysfunction and neuronal damage. Hum. Mol. Genet. *21*, 2538–2547.

Manczak, M., Calkins, M.J., and Reddy, P.H. (2011). Impaired mitochondrial dynamics and abnormal interaction of amyloid beta with mitochondrial protein Drp1 in neurons from patients with Alzheimer's disease: implications for neuronal damage. Hum Mol Genet *20*, 2495–2509.

Manczak, M., Sesaki, H., Kageyama, Y., and Reddy, P.H. (2012). Dynamin-related protein 1 heterozygote knockout mice do not have synaptic and mitochondrial deficiencies. Biochim. Biophys. Acta BBA - Mol. Basis Dis. *1822*, 862–874.

McLelland, G.-L., Soubannier, V., Chen, C.X., McBride, H.M., and Fon, E.A. (2014). Parkin and PINK1 function in a vesicular trafficking pathway regulating mitochondrial quality control. EMBO J.

Mears, J.A., Lackner, L.L., Fang, S., Ingerman, E., Nunnari, J., and Hinshaw, J.E. (2011). Conformational changes in Dnm1 support a contractile mechanism for mitochondrial fission. Nat Struct Mol Biol *18*, 20–26.

Meredith, G.E., Sonsalla, P.K., and Chesselet, M.-F. (2008). Animal models of Parkinson's disease progression. Acta Neuropathol. (Berl.) *115*, 385–398.

Meuer, K., Suppanz, I.E., Lingor, P., Planchamp, V., Goricke, B., Fichtner, L., Braus, G.H., Dietz, G.P., Jakobs, S., Bahr, M., et al. (2007). Cyclin-dependent kinase 5 is an upstream regulator of mitochondrial fission during neuronal apoptosis. Cell Death Differ *14*, 651–661.

Misko, A., Jiang, S., Wegorzewska, I., Milbrandt, J., and Baloh, R.H. (2010). Mitofusin 2 is necessary for transport of axonal mitochondria and interacts with the Miro/Milton complex. J Neurosci *30*, 4232–4240.

Montessuit, S., Somasekharan, S.P., Terrones, O., Lucken-Ardjomande, S., Herzig, S., Schwarzenbacher, R., Manstein, D.J., Bossy-Wetzel, E., Basanez, G., Meda, P., et al. (2010). Membrane remodeling induced by the dynamin-related protein Drp1 stimulates Bax oligomerization. Cell *142*, 889–901.

Mopert, K., Hajek, P., Frank, S., Chen, C., Kaufmann, J., and Santel, A. (2009). Loss of Drp1 function alters OPA1 processing and changes mitochondrial membrane organization. Exp Cell Res *315*, 2165–2180.

Morais, V.A., Verstreken, P., Roethig, A., Smet, J., Snellinx, A., Vanbrabant, M., Haddad, D., Frezza, C., Mandemakers, W., Vogt-Weisenhorn, D., et al. (2009). Parkinson's disease mutations in PINK1 result in decreased Complex I activity and deficient synaptic function. EMBO Mol Med *1*, 99–111.

Morlot, S., and Roux, A. (2013). Mechanics of Dynamin-Mediated Membrane Fission. Annu. Rev. Biophys. *42*, 629–649.

Morris, R.L., and Hollenbeck, P.J. (1993). The regulation of bidirectional mitochondrial transport is coordinated with axonal outgrowth. J Cell Sci *104 (Pt 3)*, 917–927.

Müller-Rischart, A.K., Pilsl, A., Beaudette, P., Patra, M., Hadian, K., Funke, M., Peis, R., Deinlein, A., Schweimer, C., Kuhn, P.-H., et al. (2013). The E3 Ligase Parkin Maintains Mitochondrial Integrity by Increasing Linear Ubiquitination of NEMO. Mol. Cell *49*, 908–921.

Muñoz, J.P., Ivanova, S., Sánchez-Wandelmer, J., Martínez-Cristóbal, P., Noguera, E., Sancho, A., Díaz-Ramos, A., Hernández-Alvarez, M.I., Sebastián, D., Mauvezin, C., et al. (2013). Mfn2 modulates the UPR and mitochondrial function via repression of PERK. EMBO J. *32*, 2348–2361.

Nakada, K., Inoue, K., Ono, T., Isobe, K., Ogura, A., Goto, Y.I., Nonaka, I., and Hayashi, J.I. (2001). Inter-mitochondrial complementation: Mitochondria-specific system preventing mice from expression of disease phenotypes by mutant mtDNA. Nat Med *7*, 934–940.

Nakamura, K., Nemani, V.M., Azarbal, F., Skibinski, G., Levy, J.M., Egami, K., Munishkina, L., Zhang, J., Gardner, B., Wakabayashi, J., et al. (2011). Direct membrane association drives mitochondrial fission by the Parkinson disease-associated protein alpha-synuclein. J Biol Chem *286*, 20710–20726.

Narendra, D., Tanaka, A., Suen, D.F., and Youle, R.J. (2008). Parkin is recruited selectively to impaired mitochondria and promotes their autophagy. J Cell Biol *183*, 795–803.

Narendra, D.P., Jin, S.M., Tanaka, A., Suen, D.F., Gautier, C.A., Shen, J., Cookson, M.R., and Youle, R.J. (2010). PINK1 is selectively stabilized on impaired mitochondria to activate Parkin. PLoS Biol *8*, e1000298.

Oettinghaus, B., Licci, M., Scorrano, L., and Frank, S. (2012). Less than perfect divorces: dysregulated mitochondrial fission and neurodegeneration. Acta Neuropathol *123*, 189–203.

Ong, S.B., Subrayan, S., Lim, S.Y., Yellon, D.M., Davidson, S.M., and Hausenloy, D.J. (2010). Inhibiting mitochondrial fission protects the heart against ischemia/reperfusion injury. Circulation *121*, 2012–2022.

Ono, T., Isobe, K., Nakada, K., and Hayashi, J.I. (2001). Human cells are protected from mitochondrial dysfunction by complementation of DNA products in fused mitochondria. Nat Genet *28*, 272–275.

Otera, H., Wang, C., Cleland, M.M., Setoguchi, K., Yokota, S., Youle, R.J., and Mihara, K. (2010). Mff is an essential factor for mitochondrial recruitment of Drp1 during mitochondrial fission in mammalian cells. J Cell Biol *191*, 1141–1158.

Palacino, J.J., Sagi, D., Goldberg, M.S., Krauss, S., Motz, C., Wacker, M., Klose, J., and Shen, J. (2004). Mitochondrial dysfunction and oxidative damage in parkin-deficient mice. J Biol Chem *279*, 18614–18622.

Palade, G.E. (1953). An electron microscope study of the mitochondrial structure. J Histochem Cytochem *1*, 188–211.

Palmer, C.S., Elgass, K.D., Parton, R.G., Osellame, L.D., Stojanovski, D., and Ryan, M.T. (2013). Adaptor Proteins MiD49 and MiD51 Can Act Independently of Mff and Fis1 in Drp1 Recruitment and Are Specific for Mitochondrial Fission. J. Biol. Chem. *288*, 27584–27593.

Park, J., Lee, S.B., Lee, S., Kim, Y., Song, S., Kim, S., Bae, E., Kim, J., Shong, M., Kim, J.M., et al. (2006). Mitochondrial dysfunction in Drosophila PINK1 mutants is complemented by parkin. Nature *441*, 1157–1161.

Park, S.W., Kim, K.Y., Lindsey, J.D., Dai, Y., Heo, H., Nguyen, D.H., Ellisman, M.H., Weinreb, R.N., and Ju, W.K. (2011). A selective inhibitor of drp1, mdivi-1, increases retinal ganglion cell survival in acute ischemic mouse retina. Invest Ophthalmol Vis Sci *52*, 2837–2843.

Park, Y.Y., Lee, S., Karbowski, M., Neutzner, A., Youle, R.J., and Cho, H. (2010). Loss of MARCH5 mitochondrial E3 ubiquitin ligase induces cellular senescence through dynamin-related protein 1 and mitofusin 1. J Cell Sci *123*, 619–626.

Parone, P.A., James, D.I., Da Cruz, S., Mattenberger, Y., Donze, O., Barja, F., and Martinou, J.C. (2006). Inhibiting the mitochondrial fission machinery does not prevent Bax/Bak-dependent apoptosis. Mol Cell Biol *26*, 7397–7408.

Parone, P.A., Da Cruz, S., Tondera, D., Mattenberger, Y., James, D.I., Maechler, P., Barja, F., and Martinou, J.C. (2008). Preventing mitochondrial fission impairs mitochondrial function and leads to loss of mitochondrial DNA. PLoS ONE *3*, e3257.

Pitts, K.R., Yoon, Y., Krueger, E.W., and McNiven, M.A. (1999). The dynamin-like protein DLP1 is essential for normal distribution and morphology of the endoplasmic reticulum and mitochondria in mammalian cells. Mol. Biol. Cell *10*, 4403–4417.

Del Prete, M.J., Vernal, R., Dolznig, H., Mullner, E.W., and Garcia-Sanz, J.A. (2007). Isolation of polysome-bound mRNA from solid tissues amenable for RT-PCR and profiling experiments. RNA *13*, 414–421.

Qi, X., Disatnik, M.H., Shen, N., Sobel, R.A., and Mochly-Rosen, D. (2011). Aberrant mitochondrial fission in neurons induced by protein kinase C{delta} under oxidative stress conditions in vivo. Mol Biol Cell *22*, 256–265.

Qiu, X., Cao, L., Yang, X., Zhao, X., Liu, X., Han, Y., Xue, Y., Jiang, H., and Chi, Z. (2013). Role of mitochondrial fission in neuronal injury in pilocarpine-induced epileptic rats. Neuroscience *245*, 157–165.

Richter, V., Palmer, C.S., Osellame, L.D., Singh, A.P., Elgass, K., Stroud, D.A., Sesaki, H., Kvansakul, M., and Ryan, M.T. (2014). Structural and functional analysis of MiD51, a dynamin receptor required for mitochondrial fission. J. Cell Biol. *204*, 477–486.

Rintoul, G.L., Filiano, A.J., Brocard, J.B., Kress, G.J., and Reynolds, I.J. (2003). Glutamate decreases mitochondrial size and movement in primary forebrain neurons. J Neurosci *23*, 7881–7888.

Rowland, K.C., Irby, N.K., and Spirou, G.A. (2000). Specialized synapse-associated structures within the calyx of Held. J Neurosci *20*, 9135–9144.

Sandebring, A., Thomas, K.J., Beilina, A., van der Brug, M., Cleland, M.M., Ahmad, R., Miller, D.W., Zambrano, I., Cowburn, R.F., Behbahani, H., et al. (2009). Mitochondrial alterations in PINK1 deficient cells are influenced by calcineurin-dependent dephosphorylation of dynamin-related protein 1. PLoS One *4*, e5701.

Schapira, A.H., Cooper, J.M., Dexter, D., Clark, J.B., Jenner, P., and Marsden, C.D. (1990). Mitochondrial complex I deficiency in Parkinson's disease. J Neurochem *54*, 823–827.

Schneeberger, M., Dietrich, M.O., Sebastián, D., Imbernón, M., Castaño, C., Garcia, A., Esteban, Y., Gonzalez-Franquesa, A., Rodríguez, I.C., Bortolozzi, A., et al. (2013). Mitofusin 2 in POMC Neurons Connects ER Stress with Leptin Resistance and Energy Imbalance. Cell *155*, 172–187.

Schwarz, T.L. (2013). Mitochondrial Trafficking in Neurons. Cold Spring Harb. Perspect. Biol. *5*, a011304.

Scorrano, L., Ashiya, M., Buttle, K., Weiler, S., Oakes, S.A., Mannella, C.A., and Korsmeyer, S.J. (2002). A distinct pathway remodels mitochondrial cristae and mobilizes cytochrome c during apoptosis. Dev Cell *2*, 55–67.

Shen, Q., Yamano, K., Head, B.P., Kawajiri, S., Cheung, J.T.M., Wang, C., Cho, J.-H., Hattori, N., Youle, R.J., and Bliek, A.M. van der (2014). Mutations in Fis1 disrupt orderly disposal of defective mitochondria. Mol. Biol. Cell *25*, 145–159.

Sheng, Z.-H. (2014). Mitochondrial trafficking and anchoring in neurons: New insight and implications. J. Cell Biol. *204*, 1087–1098.

Sheridan, C., and Martin, S.J. (2010). Mitochondrial fission/fusion dynamics and apoptosis. Mitochondrion *10*, 640–648.

Shin, J.-H., Ko, H.S., Kang, H., Lee, Y., Lee, Y.-I., Pletinkova, O., Troconso, J.C., Dawson, V.L., and Dawson, T.M. (2011). PARIS (ZNF746) Repression of PGC-1α Contributes to Neurodegeneration in Parkinson's Disease. Cell *144*, 689–702.

Shirendeb, U., Reddy, A.P., Manczak, M., Calkins, M.J., Mao, P., Tagle, D.A., and Reddy, P.H. (2011). Abnormal mitochondrial dynamics, mitochondrial loss and mutant huntingtin oligomers in Huntington's disease: implications for selective neuronal damage. Hum Mol Genet *20*, 1438–1455.

Shirendeb, U.P., Calkins, M.J., Manczak, M., Anekonda, V., Dufour, B., McBride, J.L., Mao, P., and Reddy, P.H. (2012). Mutant huntingtin's interaction with mitochondrial protein Drp1 impairs mitochondrial biogenesis and causes defective axonal transport and synaptic degeneration in Huntington's disease. Hum. Mol. Genet. *21*, 406–420.

Smirnova, E., Shurland, D.L., Ryazantsev, S.N., and van der Bliek, A.M. (1998). A human dynamin-related protein controls the distribution of mitochondria. J Cell Biol *143*, 351–358.

Söllner, T.H. (2003). Regulated exocytosis and SNARE function (Review). Mol. Membr. Biol. *20*, 209–220.

Song, W., Chen, J., Petrilli, A., Liot, G., Klinglmayr, E., Zhou, Y., Poquiz, P., Tjong, J., Pouladi, M.A., Hayden, M.R., et al. (2011). Mutant huntingtin binds the mitochondrial fission GTPase dynamin-related protein-1 and increases its enzymatic activity. Nat Med *17*, 377–382.

Soubannier, V., McLelland, G.-L., Zunino, R., Braschi, E., Rippstein, P., Fon, E.A., and McBride, H.M. (2012). A Vesicular Transport Pathway Shuttles Cargo from Mitochondria to Lysosomes. Curr. Biol. *22*, 135–141.

Spillantini, M.G., Schmidt, M.L., Lee, V.M., Trojanowski, J.Q., Jakes, R., and Goedert, M. (1997). Alpha-synuclein in Lewy bodies. Nature *388*, 839–840.

St. P. McNaught, K., Belizaire, R., Isacson, O., Jenner, P., and Olanow, C.W. (2003). Altered Proteasomal Function in Sporadic Parkinson's Disease. Exp. Neurol. *179*, 38–46.

Sterky, F.H., Lee, S., Wibom, R., Olson, L., and Larsson, N.-G. (2011). Impaired mitochondrial transport and Parkin-independent degeneration of respiratory chain-deficient dopamine neurons in vivo. Proc. Natl. Acad. Sci. *108*, 12937–12942.

Strack, S., Wilson, T.J., and Cribbs, J.T. (2013). Cyclin-dependent kinases regulate splice-specific targeting of dynamin-related protein 1 to microtubules. J. Cell Biol. *201*, 1037–1051.

Suomalainen, A., Elo, J.M., Pietiläinen, K.H., Hakonen, A.H., Sevastianova, K., Korpela, M., Isohanni, P., Marjavaara, S.K., Tyni, T., Kiuru-Enari, S., et al. (2011). FGF-21 as a biomarker for muscle-manifesting mitochondrial respiratory chain deficiencies: a diagnostic study. Lancet Neurol. *10*, 806–818.

Taguchi, N., Ishihara, N., Jofuku, A., Oka, T., and Mihara, K. (2007). Mitotic phosphorylation of dynamin-related GTPase Drp1 participates in mitochondrial fission. J Biol Chem *282*, 11521–11529.

Theofilas, P., Bedner, P., Huttmann, K., Theis, M., Steinhauser, C., and Frank, S. (2009). The proapoptotic BCL-2 homology domain 3-only protein Bim is not critical for acute excitotoxic cell death. J Neuropathol Exp Neurol *68*, 102–110.

Tian, C., Murrin, L.C., and Zheng, J.C. (2009). Mitochondrial fragmentation is involved in methamphetamine-induced cell death in rat hippocampal neural progenitor cells. PLoS ONE *4*, e5546.

Twig, G., Elorza, A., Molina, A.J., Mohamed, H., Wikstrom, J.D., Walzer, G., Stiles, L., Haigh, S.E., Katz, S., Las, G., et al. (2008). Fission and selective fusion govern mitochondrial segregation and elimination by autophagy. Embo J *27*, 433–446.

Tyynismaa, H., Carroll, C.J., Raimundo, N., Ahola-Erkkilä, S., Wenz, T., Ruhanen, H., Guse, K., Hemminki, A., Peltola-Mjøsund, K.E., Tulkki, V., et al. (2010). Mitochondrial myopathy induces a starvation-like response. Hum. Mol. Genet. *19*, 3948–3958.

Uo, T., Dworzak, J., Kinoshita, C., Inman, D.M., Kinoshita, Y., Horner, P.J., and Morrison, R.S. (2009). Drp1 levels constitutively regulate mitochondrial dynamics and cell survival in cortical neurons. Exp Neurol *218*, 274–285.

Varadi, A., Johnson-Cadwell, L.I., Cirulli, V., Yoon, Y., Allan, V.J., and Rutter, G.A. (2004). Cytoplasmic dynein regulates the subcellular distribution of mitochondria by controlling the recruitment of the fission factor dynamin-related protein-1. J Cell Sci *117*, 4389–4400.

Verstreken, P., Ly, C.V., Venken, K.J., Koh, T.W., Zhou, Y., and Bellen, H.J. (2005). Synaptic mitochondria are critical for mobilization of reserve pool vesicles at Drosophila neuromuscular junctions. Neuron *47*, 365–378.

De Vos, K.J., Allan, V.J., Grierson, A.J., and Sheetz, M.P. (2005). Mitochondrial function and actin regulate dynamin-related protein 1-dependent mitochondrial fission. Curr Biol *15*, 678–683.

Wakabayashi, J., Zhang, Z., Wakabayashi, N., Tamura, Y., Fukaya, M., Kensler, T.W., Iijima, M., and Sesaki, H. (2009). The dynamin-related GTPase Drp1 is required for embryonic and brain development in mice. J Cell Biol *186*, 805–816.

Walker, F.O. (2007). Huntington's disease. Lancet *369*, 218–228.

Wang, H., Song, P., Du, L., Tian, W., Yue, W., Liu, M., Li, D., Wang, B., Zhu, Y., Cao, C., et al. (2011a). Parkin ubiquitinates Drp1 for proteasome-dependent degradation: implication of dysregulated mitochondrial dynamics in Parkinson disease. J Biol Chem *286*, 11649–11658.

Wang, J.X., Jiao, J.Q., Li, Q., Long, B., Wang, K., Liu, J.P., Li, Y.R., and Li, P.F. (2011b). miR-499 regulates mitochondrial dynamics by targeting calcineurin and dynamin-related protein-1. Nat Med *17*, 71–78.

Wang, X., Su, B., Siedlak, S.L., Moreira, P.I., Fujioka, H., Wang, Y., Casadesus, G., and Zhu, X. (2008). Amyloid-beta overproduction causes abnormal mitochondrial dynamics via differential modulation of mitochondrial fission/fusion proteins. Proc Natl Acad Sci U A *105*, 19318–19323.

Wang, X., Su, B., Lee, H.G., Li, X., Perry, G., Smith, M.A., and Zhu, X. (2009). Impaired balance of mitochondrial fission and fusion in Alzheimer's disease. J Neurosci *29*, 9090–9103.

Wang, X., Winter, D., Ashrafi, G., Schlehe, J., Wong, Y.L., Selkoe, D., Rice, S., Steen, J., LaVoie, M.J., and Schwarz, T.L. (2011c). PINK1 and Parkin Target Miro for Phosphorylation and Degradation to Arrest Mitochondrial Motility. Cell *147*, 893–906.

Wasiak, S., Zunino, R., and McBride, H.M. (2007). Bax/Bak promote sumoylation of DRP1 and its stable association with mitochondria during apoptotic cell death. J Cell Biol *177*, 439–450.

Wasilewski, M., and Scorrano, L. (2009). The changing shape of mitochondrial apoptosis. Trends Endocrinol Metab *20*, 287–294.

Waterham, H.R., Koster, J., van Roermund, C.W., Mooyer, P.A., Wanders, R.J., and Leonard, J.V. (2007). A lethal defect of mitochondrial and peroxisomal fission. N Engl J Med *356*, 1736–1741.

Westermann, B. (2010). Mitochondrial fusion and fission in cell life and death. Nat Rev Mol Cell Biol *11*, 872–884.

Wikstrom, J.D., Israeli, T., Bachar-Wikstrom, E., Swisa, A., Ariav, Y., Waiss, M., Kaganovich, D., Dor, Y., Cerasi, E., and Leibowitz, G. (2013). AMPK Regulates ER Morphology and Function in Stressed Pancreatic β-Cells via Phosphorylation of DRP1. Mol. Endocrinol. *27*, 1706–1723.

Yan, M.H., Wang, X., and Zhu, X. (2013). Mitochondrial defects and oxidative stress in Alzheimer disease and Parkinson disease. Free Radic. Biol. Med. *62*, 90–101.

Yang, Y., Gehrke, S., Imai, Y., Huang, Z., Ouyang, Y., Wang, J.W., Yang, L., Beal, M.F., Vogel, H., and Lu, B. (2006). Mitochondrial pathology and muscle and dopaminergic neuron degeneration caused by inactivation of Drosophila Pink1 is rescued by Parkin. Proc Natl Acad Sci U A *103*, 10793–10798.

Yoon, Y., Pitts, K.R., Dahan, S., and McNiven, M.A. (1998). A novel dynamin-like protein associates with cytoplasmic vesicles and tubules of the endoplasmic reticulum in mammalian cells. J Cell Biol *140*, 779–793.

Young, C.N., Cao, X., Guruju, M.R., Pierce, J.P., Morgan, D.A., Wang, G., Iadecola, C., Mark, A.L., and Davisson, R.L. (2012). ER stress in the brain subfornical organ mediates angiotensin-dependent hypertension. J. Clin. Invest. *122*, 3960–3964.

Young, K.W., Pinon, L.G., Bampton, E.T., and Nicotera, P. (2010). Different pathways lead to mitochondrial fragmentation during apoptotic and excitotoxic cell death in primary neurons. J Biochem Mol Toxicol *24*, 335–341.

Yu, W., Sun, Y., Guo, S., and Lu, B. (2011). The PINK1/Parkin pathway regulates mitochondrial dynamics and function in mammalian hippocampal and dopaminergic neurons. Hum. Mol. Genet. *20*, 3227–3240.

Yuan, H., Gerencser, A.A., Liot, G., Lipton, S.A., Ellisman, M., Perkins, G.A., and Bossy-Wetzel, E. (2007). Mitochondrial fission is an upstream and required event for bax foci formation in response to nitric oxide in cortical neurons. Cell Death Differ *14*, 462–471.

Yue, Z., Friedman, L., Komatsu, M., and Tanaka, K. (2009). The cellular pathways of neuronal autophagy and their implication in neurodegenerative diseases. Biochim. Biophys. Acta BBA - Mol. Cell Res. *1793*, 1496–1507.

Zhang, N., Wang, S., Li, Y., Che, L., and Zhao, Q. (2013). A selective inhibitor of Drp1, mdivi-1, acts against cerebral ischemia/reperfusion injury via an anti-apoptotic pathway in rats. Neurosci. Lett. *535*, 104–109.

Zhang, Y., Xie, Y., Berglund, E.D., Coate, K.C., He, T.T., Katafuchi, T., Xiao, G., Potthoff, M.J., Wei, W., Wan, Y., et al. (2012). The starvation hormone, fibroblast growth factor-21, extends lifespan in mice. eLife *1*, e00065.

Zhao, J., Bolton, E.M., Bradley, J.A., and Lever, A.M. (2009). Lentiviral-mediated overexpression of Bcl-xL protects primary endothelial cells from ischemia/reperfusion injury-induced apoptosis. J Heart Lung Transpl. *28*, 936–943.

Zhou, H., Falkenburger, B.H., Schulz, J.B., Tieu, K., Xu, Z., and Xia, X.G. (2007). Silencing of the Pink1 gene expression by conditional RNAi does not induce dopaminergic neuron death in mice. Int J Biol Sci *3*, 242–250.

Zunino, R., Schauss, A., Rippstein, P., Andrade-Navarro, M., and McBride, H.M. (2007). The SUMO protease SENP5 is required to maintain mitochondrial morphology and function. J Cell Sci *120*, 1178–1188.

Zunino, R., Braschi, E., Xu, L., and McBride, H.M. (2009). Translocation of SenP5 from the nucleoli to the mitochondria modulates DRP1-dependent fission during mitosis. J Biol Chem *284*, 17783–17795.

Curriculum Vitae

Björn Oettinghaus

Allenmoosstrasse 116, 8057 Zürich, +41 765720553, bjoern.oettinghaus@gmail.ch

Date of Birth: **02/02/1983**
Nationality: **German**

Postgraduate Education

2009 — 2014

PhD in neurobiology at the University of Basel (Switzerland)

PhD project "**Drp1 ablation in the adult mouse forebrain**" under the supervision of Prof. Stephan Frank in Basel and under the supervision of Prof. Luca Scorrano in Geneva.

The project was selected for an oral presentation at the Keystone Symposia on Mitochondrial Dynamics and Physiology 2014

Secondary Education

2003 — 2008

Biology studies at the University of Constance (Germany)
focused on biochemistry and toxicology

Diploma thesis **"Construction and characterisation of clinical PINK1 mutant cell lines with a focus on mitochondrial dysfunction"** at the KU Leuven (Belgium) under the supervision of Prof. Bart de Strooper. The thesis was supported by a **DAAD scholarship**.

Graduation 04/2008 with a Diploma in Biology after 9 semesters obtained grade was 1.3 (range 1-6, with 1.0 being the highest grade and 4.0 being the minimum requirement to pass).

Intermediate Diploma 10/2005 grade obtained was 2.3 (range 1-6, with 1.0 being the highest grade and 4.0 being the minimum requirement to pass). The grade ranks within the top 15% of the class.

Extracurricular Activities

02/07 — 03/07 University of Constance (Germany), literature research for Prof. Alexander Bürkle **"Compiling a literature compendium on biomarkes of aging"**

08/06 — 10/06 University of Zurich (Switzerland), project work in the laboratory of Prof. Erik Boettger: **"Modelling of the ribosomal decoding site in *Mycobacterium smegmatis*"**

03/06 — 05/06 University of Constance (Germany), project work in the laboratory of Prof. Albrecht Wendel: **"The effect of glycyrrhizin on cytokine induced Apoptosis in HepG2 cells"**

03/04 — 04/04 Novartis, Basel (Switzerland), preclinical safety department

Social Service

2002 — 2003

Military replacement service in a children-after-school-care-facility of the protestant church Kantate Domino in Frankfurt am Main.

Primary Education

1999 — 2002

Graduation (Abitur) 06/2002 at the Liebig Gymnasium in Frankfurt am Main grade obtained was 1.9 (range 1-6, with 1.0 being the highest grade and 4.0 being the minimum requirement to pass)

Extracurricular Activities

10/01 International Biology Olympics (8th place in the federal state Hesse, Germany)

08/00 — 01/01 Exchange semester at Pine Creek High Colorado Springs, CO USA

Additional Qualifications

Qualified to work with laboratory animals, experience with microsurgical techniques on mice (cerebral microinjection and middle cerebral artery occlusion)

Languages:

German (mother tongue), English (fluent), French (advanced)

Publications

Oettinghaus B, Licci M, Scorrano L, Frank S (2012) Less than perfect divorces: dysregulated mitochondrial fission and neurodegeneration. *Acta Neuropathol* **123:** 189-203

Ferraro E, Pesaresi MG, De Zio D, Cencioni MT, Gortat A, Cozzolino M, Berghella L, Salvatore AM, **Oettinghaus B**, Scorrano L, Perez-Paya E, Cecconi F (2011) Apaf1 plays a pro-survival role by regulating centrosome morphology and function. *J Cell Sci* **124:** 3450-3463

Oettinghaus B, Frank S, Scorrano L (2011) Tonight, the same old, deadly programme: BH3-only proteins, mitochondria and yeast. *EMBO J* **30:** 2754-2756

Akshay S, Bertea M, Hobbie SN, **Oettinghaus B,** Shcherbakov D, Bottger EC, Akbergenov R (2011) Phylogenetic sequence variations in bacterial rRNA affect species-specific susceptibility to drugs targeting protein synthesis. *Antimicrob Agents Chemother* **55:** 4096-4102